2018-01-18

Towards the early detection of CO2 leaks from carbon storage sites: modelling and measurement of reaction, diffusion and mass flow of CO2 and O2 in near-surface soils

Alam, Md Monzurul

UNIVERSITY OF CALGARY

Towards the early detection of CO_2 leaks from carbon storage sites: modelling and measurement of reaction, diffusion and mass flow of CO_2 and O_2 in near-surface soils

by

Md Monzurul Alam

A THESIS

SUBMITTED TO THE FACULTY OF GRADUATE STUDIES

IN PARTIAL FULFILMENT OF THE REQUIREMENTS FOR THE

DEGREE OF DOCTOR OF PHILOSOPHY

GRADUATE PROGRAM IN PHYSICS AND ASTRONOMY

CALGARY, ALBERTA

JANUARY, 2018

Abstract

Carbon capture and storage (CCS) of CO_2 in geological reservoirs is being used to mitigate climate change and so a method and technology is needed for early leak detection. This thesis focuses on understanding the reaction, diffusion, and mass flows of O_2 and CO_2 in near surface soils with or without a CO_2 leak.

Two numerical models were developed to describe O_2 and CO_2 reactions, diffusion, mass flow and concentration gradients in the top 1 m of Alberta soils. The first model showed that under typical soil pH values, virtually all CO_2 and O_2 diffusion would occur in the gaseous phase, with less than 0.10% occurring in the aqueous phase, even for high soil water content.

The second model calculated the contribution of diffusion and mass flow for CO_2 and O_2 in the gas phase of soils having a range of respiratory quotient ($RQ=CO_2$ flux/O_2 flux) values, with or without a CO_2 leak. With RQ values ranging from 0.7 to 1.2, mass flow was predicted to account for -0.19% to 1.09% of CO_2 flux to the soil surface, respectively. When simulated rates of CO_2 leakage were set at 1 and 5 times the net biological flux from soils, the contribution of mass flow to total CO_2 flux increased to about 3% and 13%, respectively.

The model was also used to identify the Gas Concentration Ratio (GCR = [CO_2] differential between bulk air and soil surface / [O_2] differential between bulk air and soil surface) as a metric that could be used to identify soils impacted by a CO_2 leak. Three gas analysis systems were built for use with a soil column to test the accuracy of the models and the potential value of a GCR measurement.

The observed concentration gradients were found to be a good fit to the model predictions and the observed GCR measurements were able to differentiate between soils impacted by CO_2 leaks as low as 2 to 3 times the normal biological flux rate of soils (ca. 2 $\mu molCO_2/m^2/s$). This

work supports the further development and use of a portable instrument to carry out GCR measurements at CCS sites.

Acknowledgement

I sincerely thank to my supervisors, Dr. Ann-Lise Norman and Dr. David B. Layzell, for their continuous support, guidance, and teaching me from the very first day of this journey. It was not possible for me to reach this point without having yours countless help throughout my time under yours supervision. I'm very grateful to have both of you as my mentors. I would particularly want to mention Dr. Layzell and his patience to guide me during this program. This were truly encouraging and I gained so many things from you.

I would also like to thank my committee members, Dr. Maria Strack and Dr. Andrew Yau, for their great support, advice and time they spent for me during these years. I am also grateful to all Dr. Norman's group members, Nasrin Pak, Roya Grahreman, Ofelia, Michelle, Neda Amiri, Chenqi and Mark, from whom I received support through my presentations to the group and discussions on my research.

I am indebted to few people of Isotope Science Lab, particularly Steve Taylor and Nenita Lozano for their support during my lab works in early days. Very especial thank to Jesusa Overend-Pontoy for her continuous help and motivational words throughout my PhD.

I would like to acknowledge, all staff of Dept. of Physics and Astronomy, Institute of Sustainable Energy, Environment and Economics (ISEEE), Canadian Energy Systems Analysis Research (CESAR), and Faculty of Graduate Studies, University of Calgary for their various supports, teaching and research grants during my degree.

I am obliged to my parents for their supports and initial encouraging to come abroad to pursue my higher education. Finally, I thank to, my wife Tania Suraia without her mental support throughout this period I would not accomplish this, and to my daughter Samarah for being my last motivation.

Table of Contents

Abstract ii
Acknowledgement iv
Table of Contents v
List of Tables vii
List of Figures and Illustrations viii
List of Symbols, Abbreviations and Nomenclature xii

CHAPTER 1. CARBON STORAGE MONITORING: FOCUS ON SOIL O_2 AND CO_2 EXCHANGE 1
1.1 Introduction: Climate Change and GHG Emissions 1
1.2 Stoichiometric relationship of O_2 and CO_2 4
1.3 Thesis Objective 8

CHAPTER 2. CLIMATE CHANGE AND MITIGATION OPTIONS: LITERATURE REVIEW 13
2.1 Introduction: Climate Change and GHG Emissions 13
2.2 Observed Climate Change 14
2.3 Global GHG emissions: 16
2.4 Global warming and necessity for CO_2 emission reduction: 20
2.5 Canada's emission scenarios: 21
2.6 Global emission reduction strategy: 24
2.7 Carbon Capture and Storage (CCS) technology: 26
2.7.1 CO_2 Capture: 26
2.7.2 Transport of captured CO_2 28
2.7.3 CO_2 storage 29
2.8 Risk of CO_2 leakage from storage and its hazardous impact 31
2.9 Geological storage monitoring technology 33
2.10 Limitations of the current monitoring technology 42
2.11 Rationale for this research 44

CHAPTER 3. GAS EXCHANGE AT NEAR-SURFACE SOIL: MODEL DEVELOPMENT 46
3.1 Introduction 46
3.2 Objective 47
3.3 Methods 48
3.3.1 Model-A: Diffusion and Reaction Model in Gas and Liquid Phase 48
3.3.2 Model-B: Diffusion, Reaction, and Mass flow Model for Gas Phase 58
3.4 Results 63
3.4.1 Model-A Sensitivity Tests 63
3.4.2 Model-A Soil Gas Profiles 66
3.4.3 Model-B: Soil Gas Profiles and CO_2 leak Detection 70
3.5 Discussion 73

CHAPTER 4. FEASIBILITY TEST IN CONTROLLED SETUP 75
4.1 Introduction 75

4.2 Methods 76
4.2.1 The soil column 76
4.2.1.1 Soil Air Porosity (V/V) measurement with pressure method 79
4.2.2 Concentration gradients measurements in GAS-1 82
4.2.1 Gas Analysis Systems (GAS-2 and GAS-3) 85
4.2.2 Standard use of the GAS-2 87
4.2.3 Standard use of the GAS-3 88
4.2.4 Calibration of GAS-2 and GAS-3 93
4.2.4.1 Calibration of IRGA analyzer Licor-7000: 93
4.2.4.2 Calibration of oxygen sensors and Pressure Differential sensors: 95
(a) Reference O_2 *(OR) and Sample* O_2 *(OS) sensors calibration:* 95
(b) *Pressure Differential Sensor Calibration:* 95
(c) Calibration of Differential Pressure (PD) effect on the Oxygen Differential (OD) sensor 98
(d) Converting the measured OD (V) for the PD effect to OD(ppm) 100
4.2.4.3 Calibration of DOX using IRGA Li-7000 101
4.2.5 Haldane correction for net gas volume 103
4.3 Results and discussion 105
4.3.1 Characterization of soil properties: 105
4.3.1 Model vs Measurements: O_2 and CO_2 profiles for estimating soil tortuosity, τ 112
4.3.1 Gas concentration ratio (GCR) measurements using GAS-3 116
4.3.2 Leak detection by GCR measurements using GAS-3 for SOIL-B 120
4.3.2.1 Comparison of Model and measured GCR for SOIL-B 121
4.3.1 Detection limit of the GCR method 123

CHAPTER 5. CARBON SEQUESTRATION IN SOIL 127
5.1 Introduction 127
5.2 Methods 127
5.3 Results and Discussions 128
5.3.1 Comparison of model and measured GCR for SOIL-B 132
5.3.2 CO_2 accumulation in soil column 134

CHAPTER 6. CONCLUSIONS 137
6.1 Summary 137
6.1 Recommendation of Future Studies 139

REFERENCES: 143

APPENDIX A. LEAK TEST FOR GER MEASUREMENTS FOR SOIL-A 161

APPENDIX B. COMPARISON OF MODEL AND MEASUREMENTS FOR ENHANCED BOUNDARY BETWEEN SOIL AND AMBIENT AIR 165

APPENDIX C. CALCULATION OF CO_2 ACCUMULATION IN THE SOIL COLUMN167

List of Tables

Table 1-1: O_2 and CO_2 relationship in biotic and abiotic processes 6

Table 2-1: Technology available or under research for monitoring CO_2 storage 41

Table 3-1: Reference diffusivities of gases 53

Table 3-2: Particle size distribution of typical 'Sandyloam soil'. 61

Table 3-3: Factors affecting GCR in soil. This table shows model predictions at SR (at reference temp) equal to 4.65µmol/m^2/s and for both gas and liquid phase diffusion. 65

Table 4-1: Texture class of the soils used in the experiments 79

Table 4-2**:** Measured physical properties SOIL-A and B in the soil columns 106

Table 4-3 : SOIL-A characteristics for three replicate measurements using GAS-2 on 13 Jun 2016. The CalGas was created by mixing a 10.1% CO_2 in N_2 gas and Breathing air of 0.0496% CO_2 with 20.95% O_2. 110

Table 4-4: SOIL-B characteristics in GAS-3 for three consecutive sequences for soil tested on 7th Nov 2016. 118

Table 5-1: SOIL-B characteristics in GAS-3 for three consecutive sequences for soil tested on 29Mar 2017. 129

Table C-1: Total CO_2 injection over 12 days 167

Table C-2: From the concentration profile measured before injection 168

Table C-3: From the concentration profile measured 12 days after injection 168

List of Figures and Illustrations

Figure 1-1: Hypothetical leak under 0.01 - 0.025% per year and the biogenic flux range. 4

Figure 2-1: Three individually measured datasets (represented by different colors) of globally averaged land and ocean surface temperature anomalies over the period of 1850 – 2012 with respect to the average of 1961 – 1990 (top and bottom panels show anomalies for annual and decadal averages respectively) (IPCC, 2013). 16

Figure 2-2: Global trend for GHG emissions and contribution from each gas 17

Figure 2-3: Contributions to Global GHG emissions by individual compound [IPCC, 2014] 18

Figure 2-4: Increasing trend of atmospheric CO_2 over thousands of years (left) and rate of concentration growth per year (right) (WMO, 2017b). 19

Figure 2-5: Canada's national GHG emission profiles, future projection and limiting target over 2005 to 2030 (Canada NIR, 2017). 23

Figure 2-6: Canada's national GHG emission profiles, future projection and limiting target over 2005 to 2030 [Environment Canada, 2013]. 23

Figure 2-7: Global CO_2 reduction caps from different sectors to keep global warming under 2^oC (IPCC 2007). 25

Figure 2-8: Schematic of CO_2 capturing from different hydrocarbon-based energy conversion processes (Wilcox, 2012). 28

Figure 3-1: $1m^3$ homogeneous soil column of 1000 layers with each a thickness of dz. 50

Figure 3-2: Structure of Model-A where [O], [C], [BC], [CB] represents O_2, CO_2, HCO_3^- and CO_3^{2-}concentrations respectively in the gas (g) or water (w) phase in the first two modelled layers of the soil profile shown in Figure 3-1. FO, FC, FBC, FCB are flux of O_2, CO_2, bicarbonate, and carbonate respectively. SR is considered as the main factor that diffuse gas into soil (FO_g) and out of soil (FC_g); while dz, τ, V_g, V_w represents layer thickness, the path traveled, fraction of gas and liquid volume in a layer. H_O and H_C corresponds for Henry's solubility constants of O_2 and CO_2, respectively. 50

Figure 3-3: 1D steady-state gas flow model with diffusion and mass flow in the gas phase. Here MFOg, MFCg are the share of oxygen and CO_2 in soil air mass flows respectively. . 59

Figure 3-4: Model-A predictions for O_2 and CO_2 concentration (%) profiles in soil when gases diffusion occurs by gaseous and liquid phases for a soil RQ of 1.2. It is assumed that CO_2 diffusion in soil is being facilitated by HCO_3^- and CO_3^{2-} diffusion in soil water for a pH 6.4. Top panel and Lower panel corresponds to soil with gas and water porosities at (13% and 17%) and (21% and 9%), respectively. Inset shows the facilitated diffusion at depth near 80cm and below. 67

Figure 3-5: (A – B) Gradients of $[CO_2]_g$, $[CO_2]_w$, $[HCO_3^-]$ and $[CO_3^{2-}]$ for water content (17 to 21%) at pH 6.4 68

Figure 3-6: (A – B) Gradients of $[CO_2]g$, $[CO_2]w$, $[HCO3^-]$ and $[CO_3^{2-}]$ for water content (17 to 21%) at pH 7.4. 68

Figure 3-7: (A – B) Fluxes of O_2 and CO_2 molecules diffusing into and out of soil for an increase of pH 6.4 to 7.4 (at 17% water content). 69

Figure 3-8: The effects of respiratory quotient (RQ; A1-A4) and CO_2 leaks (B1-B4) on concentration gradients for O_2 (A1, B1) and CO_2 (A2, B2), the predicted GCR relative to bulk air (A3, B3) and the proportion of soil air movement through the soil driven by mass flow (MF) rather than diffusion (A4, B4). The RQ effects assumed with no leak, and the leak models were done at an RQ of 1.2 72

Figure 3-9: 1D steady-state gas flow model with diffusion and mass flow in gas phase. Here MFOg, MFCg are share of oxygen and CO_2 in soil air mass flow respectively. 72

Figure 3-10: The effects of respiratory quotient (RQ; A1-A4) and CO_2 leaks (B1-B4) on concentration gradients for O_2 (A1, B1) and CO_2 (A2, B2), the predicted $\Delta CO_2/\Delta O_2$ (GCR) relative to bulk air (A3, B3) and the proportion of CO_2 movement through the soil driven by mass flow rather than diffusion (A4, B4). The RQ effects assumed with no leak, and the leak models were done at an RQ of 1.6 72

Figure 4-1: Soil column with surface open to air showing the five sample ports (at 2, 25, 50, 75 and 98 cm depth) that were used for the measurement of the CO_2 and O_2 concentration gradients. H, approximate location of the humidity sensors. 78

Figure 4-2: (Upper panel) System used to measure soil porosity measurement. (Lower panel). The measured soil porosity (V/V) with pressure (Pa) applied in soil column. See text for details. 81

Figure 4-3: Calibration of the Qubit O_2/CO_2 analyzer with the measurements of the test gas mixtures of different O_2 and CO_2 concentrations. 83

Figure 4-4: (Left) Shows the schematic of the soil air analyzing in GAS-1 for O_2 and CO_2 concentration measurements. Sample air was extracted from 2cm, 50, 75 and 98cm depths in the soil column. (Right) shows the example of the $[O_2]$ and $[CO_2]$ % at the soil depths measured in the S147. 84

Figure 4-5: Schematic of the GAS-2A used for the measurement of gas exchange rates (GER/RQ) for CO_2 and O_2 and the concentration differentials (GCR) for CO_2 and O_2 between bulk air and the surface of the soil. The latter measurements were used to calculate the gas Concentration ratio as described in the text. A-B, 3-way valves showing positions 1 and 2; Cal, Calibration gas; DOX, Differential Oxygen Analyzer; IRGA, Infrared Gas Analyzer; PR, Pressure Regulator; R or RefGas, Reference gas = CO_2 scrubbed room air; Vr, Vs and Vc, Valves for reference, sample and common flows, respectively. 86

Figure 4-6: Schematic of the GAS-3 used for the measurement of gas exchange rates (GER/RQ) for CO_2 and O_2 and the concentration differentials (GCR) for CO_2 and O_2 between bulk air and the surface of the soil. The latter measurements were used to calculate the gas Concentration ratio as described in the text. A-D, Three way valves showing positions 1 and 2; Cal, Calibration gas; DOX, Differential Oxygen Analyzer; IRGA, Infrared Gas Analyzer; MFC, Mass Flow Controller; PR, Pressure Regulator; R or RefGas, Reference gas = CO_2 scrubbed room air; Vr, Vs and Vc, Valves for reference, sample and common flows, respectively. 90

Figure 4-7: Calibration graph of IRGA (Li-7000) in GAS-2 94

Figure 4-8: Schematic of the differential pressure (PD) sensor calibration using water manometer..... 97

Figure 4-9: Equivalent Differential Pressure (Pa) (converting manometer water column height reading to pressure) with PD (V) reading for induced air pressure in O_2 sample cell (OS) w.r.to Ref cell. 98

Figure 4-10: PD (V) effect on OD(V) (while CO_2 (V) remained unaffected)..... 99

Figure 4-11: PD (Pa) effects OD (V) reading in the DOX analyzer..... 100

Figure 4-12: Expected OD (ppm) vs Measured OD (V)..... 102

Figure 4-13: Measured gradients for O_2 and CO_2 in SOIL-A (upper panel) and SOIL-B (lower panel). Three trials were performed over 3-months for SOIL-A (with 18% of water) and two trials over 4-months period for SOIL-B column (with a decrease of water content from 18% to 14%). Errors are of ±0.14% for O_2 and ±0.33% CO_2 are not shown for simplicity. Note that CO_2 and O_2 profiles for 29Mar2017 for SOIL-B was measured after the soil was flushed of CO_2 for one day and left open to room air for several weeks. 107

Figure 4-14: PD (Pa), OD (ppm), and CS (ppm) data for gas analysing for both soil column open and closed system. Before and after running CalGas, Room Air, Soil Surface, and Soil Fluxes in sample cell, GAS was flushed by flowing 'R' gas both in reference and sample cells. Green, blue and red lines represent PD (Pa), OD (ppm) and CS (ppm) respectively, while 'dashed' blue line is for raw OD and 'solid' blue line for pressure corrected OD line. 109

Figure 4-15: Measured [O_2] and [CO_2] %at depths with model predictions for tortuosity factor, τ = 2, 3, 4 and 5. For SOIL-A (top panel) model simulation used a respiration rate of 3.54 µmol/m^2/s, and an RQ of 0.66 (measured on 13 Jun 2016). For SOIL-B (lower panel), the model used a respiration rate of 4.04 µmol/m^2/s, and an RQ of 0.99 (measured on 29 Mar 2017). 114

Figure 4-16: PD (Pa), OD (ppm), and CA (ppm) data for gas analysis for both soil column open and closed systems. Before and after running CalGas, Room Air, Soil Surface, and Soil Fluxes in sample cell, GAS-3 was flushed by flowing Ref gas both in reference and

sample cells. Green, blue and red lines represent PD (Pa), OD (ppm) and CA (ppm) respectively, while the 'dashed' blue line is for raw OD and 'solid' blue line for pressure corrected OD. 117

Figure 4-17: CO_2 and O_2 fluxes from and into the soils during Test-1 for injection of CO_2 at 1m depth. Flux measurements at the surface was started at time t = 0, prior to injection, and continued during the injection. 120

Figure 4-18: Comparison of measured and model predicted GCR for different rates of CO_2 injection. Model simulation used the respiration rate of 4 µmol/m2/s, RQ of 0.99, and 18% water that were found in soil before the test. 122

Figure 4-19: The expected biological range of the GCR at the near-surface soil for a possible range of soil RQ (based on the model). 124

Figure 4-20: Model detection limit of the GCR for various RQ and soil respiration rates. 124

Figure 5-1: CO_2 and O_2 fluxes from and into the soils during injection of CO_2 at 1-m depth (Test-2 for SOIL-B). 129

Figure 5-2: Changes in O_2 and CO_2 mixing ratios during the injection of 6 µmol/m^2/s for the first 5-days for SOIL-B. 130

Figure 5-3: Comparison of measured (solid line) and model predicted (dot-dashed) O_2 and CO_2 profiles at the 5^{th} days during the injection of CO_2 at a rate of 6µmol/m^2/s. Model simulations used the same environmental and physical properties (SR of 2.11 µmol/m^2/s, water content of 14%) measured and estimated ⊺ of 3 for SOIL-B prior to CO_2 injection at Test-2 (Table 5-1)..... 131

Figure 5-4: Comparison of measured and model predicted GCR for different rates of CO_2 injection during Test-2 for SOIL-B. Model simulation used respiration rate of 2.31 µmol/m^2/s, RQ of 0.78, and 14% water content found in soil before the test. 132

List of Symbols, Abbreviations and Nomenclature

Symbol	Definition
CA	Absolute CO_2 concentration (ppm)
μ	Air viscosity (pa × sec)
BC	Bicarbonate (HCO_3^-)
CCS	Carbon Capture and Storage
CB	Carbonate (CO_3^{2-})
CS	Differential CO_2 concentration in sample cell
DOX	Differential O_2 Analyzer
D_e	Effective gas diffusivity in soil (m^2/s)
FC	Flux of CO_2 ($\mu mo/m^2/s$)
FCB	Flux of CO_3^{2-}($\mu mo/m^2/s$)
FBC	Flux of HCO_3^-($\mu mo/m^2/s$)
FO	Flux of O_2 ($\mu mo/m^2/s$)
f_i	Fractional volume of gas
GAS	Gas Analysis System
GCR	Gas Concentration Ratio
GER	Gas Exchange Rate (closed system)
GES	Gas Exchange System
GHG	Greenhouse Gas
H_C	Henry's constant for CO_2 (unit less)
H_O	Henry's constant for O_2 (unit less)
IRGA	Infra-red Gas Analyzer
IPCC	Intergovernmental Panel for Climate Change
MF	Mass flow of air
Mt	Mega tonne
CH_4	Methane
NIR	National Inventory Report
N_2O	Nitrous oxide
S_N	Normalized soil respiration

OD	O_2 differential
ppm	Parts per million
PD	Pressure Differential
RF	Radiative forcing
Ref	Reference
RQ	Respiratory Quotient, CO_2 evolution/ O_2 uptake
Rm	Room Air
Sam	Sample
K	Soil air permeability (m^2)
V_a	Soil air volume (V/V)
SR_O	Soil O_2 uptake
r	Soil pore radius
ϕ	Soil porosity
SR	Soil Respiration
SS	Soil Surface
V_w	Soil water volume (V/V)
S	Sutherland constant
τ	Tortuosity
WMO	World Meteorological Organization

Chapter 1. **Carbon storage monitoring: Focus on soil O_2 and CO_2 exchange**

1.1 Introduction: Climate Change and GHG Emissions

Increasing CO_2 emissions from human activities elicit concerns regarding its impact on climate. Researchers around the world have examined approaches with various techniques to reduce CO_2 emissions. Among them Carbon Capture and Storage (CCS) is considered to have the greatest potential to remove CO_2. This strategy captures CO_2 from stationary sources and buries it in geological formations. Alongside renewables, energy efficiency, nuclear energy and other options, CCS can play a significant role in global actions on climate change and to stabilize CO_2 concentrations in the atmosphere at around 500 ppm (Pacala, 2004; Stauffer et al., 2011) . In geological storage, CO_2 is trapped in the subsurface by the combination of sealing buoyant CO_2 by geological structures and a series of possible geochemical reactions. The strength of all these trapping mechanisms largely depends on a group of environmental and physical factors including subsurface pressure, temperature, pore structure, capillary forces, and reservoir fluid salinity (IPCC, 2005; Ji, 2016). These dependencies create major challenges to CCS projects and the main objective of keeping injected CO_2 stored below ground. For example, an increase in pore pressure can allow existing faults to cause CO_2 to migrate upward. Also, the thermal contraction caused by changes in temperature due to injected cold CO_2 may affect warmer cap rock formations at the site and cause wellbores to fail. The greatest risks of CCS are associated with either gradual seepage over the life time of the projects or sudden catastrophic leakage.

These potential risks bring the social and environmental challenges of CCS to the front line. Public perception of risk associated with CCS arises due to concerns about the untested nature of sequestration technology and potential leak hazards over the life time of a CCS project. The environmental risks can be categorized into local and global risks. While the local risk can be caused by a high-concentration localized plume of CO_2 resulting from leaks, global risks can be caused due to low-level CO_2 leaked back into the atmosphere over the longer term with attendant effects on global climate (Herzog, 2001; Ide et al., 2006; IPCC, 2005; Sawyer et al., 2008). It is very likely that large amounts of injected CO_2 into any geological storage site will encounter man-made wellbores. The location and distribution of the overwhelming majority of these old orphans or abandoned wells formerly used by oil and gas industries remain unknown. This uncertainty in the possible migration pathways in addition to the physical complexities of the formations, certainly elevate the perception and the risks of CCS projects.

The necessity of securing the fate of CO_2 stored underground, highlights the importance of a robust CCS monitoring technology. To date, a number of techniques are being used for the monitoring and performance verification of CCS storage. Some techniques focus on background analysis of the reservoirs before and after the injections of CO_2, while other techniques are used as a precursor tool to detect the possible migration of CO_2 by continuously measuring aquifer water, soil or atmospheric air in the proximity of the leakage area (Bandyopadhyay, 2014; Chadwick et al., 2010). While most extensive techniques are essential for the assurance of stability and integrity of the formations by detecting faults, fractures and any seismic activity present in the reservoirs or providing the signal for any bulk leakage from the these CO_2 reservoirs, less extensive near-surface

and atmospheric monitoring techniques are more important particularly for direct monitoring of any small seepage from the reservoirs to ensure the environmental safety of humans and livestock (Gluyas & Mathias, 2013; USDOE, 2012; IPCC, 2005).

Although observations of engineered and natural reservoirs show that the fraction of stored CO_2 will exceed 99% over a period of 100 years for a carefully selected and well maintained storage site, more novel means for monitoring are required to maintain the integrity of global CCS projects (Bandyopadhyay, 2014; Haefeli & Bosi, 2004; IPCC, 2005). To ensure stabilization of atmospheric CO_2 concentrations and considering the large cost associated with CCS projects over long time frames for storage, leakage higher than 0.01% per year would not be acceptable for establishing CCS as an economic and viable means of an emissions reduction strategy (Haefeli & Bosi, 2004; Keeling et al., 2011). However, any small leaks that diffuse through a large surface area, due to the migration of escaped CO_2 through tortuous pathways from a few thousand meters depth to the atmosphere, may not be detectable by current monitoring techniques. This is mostly because the majority of these methods were adopted directly from other fields of study that do not have adequate sensitivity for low-level CO_2 leaks (Bandyopadhyay, 2014; USDOE, 2012). In addition to sensitivity, there are other limitations that arise for near-surface and atmospheric monitoring techniques.

For a better understanding, if we consider the scenarios of hypothetical leaks of 0.01% - 0.025 % per year from three large storage sites of 10, 20 and 30MtonCO_2 respectively, the estimated minimum CO_2 flux over a surface area of 200 m radius will be about 17 $\mu mol/m^2/s$ (Figure 1.1-1). Detection of these leaks, which lie near the range of biogenic CO_2 flux from soil, would be difficult for some existing direct monitoring

techniques (e.g. soil chamber measuring or eddy covariance methods). For example, the spatial and temporal variations of soil properties along with diurnal and seasonal changes are among some of the more important factors that affect CO_2 fluxes that may range from 2×10^{-4} to 8 µmol/m^2/s (0.001 to 30 gmCO_2/m^2/day) (Leung et al., 2006; Risk et al., 2002).

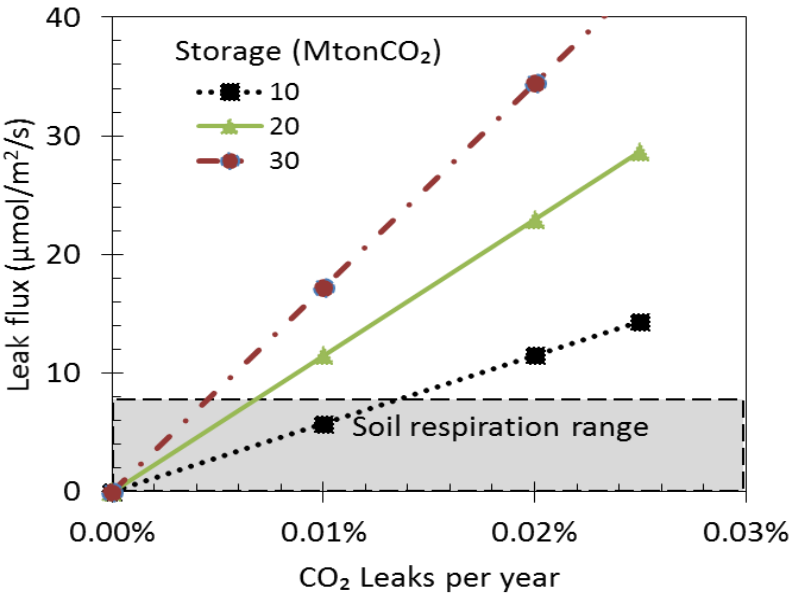

Figure 1-1: Hypothetical leak under 0.01 - 0.025% per year and the biogenic flux range.

1.2 Stoichiometric relationship of O_2 and CO_2

Public acceptance of CCS technology as a major tool for CO_2 reduction from the atmosphere requires a reliable technology that can monitor CO_2 leaks. Given the possibility of being able to directly and rapidly detect leaks, monitoring technologies especially near-surface based techniques are the main focus of this dissertation. The wide range of possible

sources of CO_2 entering the atmosphere would create major challenges for these shallow monitoring techniques to be able to distinguish a leak of sequestrated CO_2 from other sources (Schloemer et al., 2013). Research has been conducted or proposed, in recent years, to monitor leaks by measuring the relative gas mixing ratios of soil gas (O_2, CO_2, and N_2) or change in the atmospheric (O_2 and CO_2) composition. For example, Keeling *et al* (2011) has proposed the possibility of detecting a leak by atmospheric measurements of O_2/N_2 and CO_2 concentrations at the surface near potential leakage sites; Romanak *et al* (2012) has approached the problem with the sequential analysis of O_2 vs CO_2, CO_2 vs N_2, and CO_2 vs N_2/O_2 of vadose zone gases, and Pak *et al* (2016) introduced a detection method based on the deviation of differential O_2 and CO_2 ratios (with respect to background) for an atmospheric plume (Pak et al., 2016; Romanak et al., 2012). These methods rely on the stoichiometric relationship of major soil gases (O_2 and CO_2) and monitoring leaks by detecting anomalies in this relationship. Stoichiometric ratios of soil gases can be used for CCS leak detection because most biogenic (e.g. respiration, photosynthesis) and combustion (e.g. of biomass or fossil fuel) processes will affect O_2 and CO_2 concentrations in opposite ways and depends on the composition of carbon substrates (Schloemer et al., 2013). Therefore, a pure CO_2 leak from storage should have a major effect on the CO_2 concentration in near-surface soil, but have relatively little impact on the O_2 concentration, so it may be distinguishable from other process.

Table 1-1: O_2 and CO_2 relationship in biotic and abiotic processes

Process	Characteristic reactions	Respiratory quotient (RQ)
Biogenic respiration	$^{n}/_{6}\left(C_6H_{12}O_6\right)+nO_2 \rightarrow nCO_2+nH_2O$	0.95 to 1.0†
Organic compound Combustion	$C_xH_yO_zN_w+(x+w+{}^{y}/_{4}-{}^{z}/_{2})O_2 \rightarrow xCO_2+wN_2O+{}^{y}/_{2}\,H_2O$	0.5 to 0.67‡
Anaerobic fermentation	e.g., $C_6H_{12}O_6 \longrightarrow 2C_2H_5OH+2CO_2$	∞

†*Kettlewell, 2004;* ‡Pak et al., 2016

The monitoring method proposed by Keeling *et al* (2011) is based on the observation that fossil-fuel burning in air consumes O_2 and releases CO_2 while N_2 remains unchanged. Thus the combustion processes in the atmosphere will change the characteristic ratio of O_2/N_2 due to the deficits of O_2 and an excess of CO_2 depending on the fuel type. In a similar way, during the consumption or production of CO_2 in sea water, mostly inorganic chemical reactions are involved, and little change in the (O_2/N_2) ratio with reduced or elevated CO_2 is observed, while leaks from the CCS storage will have excess CO_2 with no change in the (O_2/N_2) ratio. This method was expected to be able to detect a leak of 7×10^5 μmol/s (1000 tonCO_2/year) at a distance of 1 km (Keeling et al., 2011).

The technique proposed by Romanak *et al* (2012) from their in-situ test used a similar approach for sequential analysis of the relative mixing ratios of O_2, CO_2 and N_2 in vadose zone soil (unsaturated soil between land surface and the groundwater table) to distinguish the biogenic and non-biogenic sources of CO_2. This method also relies on the fundamental stoichiometric relationship as its basis, and deviation of the characteristic

slopes of the relationship between O_2, CO_2, and N_2 in regular soil air is used in separating the CO_2 sources.

Another recently proposed method by Leeuwen & Meijer (2015) for monitoring CO_2 leaks in the atmosphere is based on the negative correlation of O_2 and CO_2 for biological activities. This method simultaneously measures the fractional mixing ratio of O_2 (converted to the ratio of O_2/N_2 in the atmosphere) and CO_2 in air and distinguishes the sources of the leaks by statistical analysis of the CO_2 vs O_2/N_2 in the air. The authors claimed to be able to detect a leak of 7×10^5 μmol/s (1000 tonCO_2/year) at a distance of 500 m with further instrumental improvements.

However, the wide variation of soil biotic and abiotic processes due to a number of "internal" and "external" factors, increases the uncertainties for detection techniques that rely on O_2 and CO_2 mixing ratio measurements. These internal factors include soil physical properties to carbon substrate composition, while external factors are barometric pressure fluctuations, wind direction, rainfall etc. (Schloemer et al., 2013). For example, O_2 in soil was found to decrease from 21% to 6% between low-elevation Tobanuco forest and high-elevation cloud forest soil (Yiqi & Zhou, 2006), and soil CO_2 concentration may range from 0.3 – 8% at depth from 10 – 100 cm depending on soil temperature and water content (Hashimoto & Komatsu, 2006; Jassal et al., 2005; Karberg et al., 2005). Soil microbial and root respiration are considered primarily responsible for altering soil O_2 and CO_2 concentrations (Oertel et al., 2016) and a majority of soil respiration occurs within 2.5 cm depth (Risk et al., 2002). The extent of soil CO_2 efflux largely depends on soil temperature, humidity, nutrient availability, and soil pH (Oertel et al., 2016).

1.3 Thesis Objective

This study aims to address the hurdles of small scale CO_2 leak detection from CCS sites with current techniques. As part of an interdisciplinary program, this dissertation is divided into three specific sections: understanding the transport mechanism of major soil gases (O_2 and CO_2) and their key controlling factors; synthesizing the soil gas dynamics with a numerical model to simulate concentration gradients across the soil depths, then test the model predictions on soils in a controlled laboratory setup.

Soil is a complex system linked to various components that are directly related with gas exchange between the layers and the atmosphere such as: soil respiration (combination of microbial and root respiration), carbon substrates, nutrients, rainfall, soil temperature, historical land use, etc. (Yiqi & Zhou, 2006). Fortunately there are a good number of reports that have been published on the soil system and the variables that can possibly affect soil gas compositions. The very first attempt aimed to narrow down key variables such as soil temperature, water content and its pH level, and soil respiratory quotient (RQ), depending on their relative impact on the soil gases as supported by the available literature (Gaumont-Guay et al., 2006; Yiqi & Zhou, 2006)

According to previous studies, soil respiration (SR, expressed as CO_2 evolution rate or O_2 uptake rate by soil) is the key factor that regulates soil gas transport through the metabolic process of synthesizing carbon substrates. This SR is highly dependent on a number of variables but mostly on the soil temperature and water content. The works of several research groups (Curiel Yuste et al., 2007; Hashimoto & Komatsu, 2006; Lloyd & Taylor, 1994; Qi et al., 2002) show that SR increases exponentially with soil temperature

due to the combination of a series of factors such as stimulated microbial respiration and easy passage of air within the soil. On the other hand, the water content in soils has large spatial and temporal variation and the linking of SR with soil moisture is more complex as studies show that while water is key to soil processes an excess of water can lead to anoxic conditions that are detrimental to soil respiration. Soil respiration is mostly measured as the CO_2 flux from soil because of the difficulty associated with measuring O_2 change due to its high mixing ratio in air.

This dissertation describes a diverse collection of background studies in a chapter dedicated to literature review (Chapter 2). Literature studies range from soil gases and their key controlling factors and processes, to the technology of monitoring CO_2 efflux from soil, especially those proposed or currently working as a tool for CCS site monitoring.

The second section of this thesis covers the development of a steady state model for gas exchange at the atmospheric boundary that will be able to take feedback from major variables to create possible scenarios for soil gases. Furthermore, this model has the option to consider the exogenous CO_2 invasion from belowground and open the possibility to distinguish invaded CO_2 from biological sources.

The third section was the most challenging and critical part of this thesis where a series of controlled lab tests were conducted to test the feasibility of using the method for leak monitoring. This experimental section combined the design and construction of a soil system to closely mimic field conditions to conduct tests for normal soil and artificial leak added conditions. The experimental section also describes the instrumentation of the lab results, as well as a comparison with model predictions, and the explanation of the anomalies that were observed during the experiments.

From these combined theoretical and experimental studies, a new method has been investigated as an early leak detection tool. This method is based on the assumptions that soil O_2 and CO_2 have a stoichiometric relationship driven by soils biotic activities, while escaped CO_2 from storage will alter this characteristic balance (which would be based on background characteristics of native soil) by introducing CO_2 gas with deficits of O_2.

This technique was developed in two steps: first, building a 1D- diffusion and reaction model that can simulate the differential Gas Concentration Ratio GCR ($\Delta CO_2/\Delta O_2$ w.r.t ambient air) for regular soil with known environmental conditions and with leak added conditions; second, verification of model predictions with a set of controlled lab experiments. The ability of our method to assess and detect small scale leaks from CO_2 storage was evaluated by comparing background GCR values with those for hypothetical small leak scenarios. To understand the variation of soil O_2 and CO_2 and their relationship with the soil's physical properties (especially soil respiratory quotient, RQ, which is the ratio of CO_2 evolution to O_2 consumption in soil) and medium for gas exchange tests, we have used two Canadian soils (collected from Calgary, AB). This study aims to develop a monitoring technique that will be able to distinguish a CO_2 leak close to background flux.

Chapter Two includes reviews of the literature on greenhouse gas emission, climate change, reduction policy, CCS technology, and the monitoring techniques.

Chapter Three includes the hypotheses, testing, development of the model, introduction of mass flow in the model, and simulations for potential leak scenarios.

Chapter Four includes the diagram for lab tests both for closed and open system gas analysis, details on the instrumentations, calibrations of instruments, and lab tests for the verification of our model predictions for CO_2 leak detection by Gas Concentration Ratio (GCR). It also includes CO_2 leak test analysis and a discussion on the limit of this method.

Chapter Five includes the analysis of enhanced CO_2 accumulation in soil during the injection of pure CO_2, as well as a proposal for testing the effect of CO_2 exposure on near-surface soil, its physiological changes, and future advancement of CO_2 monitoring by soil gas analysis.

Chapter Six includes the conclusion of the thesis.

Chapter 2. **Climate Change and Mitigation Options: Literature Review**

2.1 Introduction: Climate Change and GHG Emissions

Climate change due to the increasing trend of greenhouse gas (GHG) emissions has become a major global issue in recent years. The word climate generally means the average patterns of weather (temperature, air pressure, precipitation, wind etc.) over a certain period and expressed at either regional or global scales. These statistical patterns of weather are measured for a particular period that may range from months to millennia but with a standard time of 30 years (WMO, 2017a). However, the climate of our earth is a complex system with the sun as its main driving force. It covers a wide range of internal interactions between the atmosphere, biosphere, hydrosphere, and cryosphere (IPCC, 2013). These interactions are mainly regulated by the radiation budget of Earth which is the balance of the short-wave solar energy received from the sun, and its reflection and redistribution between components of the atmosphere and the surface such as clouds, the ocean, and the terrestrial biosphere and its absorption and re-emission in the infra-red (IR). Almost 70% of the total incoming short-wave radiation is re-distributed internally and 30% is reflected back to space (Dessler & Parson, 2010). The balance of the incoming solar radiation and outgoing IR-radiation along with some variability due to natural events (e.g., Earth's volcanic eruptions or periodic 11-year change in level of the Sun's radiation activity), ensure the normality of our Earth's climate system and its components. Any persistent anomaly of our climate system, both at regional and global scales, is termed as climate change.

However, increasing levels of atmospheric GHG (CO_2, CH_4, N_xO, etc.) across the world have been identified in the acceleration of global climate change and associated consequences. It is because GHG can trap IR-radiation from Earth's surface and re-emit this to the atmosphere, which alters Earth's energy balance (Dessler & Parson, 2010; Downie et al., 2009). This trapping of IR wavelengths by GHG results in heat retention in the atmosphere and ultimately triggers global climate change. GHG emissions mainly from fossil fuel combustion since the beginning of industrial revolution have already started affecting the natural systems and cycles of the Earth (Dawson & Spannagle, 2009). The observed cumulative effects, since the mid-20th century have exhibited several anomalies in the Earth's (both local and global) climate systems that are distinguished from historical patterns. The increasing trend of fossil fuel burning and decreasing total world forest cover are two major reasons for increasing GHG concentrations in the atmosphere (Richardson et al., 2011).

2.2 Observed Climate Change

The quest to understand GHG effects on the atmosphere started in the early 20th century, but it did not receive serious attention before the mid-century when high precision meteorological instruments became available. A number of weather stations across the world were also established around that time. This instrumental development along with growing interest about climate issues has accelerated weather data logging for various research programs (Dessler & Parson, 2010). The analysis of weather data and GHG mixing ratios in the atmosphere indicates the presence of rare and inconsistent (with

history) events in the climate system. For example, the increasing trend of surface temperature (both land and ocean) and sea levels, the shrinking trend of arctic ice sheets, and changes in precipitation events are taken as primary evidence of global climate change (Dessler & Parson, 2010; IPCC, 2013).

According to the Intergovernmental Panel on Climate Change (IPCC) 2013 report, the global combined land and ocean surface temperature record shows (Figure 1.1-1) an increase of 0.85^{o}C over the period from 1880 to 2012. This temperature anomaly has further increased to 0.94^{o}C (NOAA, 2017a) with respect to 1880 and continues with an increasing trend. These temperature anomalies are unprecedented based on the multiple proxy datasets of global surface temperature reconstructed by Mann and Jones, (2003).

The global sea ice and snow cover extents are two parameters that have a strong correlation with global climate change and are taken as key indicators by the IPCC. For example, the global sea ice extent data for the month of September was recorded as 25.63 million km^2 in 1979 and decreased at rate of 2.80% per decade to 22.90 million km^2 by 2017 (NOAA, 2017a) . Similarly, for the month of September, the total snow cover extent of North America and Greenland was 4.13 million km^2 in 1967 and found to be 4.04 million km^2 by 2016 indicates a rate of 1.08% shrinkage per decade (NOAA, 2017a).

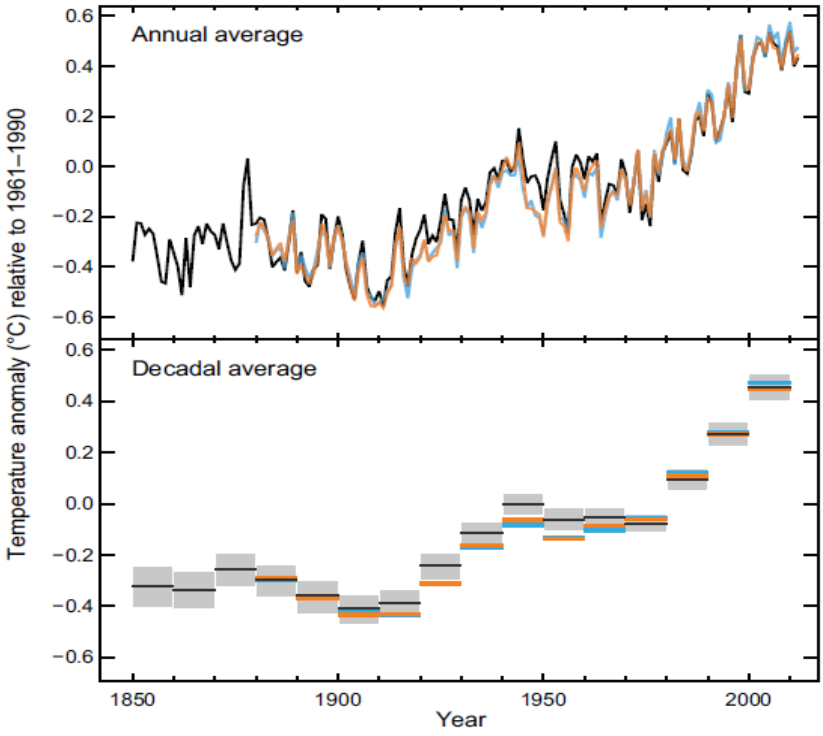

Figure 2-1: Three individually measured datasets (represented by different colors) of globally averaged land and ocean surface temperature anomalies over the period of 1850 – 2012 with respect to the average of 1961 – 1990 (top and bottom panels show anomalies for annual and decadal averages respectively) (IPCC, 2013).

Another important indicator of global climate change is the increased rate of global sea level rise; an unprecedented increase of global mean sea level (by 0.19m) was observed over the period from 1901 to 2010 (IPCC, 2013).

2.3 Global GHG emissions:

The IPCC 2014 report shows that total GHG emissions have risen more rapidly between 2000 – 2010 than was observed for 1970 – 2000 despite the mitigation policies across the world (Figure 1.1-2). The rate of increase of global GHG emissions was 0.90 $GtCO_2$

eq/year in 2000 – 2010 compared to 0.40 $GtCO_2$ eq/year over the period of 1970 – 2000 (IPCC, 2014).

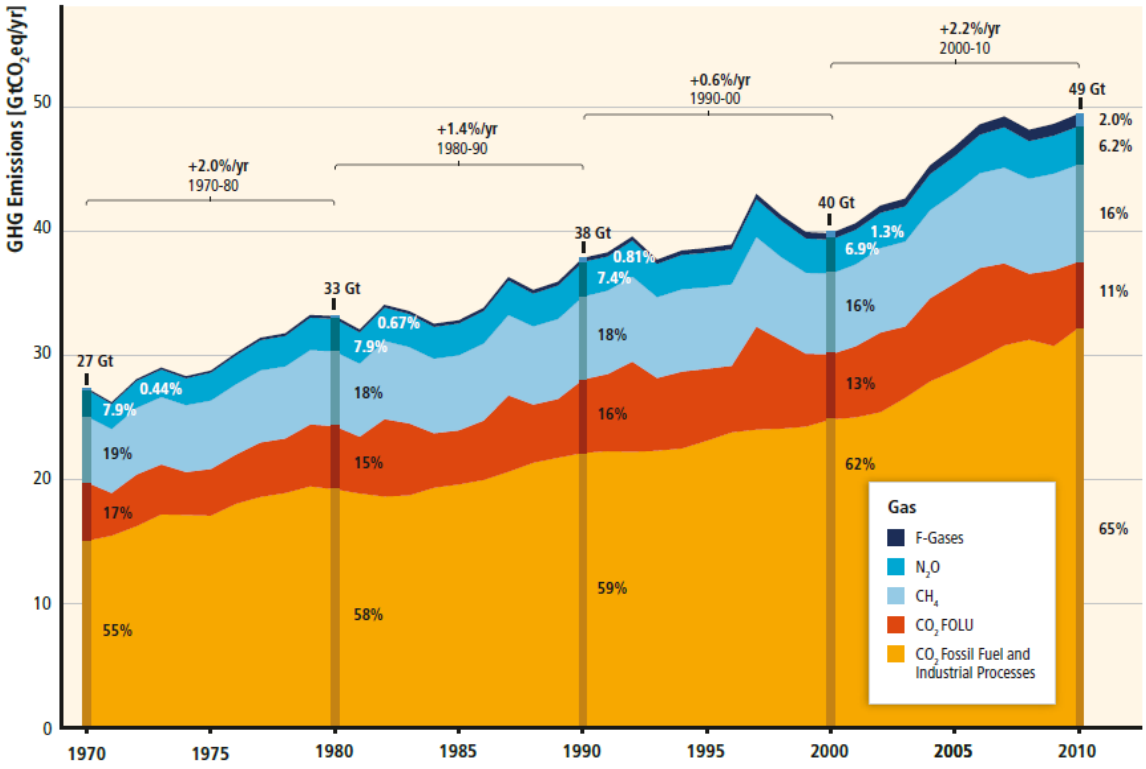

Figure 2-2: Global trend for GHG emissions and contribution from each gas over the period of 1970 – 2010 (IPCC, 2014).

As mentioned in the IPCC 2014 report on global GHG emissions (Figure 1.1-3), CO_2 emissions make up the majority (>70%) of the total GHG emissions measured worldwide followed by CH_4 and N_2O at 14.3% and 7.9%, respectively. Also, the majority of the CO_2 emissions come from fossil fuel energy, which was 36 $GtCO_2$ in 2003 and may exceed 43 $GtCO_2$/year by 2030 (Armstrong & Styring, 2015). Global GHG emissions are expected

to rise over the next few decades due to the increase of global population and economic growth. This may ultimately lead to the global mean surface temperature exceeding the threshold of 2 ^{o}C above pre-industrial levels (IPCC, 2014).

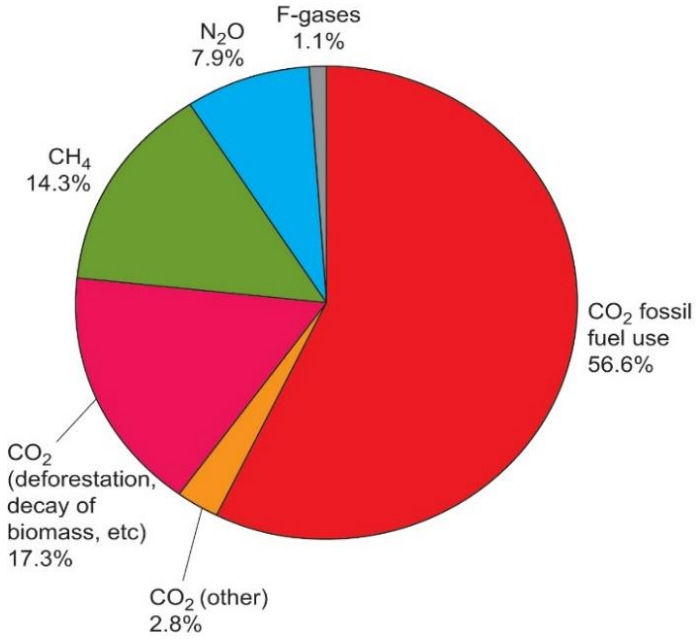

Figure 2-3: Contributions to Global GHG emissions by individual compound [IPCC, 2014]

In addition to making up the largest share of global GHG emissions, CO_2 has a high atmospheric mixing ratio and radiative forcing (RF) at 406 ppm and 1.94 Wm^{-2} respectively reported in 2017 (NOAA, 2017b).The RF of a constituent GHG is the difference between insolation absorbed by the Earth and the energy radiated back, measured at the top of the troposphere, which increases with the increase of relative atmospheric concentration of the gas (NOAA, 2017b). The atmospheric mixing ratio of

CO_2 has exceeded the level recorded over the last several hundred thousand years; the rate of increase has been rising steadily over the last decades.

The rate of CO_2 increase in the atmosphere from the year 2015 to 2016 was recorded as 3.3 ppm/year (WMO, 2017b). Considering the future growing demand for fossil fuel based energy and potential CO_2 releases to the atmosphere, the increasing trend for CO_2 concentration will continue over the 21st century (Schaeffer & van Vuuren, 2012).

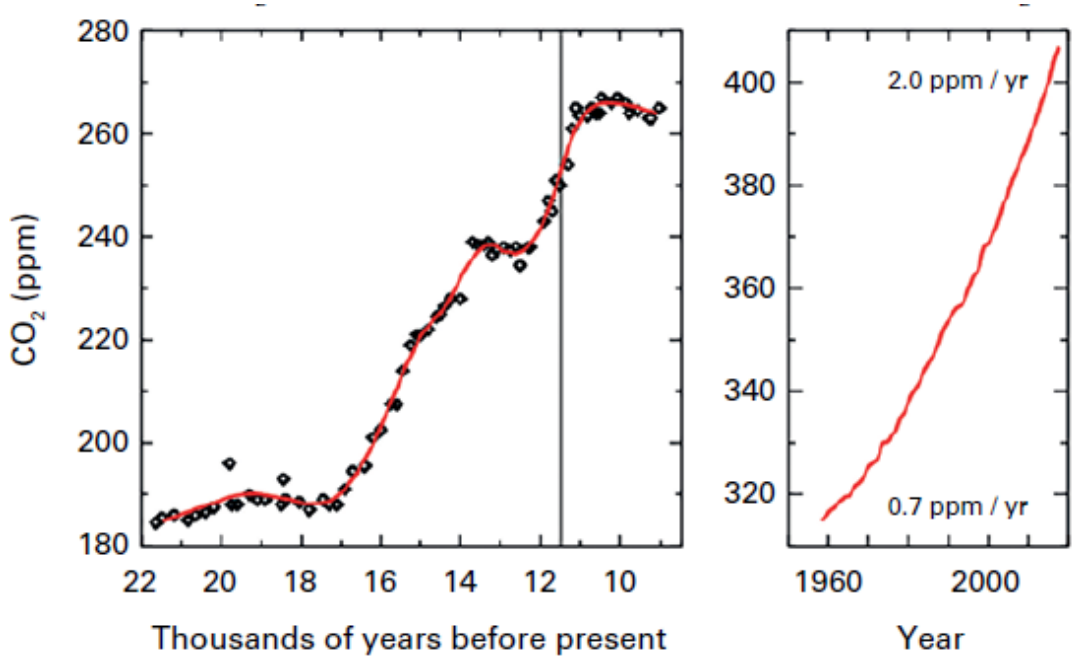

Figure 2-4: Increasing trend of atmospheric CO_2 over thousands of years (left) and rate of concentration growth per year (right) (WMO, 2017b).

2.4 Global warming and necessity for CO_2 emission reduction:

Climate change studies suggest that less CO_2 needs to be released to the atmosphere to stabilize its concentration under a threshold level to avoid negative consequences of climate change (Haefeli & Bosi, 2004). Considering the uncertainties involved with the change in energy demand and development of both alternative energy resources and usage over the upcoming decades, researchers propose different emission reduction targets. These targets of limiting accumulated global CO_2 emissions are based on the latter's global warming potential, wide range of emission sources, and on various active or future mitigation policies. According to Haefeli and Bosi (2004), to stabilize atmospheric CO_2 levels we need a reduction of about 50% of global emissions in the coming decades and 95% in the following centuries. In their model Meinhausen *et al* (2009) take the period of 2000 – 2005 as the base with an estimated accumulated CO_2 emission of 234 $GtCO_2$ and consider the current emission from proven, economically recoverable fossil fuel reserves until 2050. Their model predicts that by lowering cumulative CO_2 emissions limits from 1440 to 1000 $GtCO_2$ over the 2000 – 2050 period we can easily lower the probability of warming to exceed 2^oC relative to pre-industrial temperature, from 50% to 25% (Meinshausen et al., 2009).

Based on the 'MiniCam' modelling results, which search for economically efficient CO_2 reduction limits from various emission scenarios, a range of different cumulative reduction targets will require to maintain the atmospheric CO_2 mixing ratios to a level consistent with natural and oceanic sinks. For example, a cumulative amount of carbon that needs to be removed from the atmosphere by the end of this century would be about 366,

733 and 1260 $GtCO_2$ to keep the CO_2 mixing ratio level in air at 650, 550 and 450 ppm, respectively (Haefeli & Bosi, 2004). According to International Energy Agency (IEA) 2014 report, for a 50% chance of keeping global warming at 2^0C by the end of the 21st century a reduction of 39 $GtCO_2$/year must be reached by 2050 (Armstrong & Styring, 2015).

Based on the predictions of climate models, even a lower stabilization target of 1.5°C may have irreversible adverse effects such as increasing sea levels by 1.5 m (Greene et al., 2017). When the IEA's three projections of temperature increase scenarios are considered (using different GHG reduction levels) show that global temperature may hit 3 to 4°C by the end of this century (Armstrong & Styring, 2015).

2.5 Canada's emission scenarios:

According to Canada's National Inventory Report (NIR) of over two decades, prepared under the guidelines and methodologies of the IPCC, the five major GHG emitting sectors are defined as Energy, Industrial processes and product use, Agriculture, Waste, and Land use (Environment of Canada, 2014). The most recent NIR 2017 report shows that Canada's national GHG emissions were 729, 727, and 722 $MtCO_2$ eq. in 2013, 2014, and 2015, respectively. The majority of emissions were from the different energy sectors such as stationary power plants, transport, and fugitive emissions sources. For example, 81% of Canada's total GHG emissions in 2015 were solely from its energy sector (Canada NIR, 2017).

Figure 1.1-6 shows Canada's present emissions trends, projections, and the country's limiting target over the period of 2005 to 2030. GHG emissions from 2005 were 749 $MtCO_2$ eq., after a short decline period over four years, the trend rose to 722 $MtCO_2$ eq. in 2015 (data collected in 2016). The three lines in Figure 1.1-6 representing three possible scenarios of Canada's GHG emissions by 2030 are based on assumptions on the country's overall economic growth and energy (oil and gas) price. Having the same starting point of 2015 emissions for all three lines, the top blue line represents the higher economic growth and low energy price scenario. It predicts emissions of 747 and 790 $MtCO_2$ eq. by 2020 and 2030 respectively. The lower red line, with the assumption of lower annual economic growth and high oil and gas prices scenario, predicts emissions of 720 and 697 $MtCO_2$ eq. by 2020 and 2030 respectively. The middle black line is the reference line with average economic growth and energy prices that predicts the emissions of 731 and 742 $MtCO_2$ eq by 2020 and 2030 respectively. The dot below these lines is the country's limiting target of 523 $MtCO_2$ eq by 2030.

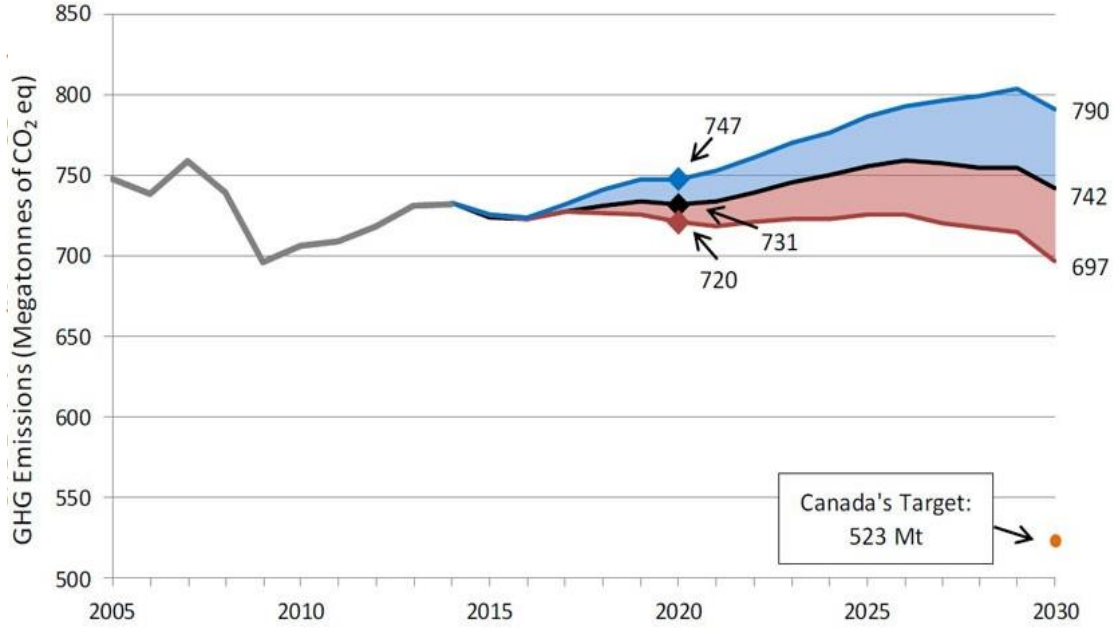

Figure 2-5: Canada's national GHG emission profiles, future projection and limiting target over 2005 to 2030 (Canada NIR, 2017).

To achieve a limiting target of 523 $MtCO_2$ eq. by 2030, which will be 30% less emission than 749 $MtCO_2$ eq. measured in 2005, Canada must eliminate about 226 $MtCO_2$ eq. per year. According to the NIR 2017 report, the reduction strategy has mostly focused on the following three pathways:

1) 89 $MtCO_2$ eq. per year reduction from federal and provincial reduction policies, achieving renewable energy targets, and international cap-and-trade credits.
2) 86 $MtCO_2$ eq. per year reduction from Pan-Canadian frame works such as coal phase out, and clean fuel standards for buildings and industry.
3) 44 $MtCO_2$ eq. per year reduction from developing green infrastructure, technology and innovation, stored carbon in forests, soil and wetlands.

2.6 Global emission reduction strategy:

In addition to countries' individual or independent efforts for removing CO_2 from the atmosphere, several emission reduction strategies are proposed or accepted by the international community. These strategies are based on different models and considerations for a wide range of variables including future energy demand, development of renewable energy, nuclear power plant utilization, Carbon Capture and Storage technology (CCS) etc. (Figure 1.1-7). However, according to the IPCC assessment report 2007, achieving a cumulative reduction of 85% cut in global GHG emissions by 2050 is only possible using a portfolio of solutions. These include two main strategies of enhanced energy efficiency together with a comparatively higher share of renewable energy production than other energy production. To avoid global warming a reduction of CO_2 within the suggested time frames is limited without a technology capable of removing largescale CO_2 emissions like CCS. It is also evident in global actions and policies on mitigating climate change that CCS is the option which has greater potential to remove a significant amount of CO_2 from the atmosphere along with other reduction options (Armstrong & Styring, 2015).

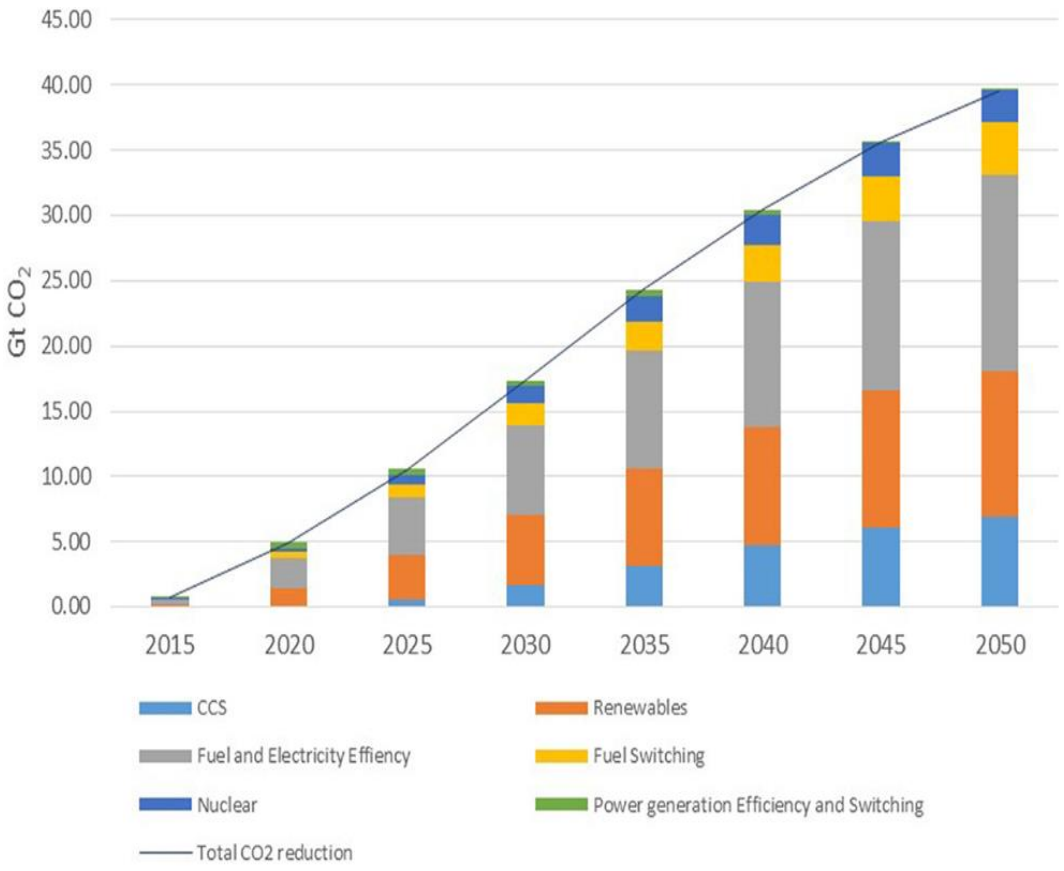

Figure 2-7: Global CO_2 reduction caps from different sectors to keep global warming under 2^{o}C (IPCC 2007).

An estimated worldwide storage capacity of CCS by 2050 is approximately 200-240 $GtCO_2$ and has the potential to remove solely about 30-37% CO_2 emissions globally compared to 2005 levels (IPCC, 2005; Stangeland, 2007). CCS, therefore, has stronger appeal in achieving the global emissions reduction target than other mitigation options while allowing the use of fossil fuels.

2.7 Carbon Capture and Storage (CCS) technology:

CCS refers to the technology of capturing CO_2 from large-scale point sources (e.g. fossil fuel-based power plants) and depositing it into selected geological storage sites or deep saline aquifers for long-term isolation from the atmosphere (Dawson & Spannagle, 2009). This CCS technology is a combination of three individual processes: i) Carbon Capture from point sources, ii) transporting CO_2 to sites, iii) depositing of liquefied CO_2 into the sites for permanent storage (IPCC, 2005).

2.7.1 CO_2 Capture:

Carbon Capture is the process of separating CO_2 from its emission sources; mainly from fossil fuel-powered electricity generating stations or industrial plants. Capturing CO_2 from the exhaust streams is a well-established technology and it allows highly concentrated (85-95%) CO_2 to be either re-used for enhanced oil recovery (EOR) (which includes the possibility of re-emitting a majority of the injected CO_2), or injected into large scale storage sites. The current capture technology mainly focuses on capturing CO_2 from the exhaust of coal fired power plants. It is expected that capturing CO_2 from other sources like natural-gas based power plants or from the atmosphere will soon be financially feasible in the near future with the advancement of research in these areas (Dawson & Spannagle, 2009).

Three types of capture technologies are currently being used or proposed for CCS projects for removing CO_2 from combustion products (flue gas with ~15% CO_2) in fossil fuel-based power plants: Post-combustion, Pre-combustion, and Oxy-combustion (Gibbins & Chalmers, 2008; IPCC, 2005). In the post-combustion technique, a very well-known

technology with limited use, a chemical solvent is used to remove CO_2 from the flue gases. In the pre-combustion technique, hydrocarbon fuels are initially converted into a mixture of H_2 and CO_2 streams by a process known as gasification or reforming. Later, CO_2 is separated from the mixture, leaving H_2 to be used as a fuel; this does not leave CO_2 as the exhaust gas. The latest capturing approach, the Oxy-fuel combustion technique, is still under development, with a relatively high potential compared to existing techniques. In this technique, pure O_2 is used instead of air for burning coal, which results in an almost 100% pure CO_2 stream gas and water vapor as exhaust (IPCC, 2005; Wilcox, 2012). The following flow chart gives the details of these three capture processes as mentioned in the IPCC 2005 special report on CCS (Figure 1.1-8).

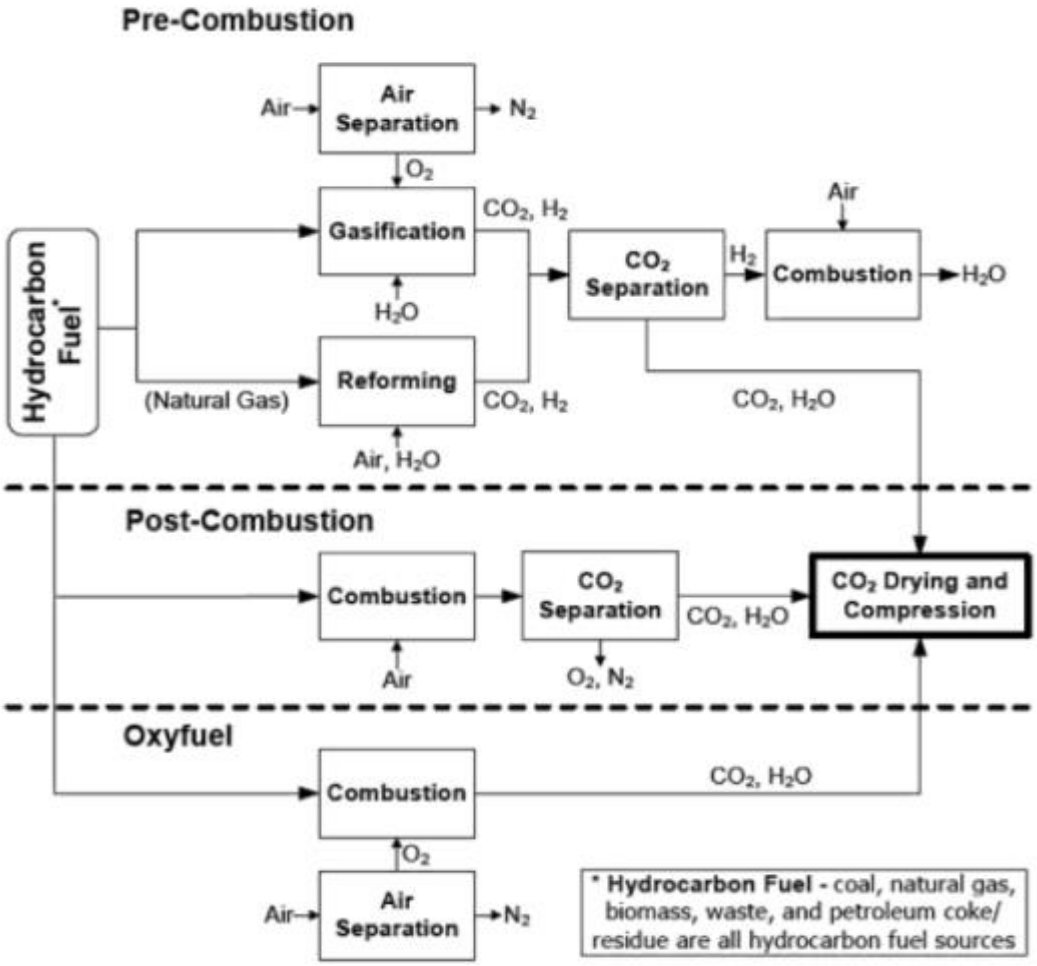

Figure 2-8: Schematic of CO_2 capturing from different hydrocarbon-based energy conversion processes (Wilcox, 2012).

2.7.2 Transport of captured CO_2

Transporting the CO_2 from capture sites to distant offshore or onshore storage sites is essential for the deployment of CSS projects. Different modes of transportation are used

for transporting compressed CO_2 to sites, such as through pipelines, by ships, or by roads (IPCC, 2005; Rackley, 2017). Among these, pipelines are the most commonly used means of transporting high volumes of CO_2 for large scale storage. In this case captured gaseous CO_2 is compressed and transported in liquid phase and pipelines are operated above the critical pressure of 7.38 MPa to maintain a certain mass flow rate and lower pressure drops across the pipelines (Rackley, 2017). The majority of the captured CO_2 is transported by means of pipelines. Most of these pipelines operate with a system of compressors with high pressure upstream and a set of intermediate booster compressor stations along the pipeline.

Transporting captured and liquefied CO_2 overseas or large distances by ships or by roads has been considered as a potential means for the growing number of small to mid-size CCS projects. For marine transportation, CO_2 can be carried by ships under a pressure of 0.7 MPa for relatively large distances such as to overseas countries, while oil tankers can be used for transporting CO_2 through roads and trains at a temperature of -20^0C and 2 MPa pressure. However, transportation by ships and oil tankers are not economically as profitable as transportation through pipelines.

2.7.3 CO_2 storage

After being transported, CO_2 in supercritical form is injected into different pre-selected geological formations. The formations are mainly depleted oil and gas reservoirs, deep saline formations, and unminable coal beds which are chosen as a part of global CO_2 reduction policy by governments across the world (Gibbins & Chalmers, 2008).

Among these, reusing CO_2 for enhancing Oil Recovery (EOR) is already an established technology that has been practiced by the oil and gas industries for several decades. This type of CO_2 usage has a strong business benefit alongside reducing CO_2 emissions from the atmosphere. For example, nearly 50 million metric tons of CO_2 per year were used to enhance oil recovery in the USA in 2010 (Ji, 2016).

To this day the total estimated potential of storage is 675-900 $GtCO_2$, 1000-10,000 $GtCO_2$ and 15-200 $GtCO_2$ by depleted oil and gas reservoirs, deep saline formations and unminable coal seams, respectively (Ji, 2016). In general, CO_2 is injected at depths deeper than 800 m at the site, which can be in both onshore and offshore sedimentary basins, where high ambient pressure and temperature will result in CO_2 in liquid or supercritical state (IPCC, 2005).

Injected CO_2 is then expected to be retained belowground by the combination of several different physical and geochemical trapping mechanisms. The physical trapping of the injected CO_2 mainly comes from the impermeable or very low permeable thick layers of the formations (shale and clay rock layers known as cap rocks) as they block the migration of CO_2 towards the surface. This physical trapping will be increased by the capillary forces of pores within the layers and by the residual trapping of CO_2 by adsorption onto grain surfaces along their migration paths within the formations (Ji, 2016; Shackley & Gough, 2006).

Geochemical trapping of injected CO_2 involves slow processes but can retain the CO_2 buried underground for thousands of years. This type of trapping occurs as the injected CO_2 comes into contact with native fluids, minerals, and rocks within the reservoirs. The geochemical entrapment happens in multiple ways over scales of thousands of years

depending on the temperature, pressure, salinity of the reservoir water and mineralogy of the reservoir rocks (Shackley & Gough, 2006). Geochemical trapping generally starts with CO_2 being dissolved and producing CO_3^{2-} in water:

$$CO_2(g) + H_2O \leftrightarrow H_2CO_3 \leftrightarrow HCO_3^- + H^+ \leftrightarrow CO_3^{2-} + 2H^+$$

The concentration of this CO_3^{2-} species in solutions either grows with time and sinks down instead of moving upward, or reacts with the rock minerals resulting in precipitations of carbonate mineral known as minerals trapping (IPCC, 2005; Ji, 2016; Shackley & Gough, 2006).

Storage sites are anticipated to be able to keep the stored CO_2 underground permanently; selection process for the potential sites is a key part of the CCS projects. Prior to any injection of CO_2, a detailed and proper physical characterization of the reservoirs is key to ensure effective sealing of the cap rocks. It is also key to know the possibility of any active, abandoned wells, or natural fractures in the site area before depositing CO_2 belowground that may compromise the integrity of the seal in the long run.

2.8 Risk of CO_2 leakage from storage and its hazardous impact

The possible existence of various natural or man-made migration pathways raise some major challenges to the stability of stored CO_2 and global CCS projects. The uncertainty of the existence of these leakage channels, especially from the century old abandoned or orphan wells in the proximity of the potential geological carbon storage site, create health and environmental safety concern over the long expected storage life time. The drilling of these wells started at the end of 19^{th} century during an oil and gas exploration period and

since then millions were drilled at different depths and formations of the reservoirs. Among these a number of wells of the mature fields have already been plugged for a few decades and discarded without any records of their sealing types or exact locations (IPCC 2005). These apparently non-documented wells near the storage sites or lacking of information about their plugging materials (mud or cement) and spatial distribution multiplies the risks of CO_2 leakage (Celia et al., 2005). According to reports, the estimated density of the abandoned wells from the legacy of oil and gas exploration in Alberta, Canada and Texas basins is 0.5 to 5 wells per km^2 with a spatial distribution from hundreds of thousands to millions, respectively (Celia et al., 2005; Gasda et al., 2004).

Future injection of CO_2 into an active storage site may capable of further leakage; as high rate of injection of compressed gas through the injection wells may lead to a high pressure gradient that can create additional stress on the impermeable layers of the storage. Exceeding this stress than the threshold level may cause deformation of these sealing layers and create faults or fractures that would eventually facilitate escaping of buoyant CO_2 from storage. Beside these, poor sealing materials of the abandoned wells with additional corrosive effect from CO_2 may also create more leakage pathways. In addition to the leakage potential through these existing or induced structural faults and fractures, there are also some meteorological factors that may increase the risks, such as ambient pressure change, surface wind, or rainfall (Liu, 2012).

Once the CO_2 escaped from below ground storage, it may eventually end up reaching shallow aquifers, near-surface soils or the surface, depending on magnitude or spatial distribution of its travel paths. The impact of the elevated CO_2 on the environment, especially on our ecosystem, has been studied by a number of researchers in recent years.

For example, Bazzaz (1990) reviewed the response of natural vegetation to elevated atmospheric CO_2; Smith et al., (2000) reviewed the enhanced production of aboveground and invasive species of arid ecosystems; and Lindroth (2010) reported increased physiological reactions on the trees in a forest ecosystem (Beaubien et al., 2008). Besides these known plants physiological effects, a major concern of the potential leaks may involve more hazardous consequences to the environment. As the IPCC (2005) report states, ambient CO_2 concentration higher than 2% has a strong effect on human and animal's respiratory physiology while exceeding 7 – 10% will lead to unconsciousness and death. Due to the uncertainty associated with potential passageways and the number of factors involved here, the magnitude of leakage from a geological storage or its possible spatial coverage is difficult to predict (Friedmann & Herzog, 2006).

When it is most plausible that the leaks from the carefully chosen geological formations is likely to stay an order of magnitude lower than the degassing of volcanic CO_2 from Lake Nyos or failure of natural gas storage near Huchinson, two catastrophic events that were observed previously, can be taken as an alarm to possible outcomes of sudden leaks and demands the need for continuous and early detection techniques for CO_2.

2.9 Geological storage monitoring technology

The natural terrestrial biosphere is considered to be able to store 99% of CO_2 it takes from the atmosphere for a period of decades to centuries (IPCC, 2005). The ocean on the other hand, the largest CO_2 natural sink, can hold up to 85% of the CO_2 stored at a depth of 300 m by various ocean chemistry mechanisms for a period of over 500 years. Unlike terrestrial

and ocean storage, it is expected that carefully selected geological storage sites can retain more than 99% of the injected CO_2 for over a period of thousands of years (IPCC, 2005). However, a sudden leak from the storage site through abandoned wells or fractures by earthquake or by accidental puncture by subsequent drilling may lead to the ultimate failure of the site. As such leakage might have significant risk for both local and global CCS establishment, the monitoring of stored CO_2 is a crucial part of CCS projects (Wilson & Jerrad, 2007).

Effective application of a monitoring technology can ensure the accurate accounting of stored CO_2 with a high level of confidence, for both health, and environmental safety, and provide a basis for the establishment of CCS and carbon trading for stored CO_2. Monitoring technology is also an integral part of the risk management strategy for geological storage projects, as it can verify the injected CO_2 remains underground permanently and ensures its ability to detect any accidental leaks at the earliest possible time before it is re-emitted to the atmosphere.

At present, several technologies are deployed for monitoring carbon storage sites across the world adapted from a variety of other applications including the oil and gas industry, disposal of liquid and hazardous waste underground, ground water monitoring, preservation and beverages industries, meteorology, and ecosystem research etc.(Wilson & Jerrad, 2007). These monitoring technologies are classified into two major categories (Chadwick et al., 2010; Gluyas & Mathias, 2013):

1) Deep-focused or monitoring CO_2 migration in the subsurface.

2) Shallow-focused or monitoring CO_2 leakage by :

i) measuring aquifer water or soil gas composition

ii) atmospheric measurement at soil surface or at a height above the ground

Deep-focused technology focuses on the migration of CO_2 plumes in supercritical phase within the subsurface regions. This category of technologies are considered as non-direct leak monitoring methods as they do not directly measure the leakage from the sites. They mainly monitor the formations and the properties of fluid in reservoirs including 3D lime-lapse seismic, downhole pressure and temperature measurement, electrical and electromagnetic measurement of subsurface fluids etc.

Among the available deep-focused or core monitoring techniques installed in carbon storage sites around the world, some are considered very powerful in surveying the subsurface baseline properties, tracking the migration of the stored CO_2 through existing fault or fractures, detecting and quantifying the leaks for simulated leakage tests. For example, time-lapse 3D seismic, cross well seismic wire line logging, as well as pressure monitoring are excellent tools for tracking the migration of CO_2 plumes within subsurface regions or to the upper layers of the reservoirs and providing information on CO_2 concentration at depth (Harris et al., 2006; Ji, 2016; Park et al., 2012). These techniques rely either on the seismic properties (mostly acoustic impedance) or the geophysical properties of the reservoir fluids (electrical conductivity, salinity etc.). The minimum resolution of surface seismic profiles can distinguish a migration of 2500 to 10,000 tCO_2 in subsurface, while by the non-seismic geophysical measurement like gravity technique has a minimum resolution an order of magnitude higher than seismic (IPCC, 2005).

The second category of monitoring techniques are known as direct monitoring methods as they directly detect CO_2 leaks by measuring the deviation of gas concentration/ fluxes/ geochemistry from baseline surveys prior to injection. These direct methods include acidity measurement of shallow aquifers, vadose zone gas analysis, eddy covariance based flux measurement of surface air etc.

Shallow-focused monitoring techniques are more direct ways of detecting leaked CO_2 before or immediately after its release to the surface. The techniques of this group can be classified into two groups due to their zone specific measurement limitation: techniques that monitor water or gas composition below the surface, and those that monitor above the surface atmosphere. For example, the migration of CO_2 towards the surface can be detected by measuring aquifer water chemistry (e.g. pH), by measuring the relative O_2, CO_2, and N_2 concentration in vadose zone gas, tracking CO_2 flux with soil chambers or eddy-covariance towers at the surface, by identifying the isotopic tracers injected with the CO_2 streams at air (Bellante et al., 2013; Romanak et al., 2013; Romanak et al., 2012; Verkerke et al., 2014). The basics of some shallow-focused techniques are discussed in the paragraphs below along with their challenges as CO_2 leak detection technology.

Shallow-focused groundwater monitoring techniques have been proposed by many researchers as a direct way of detecting the presence of leaked CO_2 in aquifer water (Cahill et al., 2014; Kharaka et al., 2017; Lee et al., 2016). The ability of gaseous or dissolved CO_2 can change chemical composition of water in various ways (e.g. dissolved CO_2 in water, alkalinity, acidification, conductivity etc.). The detection of CO_2 intrusion in groundwater can be conducted from the survey of water composition before and after CO_2 stored in the reservoirs. This survey of chemical properties is done either by inserting certain sensors

(e.g., pH and dissolved pCO_2 sensors) into aquifers through injection wells, or by routine sampling of ground water as an effective tool for CO_2 detection. In groundwater monitoring, a number of parameters can be used as an indication of CO_2 migration in aquifers, such as dissolved CO_2 level, pH, alkalinity, heavy metals, electrical conductivity (EC), and dissolved elements (Ca, Mg, Na, Al, Zn etc.) (Lee et al., 2016; Waarum et al., 2017). For example, Cahill et al (2017) examined pH, EC and dissolved elements in a carbonate-free shallow-depth aquifer over 305 days to detect the elevated CO_2 in aquifer water from a controlled release of 10 days. The presence of CO_2 was confirmed from measured changes in the dissolved elements with advective ion pulse and increasing acidification). The detection of CO_2 leakage by groundwater chemical monitoring is very challenging because small seepage of CO_2 leaks may not be noticeable during short-term period especially for large volume of ground water and site specific interactions of leaked CO_2, water and aquifer's formation (Lee et al. 2016).

Tracer based monitoring techniques involve using the inherent isotopic signature of the injected CO_2 (stable isotopes of ^{13}C and/or ^{18}O), inherent noble gases found in the reservoirs (^{3}He, ^{40}Ar), adding certain isotopes (^{14}C), and artificial chemical compound (PFCs, CFCs, SF_6 etc.) with the injected CO_2 (Roberts et al., 2017). Tracer methods have been proposed as an effective tool for various purposes of carbon storage projects ranging from monitoring migration of injected CO_2 within the reservoirs, dissolution into reservoir fluids or detecting CO_2 infusion into groundwater, degassing to surface (Györe et al., 2017). For example the inherent signature of $^{13}CO_2$ has been used for leakage monitoring from two industrial scale carbon storage sites in Canada, QUEST and Weyburn-Midale projects. The isotopic value $\delta^{13}C$ of -20.4‰ found in the captured CO_2 is selected as tracer

for recently opened (started at 2016) QUEST carbon storage project in Edmonton, Canada (Roberts et al., 2017). The major problem associated with the isotopic or chemical tracer techniques is that CO_2 detection depends on several other factors. These include precise measurement of background level of the tracer in the subsurface, seabed or land surface of the selected storage site, its intrinsic characteristics (how inert it is to chemical reactions during its travel through various pathways of different chemical composition and environment), along with resolution of the analytical tools (Roberts et al., 2017).

Surface based shallow-focused monitoring techniques are operated either from the setup at-or-above soil surface, while remote sensing techniques are based on mobile transport, airborne or satellite platforms (Jiang et al., 2013; Schütze et al., 2013; Verkerke et al., 2014). Some these techniques are used for direct monitoring of CO_2 leakage by measuring flux with soil chamber and eddy covariance, while others are used for passive monitoring by measuring the impact of CO_2 on the aboveground ecosystem. Passive detection techniques of this group are different from others as they do not require sampling analysis and instead measure the change of an indicator that has been adversely affected by the elevated level of CO_2 (e.g. vegetation stress of surrounding area). Most of these technique have wide spatial coverage such as the spatial coverage of eddy covariance which ranges from hundred m^2 to few km^2 (Schütze et al., 2013). However, each surface and atmospheric technique has its own challenge when it comes for monitoring the geological storage sites. Measuring soil gas composition, for example, can distinguish leaked CO_2 from that of soil background, but is not well-suited to monitoring over large areas. Similarly, the atmospheric techniques, especially eddy covariance tower and atmospheric tracer techniques, are not able to differentiate between release from storage

sites and ambient CO_2 due to variable natural or anthropogenic sources in the surrounding area (USDOE, 2017).

The surface based (below or above the surface) monitoring techniques mostly target the leak detectability of the method higher than a release of 0.01% CO_2 of total storage per year. The detection of leaks by these techniques depend on various factors that range from types of the leaks, its spatial distribution, interactions with the leakage pathways, soil environment, to atmospheric conditions (Romanak et al., 2017). One of the key surface based methods, proposed and tested with various researchers, is measuring the relative mixing ratios in the soil or atmosphere (O_2, CO_2, N_2, CH_4 etc.) Some of these works has been discussed briefly in the Chapter 1, Section 1.2. The basis of these methods relies on the chemical stoichiometric relationship among these gases that are used to distinguish them from each other and from that of leakage CO_2. Tests of these proposed methods, have been conducted with controlled CO_2 release by continuous or periodic measurement of soil or atmospheric air composition. Analysis of air samples are often carried out with gas chromatography, non-dispersive infra-red analyzer, and with fuel-cell oxygen analyzers (Leeuwen & Meijer, 2015; Pak et al., 2016; Romanak et al., 2012). These methods are considered very powerful, as of today, compared to other shallow-focused monitoring techniques in distinguishing the sources of CO_2 in near-surface soil or in atmosphere by analyzing the relationship of coexisting gases. The limit of CO_2 leak detection by these types of techniques reported as small as 3 ppm above the background level and can distinguish a leak from a point source (1000 tCO_2/year) at distance 500 m to 1km (Keeling et al., 2011; Leeuwen & Meijer, 2015)

Table 2-1 shows some monitoring tools that are being used or under development for detecting CO_2 leaks from geological storage sites. The majority of the passive or deep-focused techniques (seismic) and some surface technique (eddy covariance) are established by the petroleum industry over many decades, while other techniques such as remote sensing techniques are still under research level with limited verification from controlled lab or field tests (USDOE, 2017).

Table 2-1: Technology available or under research for monitoring CO_2 storage

	Monitoring technique	Measurement parameters	Challenge
Deep focused monitoring	Seismic monitoring of CO_2 migration and distribution in the storage	P and S wave velocity, Reflection horizons, Seismic amplitude attenuation, Magnitude and sources of micro seismic events	Seismic resolution decrease with depth and rock formations
	Pressure monitoring at subsurface	Anomalies in pressure profiles	Efficient for tracking bulk CO_2 migration but not for small leakage
	Geophysical properties of the storage monitoring	Electrical conductivity and electromagnetic induction measurement	Low resolution tracking CO_2 plume migration
	Gravity measurement in the subsurface	Density changes in the subsurface fluid	Lower resolution than seismic technique not adequate for early leak detection
Shallow-focused monitoring	Water composition in aquifer monitoring	CO_2, HCO_3^-, Salinity measurements	Small seepage may not be enough to change water chemistry
	Soil gas composition in near-surface	Relative concentration and relationship of O_2, CO_2, and N_2	Difficult to cover large surface area of the storages
	Natural or introduced tracer in CO_2 storage	Travel time, Partitioning of CO_2 in brine or oil, Identification of CO_2 sources	Tracer migration may not be same as CO_2 migration, dispersion of certain tracers in atmosphere is different than CO_2
	Atmospheric flux measurement	CO_2 flux monitoring at surface or at a height above	Natural and temporal variability of CO_2 may mask small seepage
	Airborne/Satellite-based remote sensing	Remote sensing of CO_2 release to atmosphere, Hyperspectral imaging of ecosystem vegetable stress	Long path length through the atmosphere or lack vegetation at surface may hide low-level leaks

(IPCC, 2005; Liu, 2012; USDOE, 2017)

2.10 Limitations of the current monitoring technology

Most standard deep-focused techniques (e.g., both active and passive seismic monitoring) relies on the geophysical properties of the storage site and the nature of the injected CO_2 (migration, density, mixing with reservoir waters etc.) and the data quality of the surveys (Chadwick et al., 2010; Gendrin et al., 2013; Harris et al., 2006). It is, therefore, these core monitoring techniques that are considered effective in terms of verification of reservoir performance, tracking bulk CO_2 migrations in the sub-surface (usually more than tonnes of CO_2), but may not be feasible for detecting trace amounts of CO_2 leaks over the expected long life time of the CCS project.

On the other hand, near-surface and surface based techniques require a detailed analysis of background history of the site including its physical and environmental properties that may vary over the life time of a storage site. Again, the accuracy of some of these techniques becomes limited as the detection of a leak relies on the leakage path intersecting with the measured path, or sometimes during unfavorable environmental conditions (e.g. wind condition) leaked CO_2 may disperse too quickly to be detected. Surface based atmospheric monitoring techniques particularly become less effective in terms of covering a wide surface area of the storage sites. For example, a hyperspectral remote sensing technique that can cover a relatively large surface area has shown only a success rate of 47% at identifying a CO_2 vent (Gluyas & Mathias, 2013).

Techniques that are currently installed for direct measurement of CO_2 leaks include vadose zone gas concentrations, soil CO_2 flux, and ecological CO_2 flux measurement with mostly open or short-path laser absorption based instruments with remote sensing or eddy

covariance tower setups. The detection sensitivity of these techniques not only depends on the instruments themselves but also on the environment and the ways measurements are carried out. As mentioned in the IEAGHG 2012 report, a leakage of 26 – 263 μmol/m^2/s (0.1-1 $kgCO_2$/day) will remain indistinguishable at the surface by current atmospheric and shallow surface based emission monitoring techniques such as eddy covariance and soil gas flux measurements (IEAGHG, 2012).

To date, the minimum CO_2 release that can be measured by these techniques are reported for the Solfatara volcano flux of about 263–1000 μmol/m^2/s (1– 4 $kgCO_2/m^2$/day) by (Werner et al., 2003); for small seepage of 8×10^4 μmol/s (300 $kgCO_2$/day) at controlled CO_2 release sites done by zero emission research by Lewicki et al., (2007); for a controlled leakage of 1×10^7 μmol/s (43000 $kgCO_2$/day) by Loh et al., (2009); and a leak of 7100 μmol/s (27 $kgCO_2$/day) from a point source can be detected at a distance 0 – 80 meter downwind by Leuning et al., (2008). So far, the lowest CO_2 leaks detected by the surface based monitoring techniques is nearly 7×10^5 μmol/s by Keeling et al., (2011) and Leeuwen & Meijer, (2015) . It is, therefore, evident that distinguishing between small scale leakage signals and natural fluctuations in CO_2 fluxes still pose significant challenges for existing detection techniques.

Therefore, there is the need for additional studies and development of technology for geological storage site monitoring especially when it comes to small leakage rates, covering a large surface area, and early detection before release to the atmosphere. These future CO_2 monitoring methods could help facilitate global emission reduction strategies by improving the limits and accuracy of detection, estimating the extent of leakage and locating possible CO_2 escape routes.

2.11 Rationale for this research

Addressing the limitations of the existing techniques and the necessity of economically feasible early CO_2 leak monitoring methods, we have developed a new technique of analysing near surface soil gases for detecting small scales leaks that lies within the range of natural soil CO_2 flux and under the acceptable 0.01% - 0.025% leaks per year from a storage (Keeling et al., 2011; Miles et al., 2005).

This thesis is focused on understanding near surface soil O_2 and CO_2 profiles, assessing how they respond to natural biogeochemical processes and environmental factors and then use these insights to develop a method for the early detection of CO_2 leaks from carbon storage sites. To begin with, two hypotheses have been proposed and tested using a one dimensional, steady state numerical model for gas exchange between the soil and atmosphere. The First hypothesis addresses the possibility of facilitated diffusion of CO_2 in liquid phase, while the second hypothesis used an integrated reaction, diffusion, and mass flow model of gases at near surface soil layers. Our model results have been tested with an experimental setup using two representative Alberta soils and for a range of possible CO_2 leak rates calculated for different storage sites. The analysis of the theoretical model and experimental work provides a background to develop a novel method for early detection of CO_2 leaks from geological storage sites.

Chapter 3. **Gas Exchange at Near-Surface Soil: Model Development**

3.1 Introduction

Monitoring CO_2 leaks from CCS by atmospheric or soil gas measurements (eddy covariance, soil chamber etc.) are the least expensive and most direct ways for leak detection. The effect of native soil properties on the below or above ground air composition suggests that any atmospheric or soil gas measurements without quantifying these effects may increase the measurements' uncertainties. The transport of gases at the atmospheric boundary between soil and air is considered to occur mostly by the diffusion of gases due to the concentration gradients, but the characterization of the gases in near-surface soils will not be completed without accounting for their variability from other factors. These factors may range from barometric pressure at the surface, the availability of pore spaces, or the tortuous paths that gases travel in soils.

In this study, a method of simultaneous measurements of the relative changes in soil O_2 and CO_2 mixing ratio were examined with respect to the atmosphere. This method illustrates, with consideration of the possible influences that may arise from soil properties, the superposition of diffusive and pressure driven flows of gases to depict the most possible scenarios of gases near the surface. The development of this method has been done in two steps: synthesizing published data on the major factors influencing the gas exchange dynamics at the soil and atmosphere boundary, and then building numerical models to simulate O_2 and CO_2 profiles for regular soils with varying soil characteristics conditions and possible invasion of CO_2 leaks from CCS storage.

3.2 Objective

The specific goals for developing a model of O_2 and CO_2 gas exchange between soil and the atmosphere are:

i) To understand how major soil properties (soil water content, respiratory quotient (RQ), pH level, tortuosity) affecting soils will impact O_2 and CO_2 concentration gradients in near-surface soil layers.

ii) Using this knowledge to build a method to distinguish leaked CO_2 from that of soil background.

Two hypotheses have been tested in this model development; The first hypothesis considered the facilitated diffusion of HCO_3^- and CO_3^{2-} in soil water, similar to the process observed by Hunt *et al.*, (1988) on species in legume nodules. Based on this, a gas diffusion and reaction model that considers dissolution of CO_2 in soil water and equilibrium reactions of HCO_3^- and CO_3^{2-} to explore their contribution in enhancing CO_2 flux from soil to air. This hypothesis was tested by developing a static 1-D model with the diffusion and reactions associated with soil O_2 and CO_2 concentrations.

A second hypothesis considered the case when CO_2 evolution exceeded O_2 uptake by soil (i.e. RQ>1), and higher O_2 diffusivity than CO_2 would create a positive atmospheric pressure at soil depth which will be increased further by the addition of any CO_2 leak into the soil. This pressure gradient, eventually, would drive mass flow of air out of the soil, which would then impact CO_2 and O_2 concentration gradients in opposite ways. To test the contribution of mass flow to soil O_2 and CO_2 concentrations, pressure driven flow was added in our gas diffusion and reaction model.

3.3 Methods

The transport of gases across the soil-air interface is mainly driven by molecular gas diffusion with only a small portion via pressure driven mass flow (Kayler et al., 2009). Although soils contain significant amounts of water, the contribution into gas transport from liquid phase diffusion of the gases has not received much attention from scientists. The transport of gases in liquid phase has been largely overlooked due to their lower (roughly by 4-orders of magnitude) diffusivities in water versus air.

A previous study of gas diffusion within N_2-fixing legume nodules, where diffusion is mainly in the aqueous phase (99.85%), showed that CO_2 diffusion was strongly facilitated by HCO_3^- which was assumed to be in equilibrium with dissolved CO_2 (Hunt et al., 1988). This facilitated diffusion was predicted to generate a negative atmospheric pressure inside the nodule pulling O_2-rich air into the centre of the nodule through the few gas-filled intercellular spaces in the cortical tissue. Therefore, a complete analysis of CO_2 facilitated diffusion in liquid phase and the biogeochemical processes of near surface soil with their relationship to the environment may help to identify gas composition at the atmospheric boundary that is indicative of a CCS leak.

3.3.1 Model-A: Diffusion and Reaction Model in Gas and Liquid Phase

To test the first hypothesis, a 1-dimensional, steady-state model was built to represent a $1m^3$ homogeneous soil from Alberta. The soil volume (Figure 1-1) was assumed to consist of 1000 layers with a surface area of $1m^2$ and set values for fractional volume of air, soil

particles, water, temperature, pH level and RQ. The reaction and diffusion of O_2 and CO_2 as well as HCO_3^- and CO_3^{2-} in gas and liquid phases were modeled as shown in Figure 1-2.

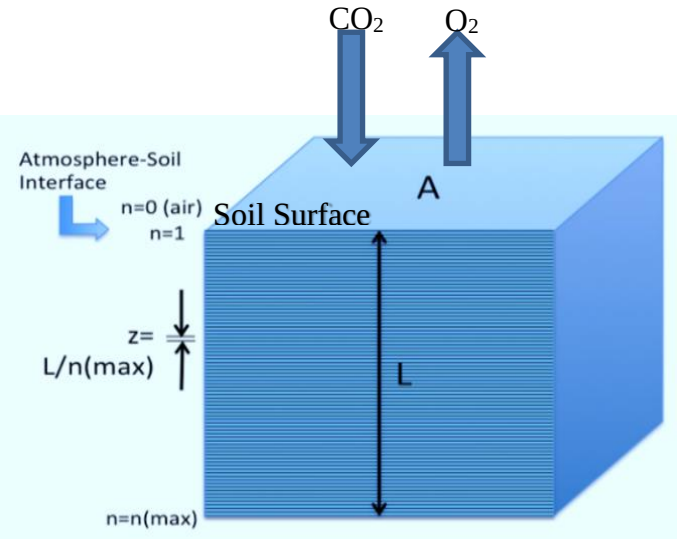

Figure 3-1: 1m^3 homogeneous soil column of 1000 layers with each a thickness of dz.

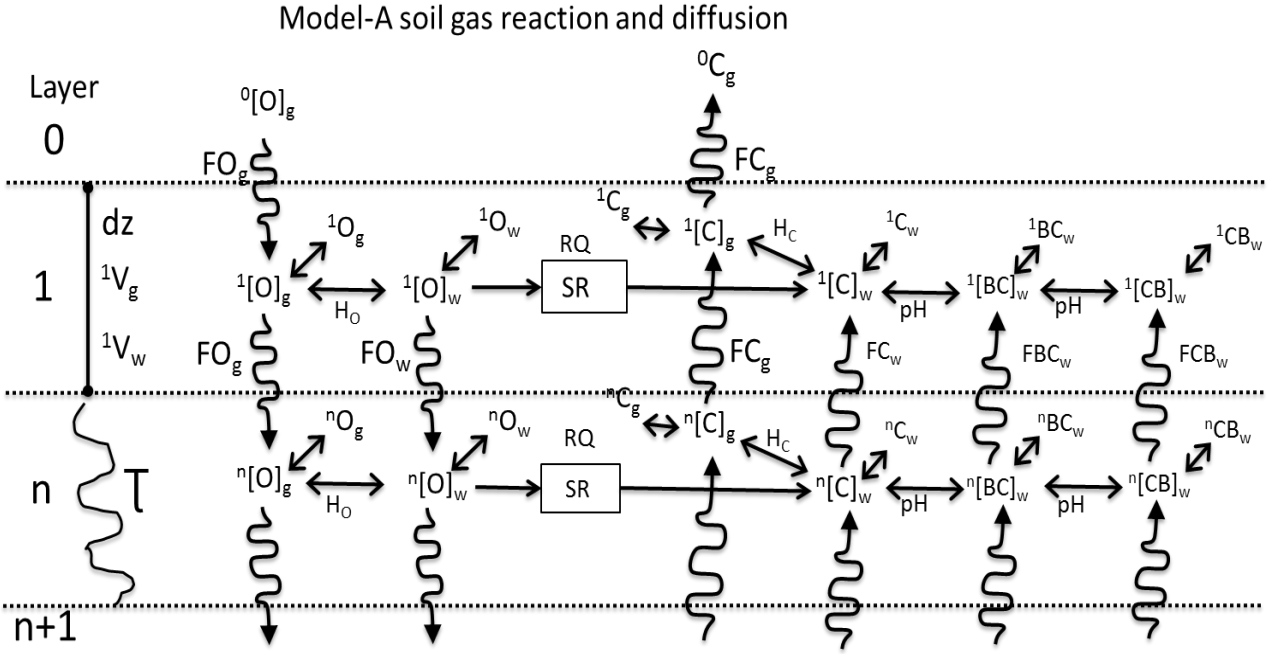

Figure 3-2: Structure of Model-A where [O], [C], [BC], [CB] represents O_2, CO_2, HCO_3^- and CO_3^{2-}concentrations respectively in the gas (g) or water (w) phase in the first two modelled layers of the soil profile shown in Figure 3-1. FO, FC, FBC, FCB are flux of O_2, CO_2, bicarbonate, and carbonate respectively. SR is considered as the main factor that diffuse gas into soil (FO_g) and out of soil (FC_g); while dz, ⊺, V_g, V_w represents layer thickness, the path traveled, fraction of gas and liquid volume in a layer. H_O and H_C corresponds for Henry's solubility constants of O_2 and CO_2, respectively.

For the mass conservation of a species (O_2 and CO_2) in a layer volume, we can write the rate of change of concentration (C) of the gas in terms of its flux gradient (dF/dz) and soil respiration (SR) which is defined as the source or sink term for soil CO_2 and O_2 respectively (Jassal et al., 2005; Šimůnek & Suarez, 1993):

$$\frac{dC}{dt} = -\frac{dF}{dz} + SR \tag{3.1}$$

At steady-state, dC/dt = 0,

$$\frac{dF}{dz} = SR \tag{3.2}$$

The SR is measured either as CO_2 evolution (SR_C, μmol/m^3/s) or O_2 uptake rate (SR_O, μmol/m^3/s) in the soil. Under steady state conditions and in the absence of any external sources and sinks of soil gases, it is expected that total CO_2 production or O_2 consumption rate (due to both biotic and abiotic processes in equilibrium) have a stoichiometric relationship in soil. The ratio of soil CO_2 evolution with O_2 uptake by soil is generally called soil respiratory quotient (RQ),

$$RQ = \frac{SR_C, \quad CO_2 \, evolution}{SR_O, \quad O_2 \, uptake} \tag{3.3}$$

Using equation (3.2), when a equilibrium condition is reached gaseous and liquid phase of soil gases:

$$^{n}F - ^{n+1}F = SR\left(^{n}z - ^{n+1}z\right) \tag{3.4}$$

where ^{n}F and ^{n+1}F are the incoming and outgoing diffusive flux from the n-th layer, and can be defined by Fick's gas diffusion law (Risk et al., 2002):

$$^{n}F = -^{n}D_e \frac{(^{n}C - ^{n+1}C)}{\left(^{n}z - ^{n+1}z\right)} \tag{3.5}$$

where ${}^{n}C$ and ${}^{n+1}C$ are CO_2 (or O_2) concentrations at the n-th and (n+1)-th layer, and ${}^{n}D_e$ is the effective diffusion coefficient (m^2/s) of the gas in soil (details in later section).

For the straight distance between two consecutive layers, Δz, we can write,

$$ {}^{n}F = -{}^{n}D_e \frac{({}^{n}C - {}^{n+1}C)}{\Delta z} \tag{3.6} $$

From the equation (3.6), concentration profiles of CO_2 (and O_2) can be calculated as:

$$ {}^{n+1}C = {}^{n}C + \left(\frac{{}^{n}F \times \Delta z}{{}^{n}D_e} \right) \tag{3.7} $$

The effective diffusivity of a soil gas in gaseous phase is a function of soil air pore space (V_g) and the tortuosity (τ_g), and can be written as (Moldrup et al., 2001):

$$ {}^{n}D_{e,g} = \frac{{}^{n}V_g \times {}^{n}D_g}{\tau_g^2} \tag{3.8a} $$

where τ_g of soil is a dimensionless parameter which can be defined as the ratio of the tortuous path traveled by the gas to apparent path distance. Tortuosity influences the transport of water, solutes, and gases in soil and alters the concentration gradients of soil gases (Moldrup et al., 2001). For simplicity, we assume that tortuosity is constant in the 1 m^3 homogenous soil layers.

Similarly, the effective diffusivity of a soil gas in liquid phase can be written as:

$$ {}^{n}D_{e,w} = \frac{{}^{n}V_w \times {}^{n}D_w}{{}^{n}\tau^2_w} \tag{3.8} $$

The diffusivity of a gas both in gaseous and liquid phase has temperature and pressure dependency as given by (Campbell, 1985):

$$D_g = {}^{ref}D_g \left(\frac{{}^{n}T}{{}^{ref}T} \right)^{\delta} \left(\frac{{}^{ref}P}{{}^{n}P} \right) \quad (3.9a)$$

$$D_w = {}^{ref}D_w \left(\frac{{}^{n}T}{{}^{ref}T} \right)^{\delta} \quad (3.9b)$$

Where, subscript 'g' for gas phase, 'w' for liquid phase; and the empirical value of δ is 2.0 and 1.75 for O_2 and CO_2 respectively in gas phase; and δ is 1.75 both for O_2 and CO_2 in liquid phase as mentioned by Campbell (1985).

Since the diffusivities in gas and water phases are significantly different and have strong correlations with temperature and pressure, corrections were made using the reference diffusivities listed in Table 3-1.

Table 3-1: Reference diffusivities of gases

Species	**Gas phase (m^2/s)**	**Liquid phase (m^2/s)**
O_2	1.77E-05*	2.00E-09*
CO_2	1.39E-05*	2.00E-09*
BC (HCO_3^-)	-	7.02E-10**
CB (CO_3^{2-})	-	5.45E-10**
H_2O	2.18E-05†	
N_2	1.79E-05†	

*† Massman 1998, * Campbell 1985, ** Zeebe 2011*

Soil properties and meteorological conditions are important in regulating soil gas composition, however, it is soil's biotic respiration (SR) considered as the main driving force of O_2 and CO_2 fluxes between soil and air (Oertel et al., 2016). The rate of SR may vary in soil layers depending on the soil temperature and water availability. The estimation

of mean SR is calculated based on its temperature sensitivity given by Lloyd and Taylor (1994):

$$SR(T) = SR_{ref} \times Q_{10}^{\left(\frac{T-T_{ref}}{10}\right)} \quad (3.10)$$

Where, SR_{ref} is soil respiration rate at the reference temperature T_{ref} and Q_{10} is the empirically fitted temperature sensitivity factor that gives the relative change in SR for a 10^{o}C temperature increase (Gaumont-Guay et al., 2006; Lloyd & Taylor, 1994; Qi et al., 2002).

Although research shows that Q_{10} factor may vary for a 1.3 to 3.3 (Lloyd & Taylor, 1994), considering the expected temperature range (20 to 30^{0}C) for our future lab tests, a Q_{10} of 2 was used for our model.

The temperature dependant SR, corresponding to soil temperature profile, was then multiplied with a normalized soil respiration *(S_N)* factor (unit less) at 15% water content V_w (V/V) derived from a water dependent soil respiration relationship found by Yu *et al.*, (2011):

$$S_N = 3.7602 \times V_w + 0.3534 \quad (3.11)$$

The soil respiration as a function of temperature and water content used in our model is:

$$SR(T, w\%) = SR_{ref} \times S_N \times Q_{10}^{\left(\frac{T-T_{ref}}{10}\right)} \quad (3.12)$$

It can be assumed that for longer water retention times in soil, CO_2 (w) and carbonate species will reach equilibrium. The conversion of gaseous CO_2(g) to CO_2(w), and the chemical reactions of CO_2 (w) with H_2O(w) that produce HCO_3^- and CO_3^{2-} are:

$$CO_2\,(g) \leftrightarrow CO_2(w) \quad (3.13)$$

$$CO_2\,(w) + H_2O \leftrightarrow H^+ + HCO_3^- \quad (3.14)$$

$$HCO_3^- \leftrightarrow H^+ + CO_3^{2-} \tag{3.15}$$

For equilibrium reaction (eq. 3.14):

$$[HCO_3] = \frac{K_1 \times [CO_2]}{[H^+]} \frac{mol}{m^3} \tag{3.16}$$

For equilibrium reaction (eq. 3.15):

$$[CO_3^{2-}] = \frac{K_2 \times [HCO_3^-]}{[H^+]} \frac{mol}{m^3} \tag{3.17}$$

At T = 25°C and for pH=6.0,

$$K_1 = 4.6 \times 10^{-7} \frac{mol}{L},\ K_2 = 4.69 \times 10^{-11} \frac{mol}{L}, \text{ and } [H^+] = 10^{-pH} \frac{mol}{L}$$

The acid dissociation constants K_1 and K_2 are calculated from temperature corrected pK_1 and pK_2 for fresh water (with salinity, s=0) based on the equation given by Harned and Jr, (1943).

For the combination of gaseous and aqueous flux of O_2 and CO_2, we can write the equation (3.2) as,

$$\frac{d}{dz}(FO_g + FO_w + FC_g + FC_w + FBC_w + FCB_w) = SR \tag{3.18}$$

where FC, FO, FBC, and FCB stands for CO_2, O_2, Bicarbonate (HCO_3^-), carbonate (CO_3^{2-}) flux, respectively. Integrating for the limit of n-th to (n+1):

$$^n(FO_g + FO_w + FC_g + FC_w + FBC_w + FCB_w) -^{n+1}(FO_g + FO_w \\ FC_g + FC_w + FBC_w + FCB_w) = SR(^n z -^{n+1} z) \tag{3.19a}$$

$$^n(FO_g + FO_w + FC_g + FC_w + FBC_w + FCB_w) -^{n+1}(FO_g + FO_w \\ + FC_g + FC_w + FBC_w + FCB_w) = SR \times \Delta z \tag{3.19b}$$

If the flux of O_2 and CO_2 entering and leaving from a layer (both in gaseous and aqueous phase) is driven by the consumption of O_2 (SR_O) and production of CO_2 (SR_C), we can split the above equation into:

$$^{n}(FO_g + FO_w) - ^{n+1}(FO_g + FO_w) = SR_O \times \Delta z \quad (3.20a)$$

$$^{n}(FC_g + FC_w + FBC_w + FCB_w) - ^{n+1}(FC_g + FC_w + FBC_w + FCB_w) = SR_C \times \Delta z \quad (3.20b)$$

Therefore, for the mass balance of moles in a soil layer, we can write:

$$^{n}FO_g = \frac{^{n+1}[FO_g \times V_g + FO_w \times V_w] + ^{n}[SR_O \times \Delta z - FO_w \times V_w]}{^{n}V_g} \quad (3.21a)$$

$$^{n}FC_g = \frac{^{n+1}[FC_g \times V_g + (FC_w + FBC_w + FCB_w)V_w] + ^{n}[SR_C \times \Delta z - (FC_w + FBC_w + FCB_w)V_w]}{^{n}V_g} \quad (3.21b)$$

where V_t, V_g and V_w are for the total, fractional air and water content; SR_O and SR_C for soil respiration as O_2 consumption and CO_2 production rates.

The fluxes of O_2 and CO_2 in liquid phase in equation (3.21 a and b) were derived from concentration gradients which were calculated assuming equilibrium condition with gas phase using their solubility constants. The temperature dependent solubility constants were corrected by the following relationship:

$$H_O = h_1 T^3 + h_2 T^2 + h_3 T \quad \text{(dimensionless)} \quad (3.22a)$$

$$H_C = \frac{1370}{Exp(h_4 + \frac{h_5}{^{n}T} - \frac{h_6}{^{n}T^2} bar)} \quad \text{(dimensionless)} \quad (3.22b)$$

where h_1, h_2, h_3 are coefficients for temperature dependent O_2 solubility in water, H_O, (Tromans et al., 1998) and h_4, h_5, h_6 are coefficients for temperature dependent CO_2 solubility in water, H_C, (Crovetto, 1991).

The flux of HCO_3^- and CO_3^{2-} in equation (3.21 a and b) were calculated from their concentrations at equilibrium reactions using Fick's law:

$$^nFBC_w = -^nD_{HCO_3^-}\frac{^n[HCO_3^-] - ^{n+1}[HCO_3^-]}{\Delta z} \quad (3.23a)$$

$$^nFCB_w = -^nD_{CO_3^{2-}}\frac{^n[CO_3^{2-}] - ^{n+1}[CO_3^{2-}]}{\Delta z} \quad (3.23b)$$

where the diffusion coefficients of $D_{HCO_3^-}$ and $D_{CO_3^{2-}}$ are estimated from their relationship with temperature as given by Zee be (2011):

$$D_i = {}^{ref}D_i\left[\frac{T}{T_{ref}} - 1\right]^{\delta_i} \quad (3.24)$$

with $^{ref}D_i$ as the reference diffusivities (Table 3-1), with empirical parameter δ_i of 2.39 and 2.19 for HCO_3^- and CO_3^{2-} respectively.

Equations (3.21 a and b) are used to estimate the diffusive fluxes of O_2 and CO_2 (corrected for their temperature and water dependency). These inputs are then used in the equation (3.7) to calculate the concentration profiles of O_2 and CO_2 across the soil depth. The boundary conditions set to solve equation (3.8) are:

At soil surface, n = 0^{th} layer,

$^0[O_2]$ = 20.90%, $^0[CO_2]$ = 0.04%, $^0[N_2]$ = 78.10%, $^0[Ar]$ = 0.96%

^{0}T = 290.19 K, and $^{0}P_{atm}$ = 89,000 Pa.

The concentration gradients of CO_{2w}, HCO_3^- and CO_3^{2-} over the 100 cm depth of the soil column were estimated from the model simulation to analyze their role in aqueous phase in enhancing diffusive flux of CO_2 from soil to atmosphere. Further, a unique parameter is introduced in this dissertation as the Gas Concentration Ratio (GCR) and calculated as the ratio of differential concentrations (ΔCO_2 and ΔO_2) at the n-th layer with respect to ambient air (at 0^{th} layer) as:

$$GCR = \left| \frac{^{0}[CO_2] - ^{n}[CO_2]}{^{0}[O_2] - ^{n}[O_2]} \right| \tag{3.25}$$

The GCR values are then used to compare the individual contribution from soil properties (w%, pH, and RQ) on the transport of gases in near-surface soils.

3.3.2 Model-B: Diffusion, Reaction, and Mass flow Model for Gas Phase

The fluctuation of atmospheric or soil air pressure may affect the total gas exchange mechanism in near-surface soil. This fluctuation of total pressure may arise from the barometric temperature, wind flow or humidity changes. For example, the chinook events that are observed in Calgary and surrounding areas during the period of October to March every year, can lead to a sharp change in barometric pressure from the combination of strong wind flows (>16 km/hour), sudden increase of temperature higher than normal daily mean, and a substantial decrease in relative humidity (Schieman et al., 2009). In addition to the abrupt barometric pressure changes a small bulk soil air pressure difference may

arise from the difference of diffusivities of counter fluxes (O_2 from atmosphere to soil and CO_2 from soil to atmosphere) and from the unequal rate of CO_2 evolution and O_2 uptake in soils. The arise of bulk pressure difference may lead to mass flow of soil air and affect the total gas exchange at the atmospheric boundary (Kayler et al., 2009). Therefore, Model-A was modified to consider the mass flow (MF) of soil air due to possible bulk pressure differences between the soil and atmosphere or simply between the layers in soil, as well as its feedback on the components of soil air.

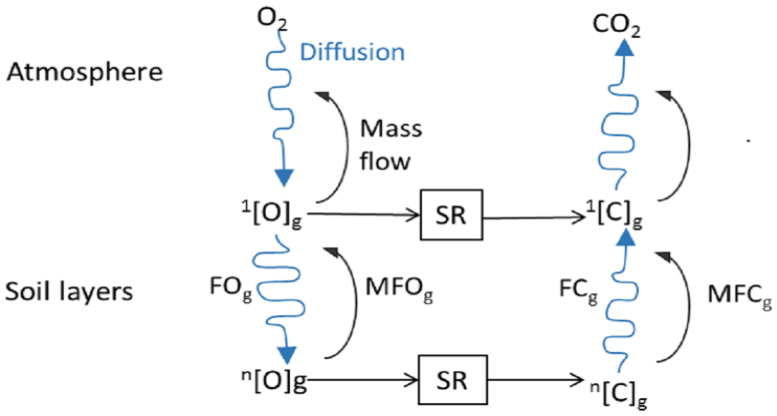

Figure 3-3: 1D steady-state gas flow model with diffusion and mass flow in the gas phase. Here MFOg, MFCg are the share of oxygen and CO_2 in soil air mass flows respectively.

For the presence of bulk pressure gradients between layers, total flux of a gas into or out of the soil will be the combination of its diffusive flux (due to partial pressure gradient, derived from Fick's law) and mass flow (due to total pressure gradient, derived from Darcy's law) (Ball, 1981; Lewicki et al., 2007):

$$F_i = F_i^{DF} + (F_i^{MF} \times f_i) \tag{3.26}$$

$$F_i = -D_i \frac{\partial C_i}{\partial z} - \left(\frac{P}{RT} \frac{K}{\mu} \frac{\partial P}{\partial z} \right) \times f_i \text{ mol/m}^2\text{/s} \tag{3.27}$$

where *'i'* stands for the corresponding soil gas (e.g. O_2 or CO_2), C_i and f_i are concentration and fractional concentration of the *i-th* gas, K is the intrinsic permeability of soil air (m^2), μ is dynamic viscosity of soil air (Pa × Sec). This equation can be rearranged using the partial pressure of the gas and the total soil air pressure gradients:

$$F_i = -\frac{D_i}{RT} \frac{\partial p_i}{\partial z} + \left(\frac{p_i}{RT} \frac{K}{\mu} \frac{\partial P}{\partial z} \right) \text{mol/m}^2\text{/s} \tag{3.28}$$

The air permeability of soil (K) is a critical parameter for pressure driven flow in porous media and is strongly related to soil porosity and pore size distribution. It was estimated by equating the Darcy's law of gas viscous flow through a soil filled tube and Poiseuille's law for viscous flow of gases through 'n' parallel tubes of equal radius 'r' as described by Ball *et al* (1981):

$$K = \frac{r^2 \Phi}{8\tau^2} \text{ m}^2 \tag{3.29}$$

where Φ is the total porosity of the soil (fractional volume of air and water content in soil); the tube radius 'r' is assumed here as analogous to the average pore radius in soil and estimated for a typical soil ('Sandy Loam') with the texture characteristics given in Table 3-2:

Table 3-2: Particle size distribution of typical 'Sandyloam soil'.

Soil Type	**'Sandyloam Soil'‡**		
compositions	*clay*	*sand*	*silts*
Fraction of particles	0.19	0.60	0.21
particle diameter(mm)	1.50×10^{-3}	1.75×10^{-1}	2×10^{-2}

‡(USDA, 1993)

From the fractional concentration and particle size distribution, we estimate the average particle diameter of 'Sandyloam soil' as 0.11 mm.

We also assume that the soil composition, compaction, particle and pore distribution are completely homogeneous. Having this homogeneity, if 70% of the total volume is occupied by solid particles and the rest of the volume (30%) is porous (including both gas and liquid percentage), then for cross-sectional area of any soil layer we can write:

$$\frac{particle\ cross\,section\ area}{pore\ cross\,section\ area} = \frac{70\%}{30\%} \tag{3.30}$$

From this assumption, we get average pore diameter of 'SandyLoam Soil' as 71×10^{-6} m. The dynamic viscosity μ has temperature dependence which was corrected with Sutherland's law (White, 1991):

$$\frac{\mu}{\mu_{ref}} \approx \left(\frac{T}{T_{ref}}\right)^{3/2} \frac{T_{ref}+S}{T+S} \tag{3.31}$$

where S is an effective temperature (in Kelvin), called the Sutherland constant, and is characteristic of the gas. The value of S is 111(K) for air.

The concentration gradients of O_2 and CO_2 along the soil depth were calculated for a range of soil properties. This includes water content (w%) of 17 to 21% of the total soil volume, pH of 6.4 to 7.4, respiratory quotient (RQ) of 0.7 to 1.2, and soil respiration (SR) rate of 2 to 6 $\mu molCO_2/m^2/s$. The temperature 17^oC and SR were assumed to be constant throughout the column. These soil properties represent the characteristics of Calgary soil. For example, for the month of July 2012, the average soil water content was recorded between 17 to 21%, and the average max temperature was recorded as 17^oC in soil (up to 100cm depth) at Airdrie weather station (ACIS, 2012).

Initially, the concentration profiles of O_2 and CO_2 and their differential ratios (GCR) at different soil depths were calculated from Model-A for a variation in soil properties. Later, a range of CO_2 leaks (based on the possible storage size and an arbitrarily chosen soil surface area) in the gas phase were added at 1m depth (1000-th layer) of Model-B to simulate the invasion of escaped CO_2 in near-surface soil. For addition of CO_2 at 1m depth as representative of CO_2 escaped from underground storage, we considered only the possible small scale leak scenarios that are around, or below, the acceptable leakage of an economical large storage site reported by Haefeli et al (2004), Milles et al (2005), Keeling et al (2011). For example, based on these reports, a leak of 0.01% - 0.03% of total CO_2 per year from the total storage of 100 $MtCO_2$ spanning over an area of radius 300 m, can create an efflux of about 25 $\mu molCO_2/m^2/s$ (Miles et al., 2005). This flux can be compared to the typical range in soil flux of 0.2 – 8 $\mu molCO_2/m^2/s$ (Leuning et al., 2008).

For the addition of leak flux (F_{leak}, $\mu mol/m^2/s$), the total number of moles of CO_2 in the volume of 1000-th layer (at 1m depth) will be the sum of moles driven by the diffusive flux, the fraction of CO_2 driven by mass flow, and the moles of pure CO_2 added

from the leak flux. The sum of total CO_2 moles gives the total flux of CO_2 at the 1000-th layer as:

$$^{1000}F_{CO_2} = {}^{1000}F_{CO_2}^{DF} + F_{CO_2}^{MF} + F_{leak} \tag{3.32}$$

The concentration profiles (Equation 3.7) and the GCR values (Equation 3.25) from Model-B for leak added conditions were compared to that found from Model-A for normal conditions to distinguish CO_2 leaks.

3.4 Results

3.4.1 Model-A Sensitivity Tests

Sensitivity tests of Model-A for soil properties (RQ, w%, and pH) for multiple phase (gaseous and liquid) and single phase diffusion and reactions are quantified in Table 3-3.

These tests show that soil RQ, as expected, is the key factor that drives the concentration gradients across the soil layers, followed by soil water content (w%) and the pH level of soil water respectively. For example, RQ of 0.70 to 1.20 results in GCR values of about 0.90 for any pH level between 6.4 to 8.4 and water content between 17 to 21%. We also find that the GCR values predicted by the model do not depend on soil depths; the ratio of the mixing ratio differentials ΔO_2 and ΔCO_2 (w.r.t to ambient air) would be the same regardless of whether they were measured at 1cm or 100 cm below the surface.

Although an increase of water content from 17 to 21% can increase the concentration differentials of O_2 and CO_2, the GCR value remains constant. This is because the increase of soil water content stimulates soil biological activities, which produces higher consumption of O_2 and production of CO_2. Soils in Calgary are not expected to have

pH values higher than 8.4, however, an extreme case of pH 9.4 was also tested here. It shows that at pH 9.4, the ΔCO_2 decreases at both depth while ΔO_2 remains the same (or with minor changes, Table 3-3). The lower GCR values observed in Table 3-3 for pH 9.4 are because higher diffusive fluxes of HCO_3^- and CO_3^{2} in soil water combined with high pH facilitate CO_2 diffusion from the soil to the atmosphere.

Table 3-3: Factors affecting GCR in soil. This table shows model predictions at SR (at reference temp) equal to 4.65µmol/m^2/s and for both gas and liquid phase diffusion.

Soil Properties				**Between 0 – 1 cm depth**			**Between 0 – 100 cm depth**		
RQ	*pH*	*W%*	*Air%*	*ΔO_{2g}*	*ΔCO_{2g}*	*GCR*	*ΔO_{2g}*	*ΔCO_{2g}*	*GCR*
-	-	*V/V*	*V/V*	*mol/m^3*	*mol/m^3*	-	*mol/m^3*	*mol/m^3*	-
0.70	6.4	17%	13%	0.033	0.30	0.907	1.655	1.501	0.907
	7.4	17%	13%	0.033	0.030	0.906	1.655	1.499	0.906
	8.4	17%	13%	0.033	0.033	0.899	1.655	1.488	0.899
	9.4	17%	13%	0.033	0.027	0.830	1.652	1.371	0.830
	6.4	21%	9%	0.054	0.049	0.907	2.709	2.456	0.907
1.0	6.4	17%	13%	0.023	0.030	1.283	1.168	1.499	1.283
	7.4	17%	13%	0.023	0.030	1.282	1.168	1.498	1.282
	8.4	17%	13%	0.023	0.030	1.272	1.168	1.486	1.272
	9.4	17%	13%	0.023	0.027	1.176	1.165	1.370	1.176
	6.4	21%	9%	0.038	0.049	1.283	1.912	2.453	1.283
1.2	6.4	17%	13%	0.019	0.030	1.530	0.979	1.499	1.530
	7.4	17%	13%	0.019	0.030	1.529	0.979	1.498	1.529
	8.4	17%	13%	0.019	0.030	1.518	0.979	1.486	1.518
	9.4	17%	13%	0.019	0.027	1.403	0.976	1.370	1.403
	6.4	21%	9%	0.032	0.049	1.530	1.603	2.452	1.530

These sensitivity tests for Model-A confirm that the concentration gradients of O_2 and CO_2 in soil are mainly regulated by the soil RQ, which leads to a linear relationship

with the expected ratio in concentration gradients (GCR). It also shows that the facilitated diffusion in liquid phase can only be considerable for high pH (e.g. pH 9.4).

3.4.2 Model-A Soil Gas Profiles

The profiles of O_2 and CO_2 in soils were simulated from Model-A for different soil water content with the same RQ and pH value (Figure 1-4). It can be seen that the contribution of liquid phase diffusion (from HCO_3^- and CO_3^{2-}) under both soil water conditions are negligible. However, to quantify the individual role of HCO_3^- and CO_3^{2-} in driving CO_2 diffusion faster (facilitated diffusion), concentration gradients and their fluxes were analyzed for a change in soil properties (Figure 1-5 to Figure 1-7).

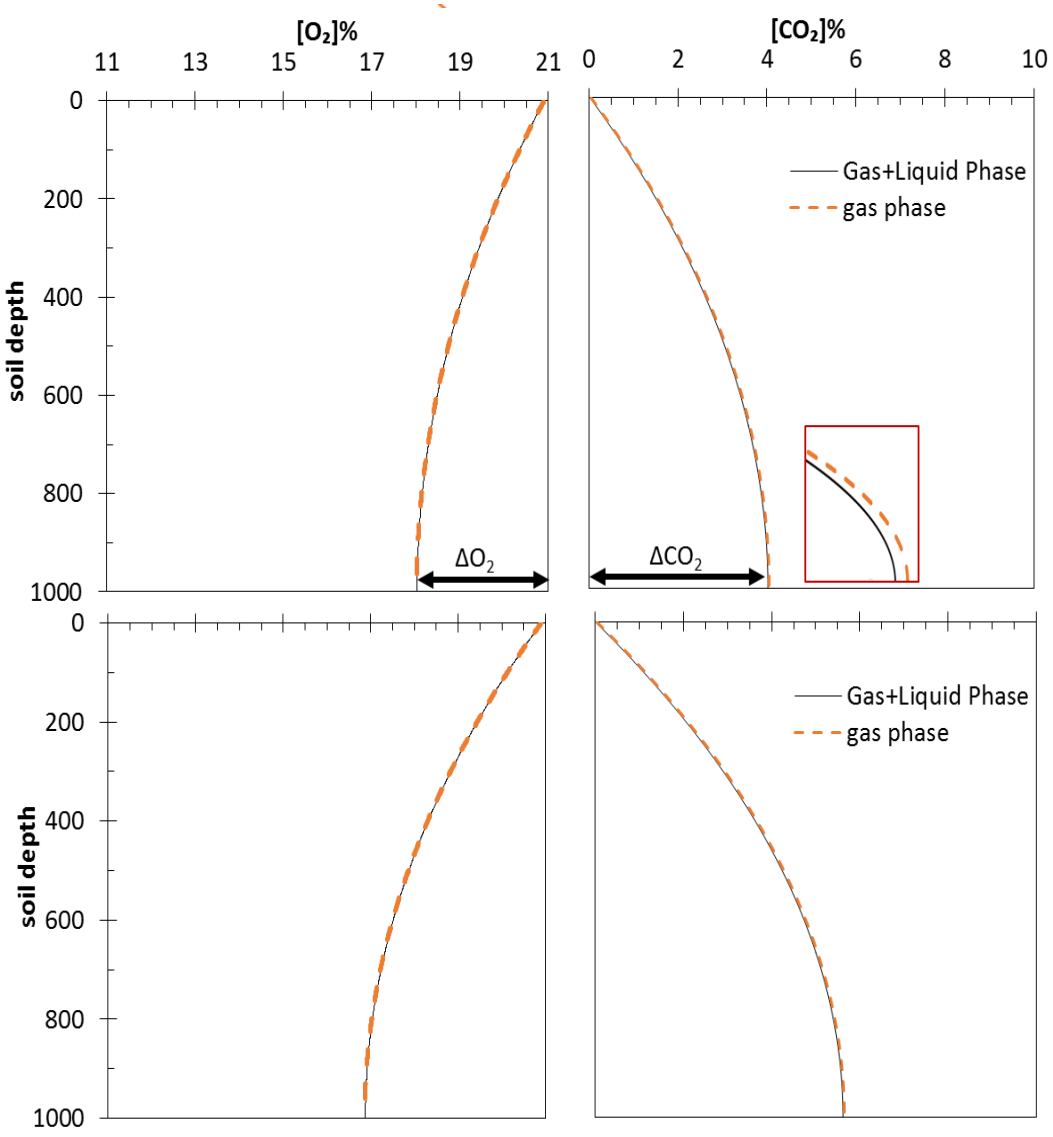

Figure 3-4: Model-A predictions for O_2 and CO_2 concentration (%) profiles in soil when gases diffusion occurs by gaseous and liquid phases for a soil RQ of 1.2. It is assumed that CO_2 diffusion in soil is being facilitated by HCO_3^- and CO_3^{2-} diffusion in soil water for a pH 6.4. Top panel and Lower panel corresponds to soil with gas and water porosities at (13% and 17%) and (21% and 9%), respectively. Inset shows the facilitated diffusion at depth near 80cm and below.

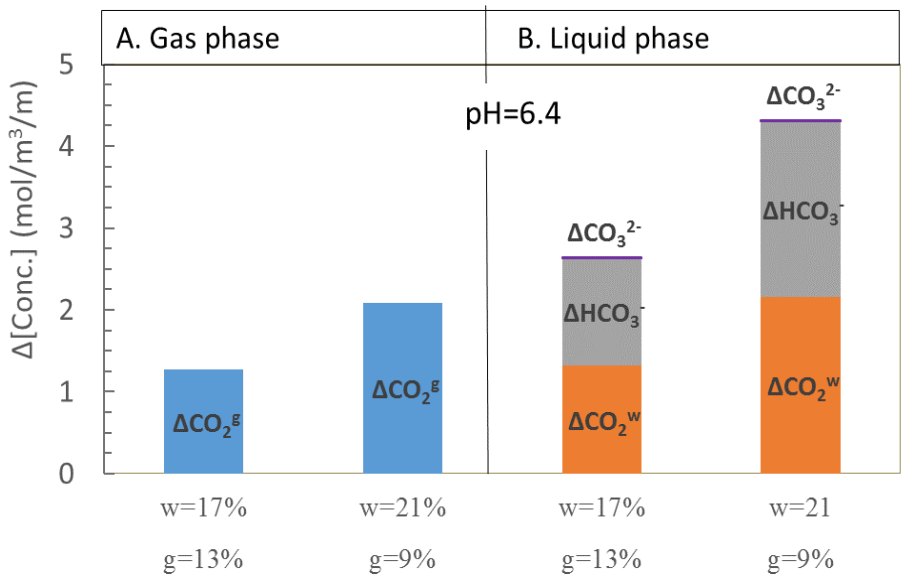

Figure 3-5: (A – B) Gradients of $[CO_2]_g$, $[CO_2]_w$, $[HCO_3^-]$ and $[CO_3^{2-}]$ for water content (17 to 21%) at pH 6.4

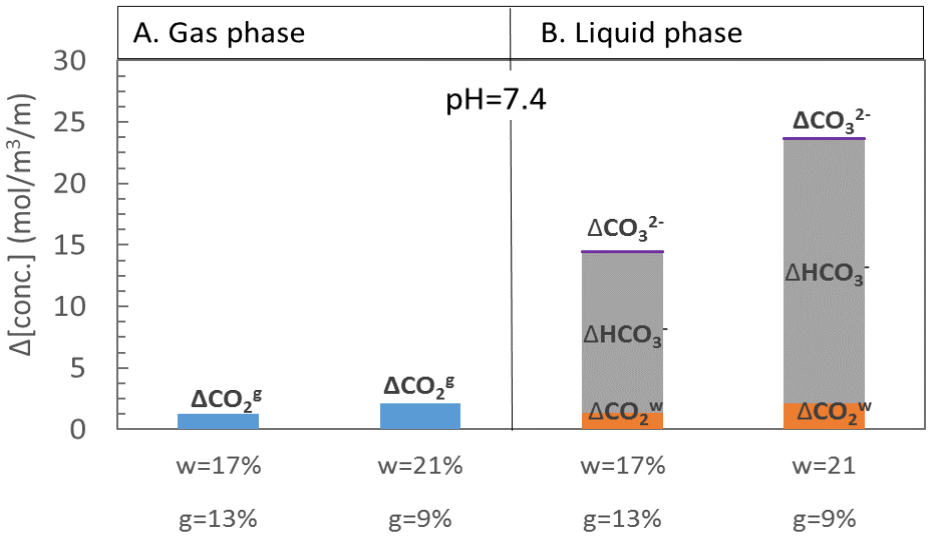

Figure 3-6: (A – B) Gradients of [CO2]g, [CO2]w, [HCO3-] and $[CO_3^{2-}]$ for water content (17 to 21%) at pH 7.4.

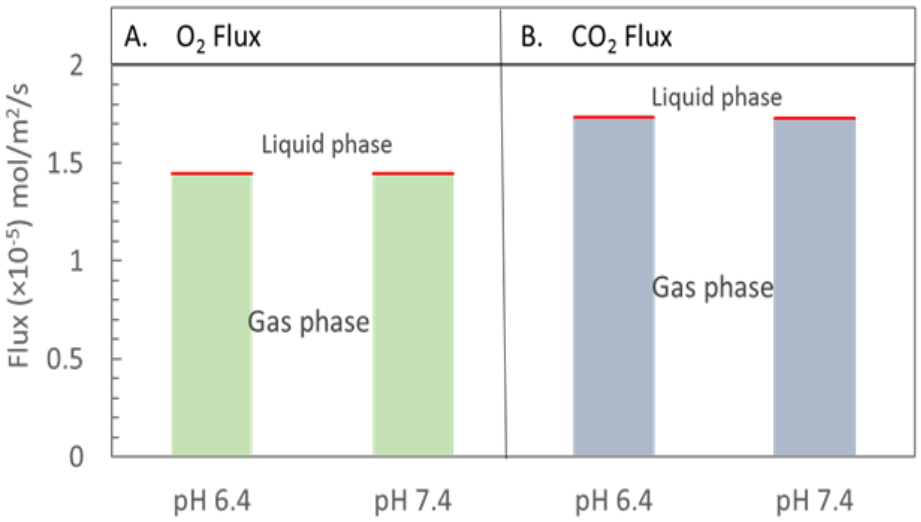

Figure 3-7: (A – B) Fluxes of O_2 and CO_2 molecules diffusing into and out of soil for an increase of pH 6.4 to 7.4 (at 17% water content).

In addition to the initial model simulations for a wide range of soil properties, the effect on the concentration gradients of HCO_3^- and CO_3^{2-} and their contribution in diffusing CO_2 out from soil were also analyzed. Model-A predictions show that at any pH level an increase of soil water content (17 to 21%) produces a negligible gradient of $[CO_2]g$ (Figure 1-5A & Figure 1-6A), and small gradients of $[CO_2]_w$, $[HCO_3^-]$, and $[CO_3^{2-}]$ in water phase along the 1m depth (Figure 1-5B & Figure 1-6B). Contrary to this, Model-A predicts that an increase of pH from 6.4 to 7.4 (for the same water content) causes 10-fold higher gradients in $[HCO_3^-]$ and $[CO_3^{2-}]$ (Figure 1-5B & Figure 1-6B) while gas phase $[CO_2]_g$ gradients were not affected by the pH change (Figure 1-5A & Figure 1-6A).

Despite the observed increases in the gradients of HCO_3^- and CO_3^{2-} at higher pH, estimated fluxes (Figure 1-7) show that more than 99% of total O_2 and CO_2 diffusion in

soil occurs within the gas phase; water phase diffusion accounts for a very small proportion. The 1.2-fold higher CO_2 flux than O_2 flux in soil is due to the assumed soil biological respiratory quotient (RQ = CO_2 production rate / O_2 consumption rate). However, even at higher pH, CO_2 flux in the water phase accounted for only 0.08% of total CO_2 diffusion (Figure 1-7B). The negligible role for facilitated diffusion by bicarbonate and carbonate was due to the difference of the effective diffusion coefficient of CO_2 in gas and in water.

3.4.3 Model-B: Soil Gas Profiles and CO_2 leak Detection

Model-B simulations are given in Figure 1-8 where the upper panel (A1 to A4) provides results for variations in soil RQ 0.7 to 1.2 without any CO_2 leak, and the lower panel (B1 to B4) provides results for different CO_2 leak rates (2 – 10 μmol/m^2/s) at RQ of 1.2. Model-B simulations use soil properties of 2 μmolO_2/m^2/s for SR_O, and 17% volumetric water content with 13% air porosity.

As expected, regular soils with a range of RQ (0.7 to 1.2) reflects the characteristic profiles of O_2 and CO_2 at the soil surface and across 1m depth. For the high CO_2 production rate (against constant O_2 uptake at constant RQ), the CO_2 profiles below the surface will reach higher levels but may not lead to any distinction near the surface (Figure 1-8 A2). The GCR and MF values, on the other hand, have a common unique feature of increased values at the surface; both of these reflect the increase of CO_2 production rates. Between these two the GCR remains constant along the depth for constant RQ and CO_2 production, while MF% decreases with depth. Also, at higher RQ values, the model predicted an increased role for mass flow (MF) in bringing soil air to the surface of the column (Figure

1-8 A4). The most important factor is that both GCR and MF values lie within a certain range that could be used as characteristic of native soils with known properties. For example, for an RQ of 0.7 to 1.2 at constant O_2 consumption of 2 μmol/m^2/s, the GCR and the MF at the soil surface ranges about 0.9 to 1.50 and -0.19% to 1.09% respectively; both should be distinguishable from air even at the soil surface (Figure 1-8 A3 to A4).

When the model was used to simulate CO_2 leaks into layer 1000 of soils having a set RQ of 1.2, much larger gradients were predicted throughout the soil profile (Figure 1-8 B2) even when the CO_2 leak rate was similar or 2 to 5 times higher than the biological flux of CO_2 in soil of 2 μmol/m^2/s. But, this increase of the soil CO_2 concentrations due to addition of leaked CO_2 would not be noticeable at the surface or layers immediately below and requires more measurements at deeper depths. The values of GCR (ΔCO_2: ΔO_2) (Figure 1-8 B3) and the contribution of mass flow to CO_2 flux (MF%) (Figure 1-8 B4), on the other hand, would be very different from the values that were modeled in the absence of a CO_2 leak (Figure 1-8 A3, A4) and would be informative distinguishing the sources of CO_2.

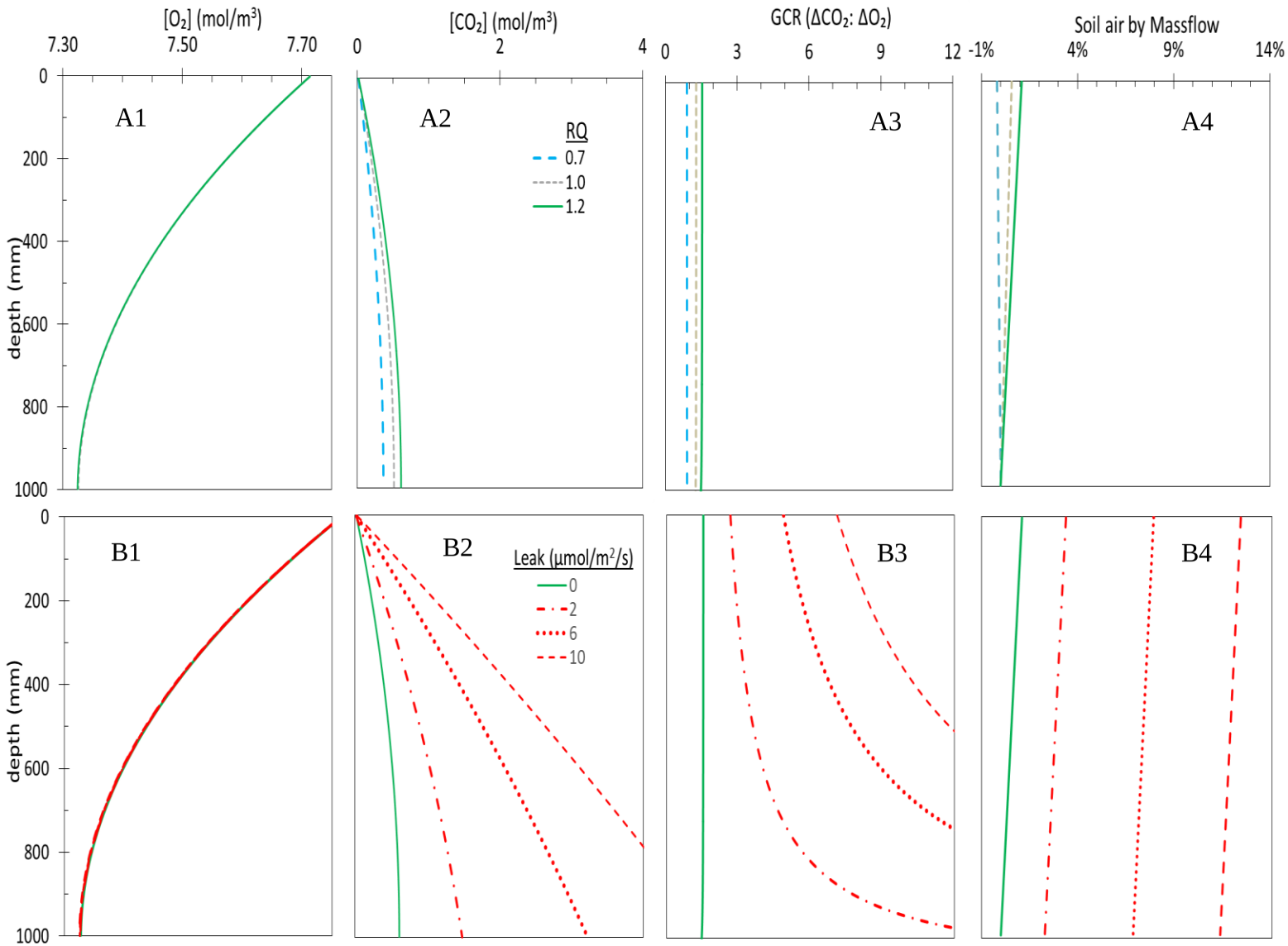

Figure 3-8: The effects of respiratory quotient (RQ; A1-A4) and CO_2 leaks (B1-B4) on concentration gradients for O_2 (A1, B1) and CO_2 (A2, B2), the predicted GCR relative to bulk air (A3, B3) and the proportion of soil air movement through the soil driven by mass flow (MF) rather than diffusion (A4, B4). The RQ effects assumed with no leak, and the leak models were done at an RQ of 1.2

3.5 Discussion

From simulations of Model-A for different soil w% and pH levels (Figure 1-5 to Figure 1-7), we find that facilitated diffusion of CO_2 by the carbonate species in regular soil (with normal soil temperature, w% and pH level) is negligible compared with the magnitude of the gaseous CO_2 flux from the soil. This confirms that gas exchange between normal soil and atmosphere mainly occurs in the gas phase. However, more studies are required when soils have high water contents or water saturated soil.

Simulations of Model-B (Figure 1-8) for differential gas concentration ratio GCR (w.r.t. to bulk air) shows that GCR can be used to distinguish an invading CO_2 leak compared to CO_2 from biological activities. The GCR at the soil surface will shift towards higher values than background for the addition of pure CO_2 ($\geq$2 $\mu mol/m^2/s$) at depths near the surface. This result highlights the potential of our model for detection and quantification of CO_2 leaks from belowground by analyzing the unique GCR values at the soil surface (knowing the existing properties of the soil). The detection sensitivity of the model, further, will be enhanced by the measurement of the fraction of soil air driven by the total pressure (MF), as this will increase significantly with the incremental CO_2 leak at soil depths. For example the percentage of soil air driven out from the soil will increase from about 3 to 13% for an increase in a CO_2 leak from 2 to 10 $\mu mol/m^2/s$ at soil depth.

In the next chapter a series of gas analysis systems (GAS-1, 2, and 3) were developed to test the feasibility of using our Model-B (gas diffusion, reaction and mass flow model) for detecting sequestrated CO_2 leaks.

Chapter 4. **Feasibility test in controlled setup**

4.1 Introduction

Monitoring CO_2 leaks to the atmosphere from a Carbon Capture and Storage (CCS) site should be reflected as an elevated surface level flux of CO_2, a process that can be measured using an infra-red gas analyzer integrated with measurement chambers (e.g. Licor Model 8100A). However, such instruments are expensive and they take a significant amount of time to obtain a measurement. Moreover, CCS leaks resulting in flux rates of less than 10 μmoles/m^2/sec could be difficult to differentiate from background levels of soil respiration, a process that also results in CO_2 flux to the atmosphere.

A cost-effective technology is needed that can rapidly sample the CO_2 that is present at the soil surface and determine whether it has originated from natural soil processes, or from a CCS leak. The ability to detect low fluxes of CO_2 from CCS sites would be particularly useful in allowing rapid remediation of the leak and to avoid possible environmental and health impacts from larger CCS leaks.

In a previous chapter, we proposed that simultaneous measurements of O_2 and CO_2 concentration gradients between the soil surface and bulk air (i.e. the Gas Concentration Ratio, GCR) should provide a rapid, cost-effective assessment of the relative contribution to the CO_2 leaving soil that comes from natural soil processes versus a CCS leak. This is because natural soil processes leading to CO_2 production are also associated with O_2 uptake and reduction in O_2 concentration, whereas a CCS leak of pure CO_2 would only impact O_2 concentration by volumetric dilution.

To explore this proposal, a detailed numerical model was created to describe CO_2 and O_2 reaction, diffusion and mass flow in soils having a wide range of bio-physical properties (including temperature, water content, porosity and respiratory quotient). For a given set of bio-physical soil properties, with or without a CO_2 leak, the model was able to predict the concentration gradients of O_2 and CO_2 into the soil and the resulting GCR.

The purpose of the current study was to test the model developed previously using a column of soil upon which measurements can be made to characterize the properties of the soil being studied, the gradients of CO_2 and O_2 and the GCR in the absence and presence of a simulated CO_2 leak. We hope to use the insights gained from this work to design a new instrument for the early detection of CO_2 leaks from CCS sites.

4.2 Methods

A soil column and two Gas Analysis Systems (GAS-1 and GAS-2) were built to allow measurements (with or without a simulated CO_2 leak) of the gradients of CO_2 and O_2 concentration within the soil column (GAS-1), the fluxes of CO_2 and O_2 at the soil surface, and the differential gas concentration ratio (GCR) of ΔCO_2: ΔO_2 between the soil surface and bulk air (GAS-2).

4.2.1 The soil column

A cylinder of acrylic (103.3 cm long, 10 cm ID, 0.7 cm wall thickness) was fitted with a sintered glass disk (with 93 mm diameter X 8 mm thick with pore size of 4-8 μm, model 7176-166, ACE Glass Inc.) positioned 2 cm from the bottom of the cylinder with a second

cylinder (2 cm long, 9 cm ID, 0.7 cm wall thickness) to create a chamber with a volume of 124±13 cm^3 (Figure 1-1).

The column was machined to allow the placement of 1/8" NPT 1/4" Swagelok fittings at approximately 2, 25, 50, 75, 98, and 102 cm from the top of the soil in the column. The ferrules in the fittings were replaced with silicone septa (5 mm OD X 3.2 mm, Norwesco Industries Ltd.) to allow a syringe to be used to remove gases from locations throughout the soil chamber (Figure 1-1). Additional 1/16" NPT to 1/8" Swagelok fittings was also used to provide access to the lower chamber (i.e. at 102 cm from the top of the soil column) to allow the injection of pure CO_2 using a high precision mass flow controller (range 0–1 ml/min, Model no. 32915-74, Cole–Parmer Instrument Company).

A cap for the top of the column was made from a 0.64 cm thick acrylic sheet glued to a 1.3 cm long cylinder having an ID of 11.5 cm so it could slide over the top of the column (Figure 4-2). Three ports were created in the acrylic sheet and threaded to hold 1/8" NPT X 1/4" Swagelok fittings that were used to create a 122±8 cm^3 headspace at the top of the column. Two of these ports were connected with tubes that carried gases into and out of the top headspace, and another port was used to measure the pressure within the closed soil chamber using a highly sensitive pressure transducer (Range 0 – 25 Pa, Model no. PX653-0.1D5V, Omega Environmental Inc.).

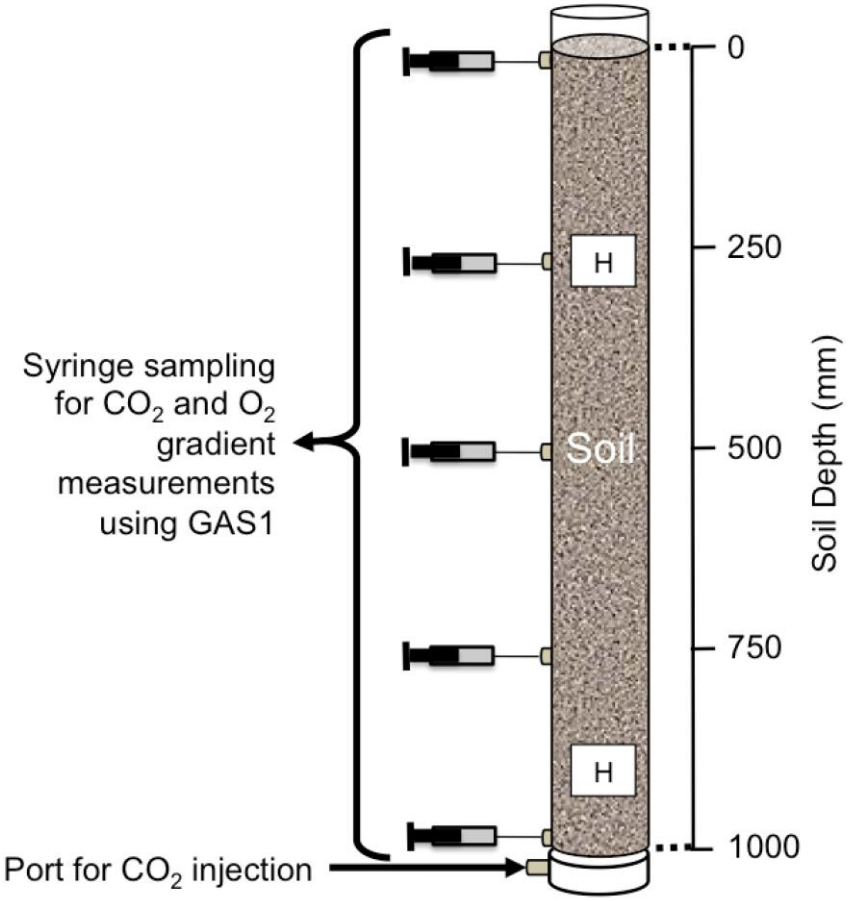

Figure 4-1: Soil column with surface open to air showing the five sample ports (at 2, 25, 50, 75 and 98 cm depth) that were used for the measurement of the CO_2 and O_2 concentration gradients. H, approximate location of the humidity sensors.

The column was filled with 1000 mm of sieved (<2 mm diameter) well-mixed soils collected from the campus of the University of Calgary, Calgary, AB. Soil-A was collected under grass while Soil-B was collected from a community garden. Table 4-1 provides details on the soil properties as determined by the 'manipulative test' (FAO, 2017). It

shows that textures of these two soils are slightly different to each other as SOIL-A was found as “Loamy Sand” and SOIL-B as “Sandy Loam”.

Table 4-1: Texture class of the soils used in the experiments

Soil Sample	Location of the samples (UTM)	Measured Bulk Density (gm/cm^3)	Measured Texture Class	Relative texture (%)		
				Sand	*silt*	*Clay*
SOIL-A	11 U 701095 5662547	1.48±0.07	“Loamy Sand”	70 – 86	0 – 30	0 – 15
SOIL-B	11 U 700373 5662148	1.32±0.06	“Sandy Loam”	50 – 70	0 – 50	0 – 20

Distilled water (DW) was added to the soil to achieve a water content of 15-20% (V/V) and the soil was mixed to homogeneity before placing it in the chamber. Two resistance humidity sensors (dimensions 8.9 X 1.8 X 0.7 cm) were buried in the soil at about 25 cm and 90 cm depth and used to monitor soil water content (V/V) during the experiments. As described below, the pressure measurement approach was used to measure the volumetric gas content within the soils which was found about 25 – 30% (V/V) (Section 4.2.1.1).

4.2.1.1 Soil Air Porosity (V/V) measurement with pressure method

The porosity (V/V) of the soil in the column was measured using a volume-pressure technique similar to Annan et al., (1989). The soil column was capped and connected to a

1L Mason jar, a differential pressure sensor (Range 0 – 100 kPa, Model. MPXV5100DP, Freescale Semiconductor Inc.), and a 3-way valve through a Teflon tubing (vol. of 10 ml) as shown in Figure 1-2.

In this technique a Mason jar volume was taken as reference volume (V_r) and the pressure inside it was increased by injecting air with a 60 ml syringe through the septa, while the soil column was open to atmospheric pressure (P_s) for the valve in position 1. By moving the valve to position 2, air from the compressed jar was allowed to expand to the soil column (Figure 1-2). The pressure inside the jar before (P_r) and after allowing the air expansion were recorded with the differential pressure sensor.

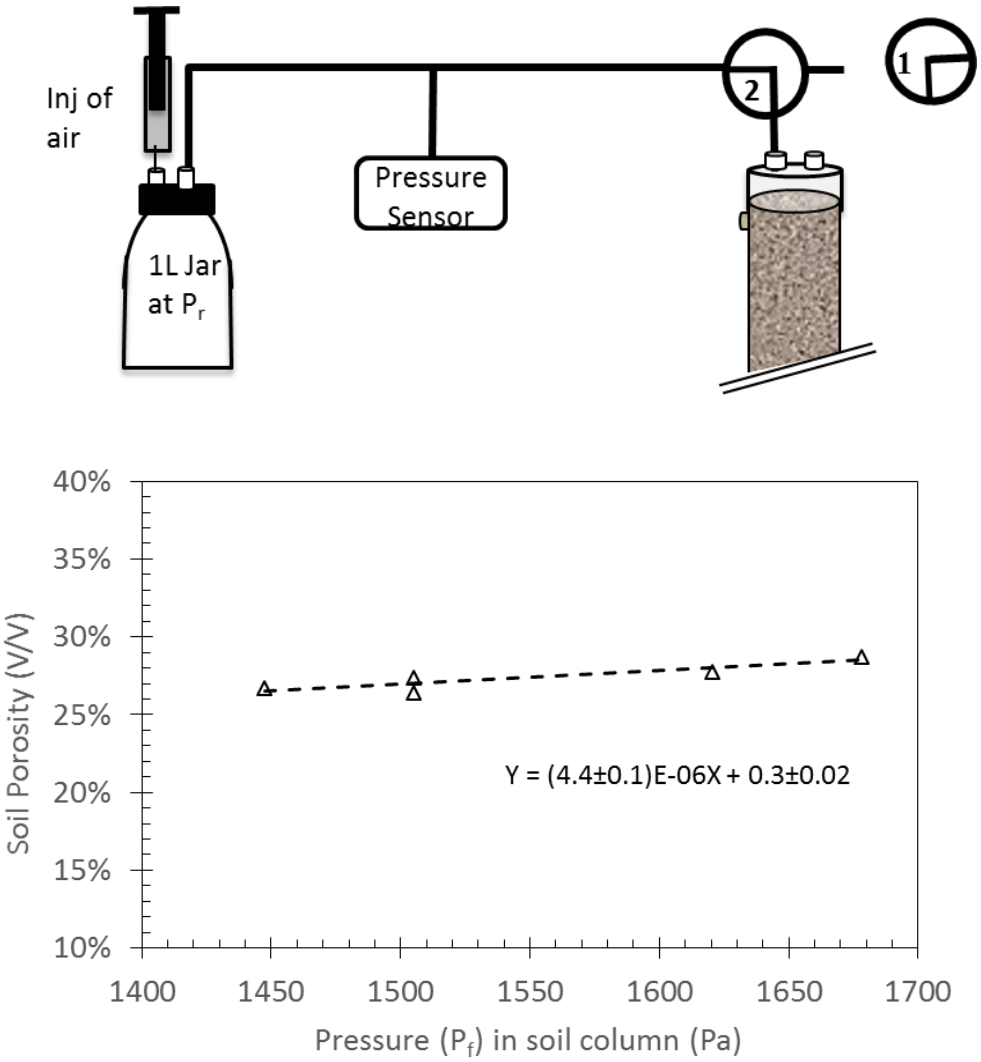

Figure 4-2: (Upper panel) System used to measure soil porosity measurement. (Lower panel). The measured soil porosity (V/V) with pressure (Pa) applied in soil column. See text for details.

If the initial air volumes in the jar and soil column are V_r and V_s, the initial pressure P_r and P_s, and the final pressure of the entire system is P_f, according to Boyle's Law (PV = constant in closed system) we can write:

$$P_r V_r + P_s V_s = P_f (V_s + V_r) \tag{4.1}$$

$$V_s = \left(\frac{P_f - P_r}{P_s - P_f} \right) \times V_r \tag{4.2}$$

So, air volume in the soil is, $V_a = V_s - V_t - V_b$

where, V_s, V_t, V_b are the volume of the headspace and the bottom chamber of the soil column.

Hence, the air porosity in the soil column, $\phi = \frac{V_a}{Soil \quad Vol.}$

4.2.2 Concentration gradients measurements in GAS-1

The 'GAS-1' includes a single inlet laser diode O_2 analyzer and an IR-CO_2 detector (Model S147, Qubit Systems Inc, Kingston, Canada), a syringe pump (Model NE-300, New Era Pump System Inc.). This GAS-1 can measure a relatively high range of concentration change (up to a Δ[Conc.] of 10%) of the O_2 and CO_2 by the Qubit S147 analyzer.

A two-point calibration of the Qubit S147 analyzer of GAS-1, for both the O_2 and CO_2 sensors, was performed using the experimental setup shown in Figure 1-4A. For the O_2 senor calibration 20.95% and 9.95% O_2, and for the CO_2 sensor 10.10% and 0% CO_2 gases were used to set the maximum and minimum points of the analyzers respectively. After calibration, the analyzer was tested for a set of lab prepared gas mixtures (10.48% O_2 with 5.08% CO_2; 4.89% O with 5.09% CO_2; and 15.71% O_2 with 2.56%CO_2) in GAS-

1 (Figure 1-3). We found that the GAS-1 analyzer measured the concentrations with an average deviation of only ±0.14% for O_2 and ±0.33% CO_2 from their actual concentrations in the mixtures.

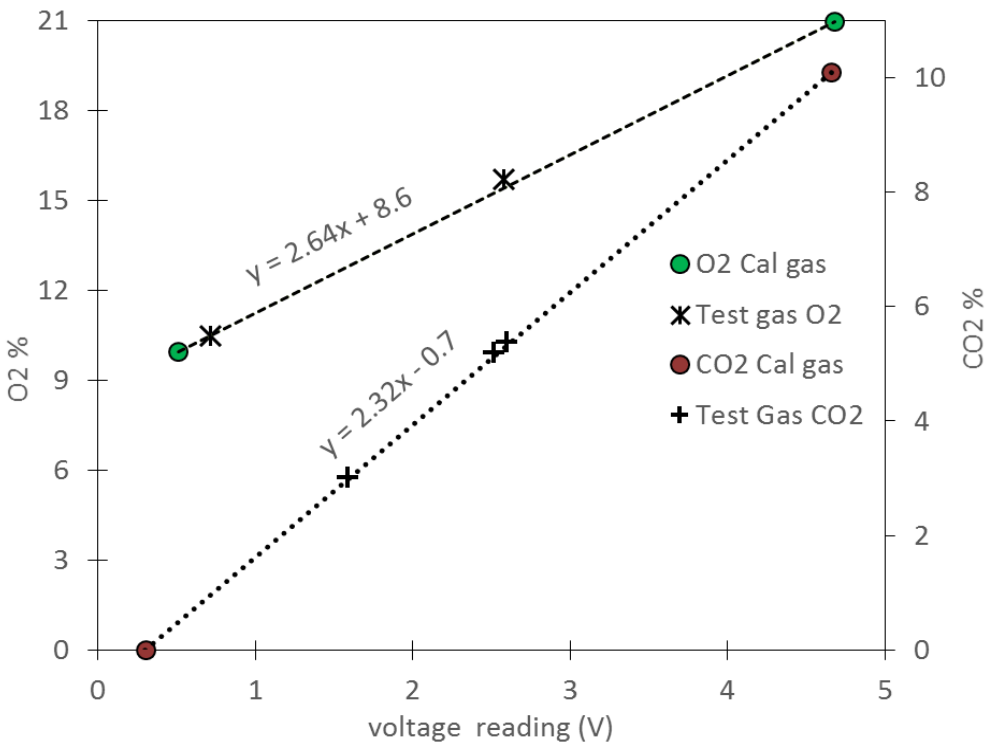

Figure 4-3: Calibration of the Qubit O_2/CO_2 analyzer with the measurements of the test gas mixtures of different O_2 and CO_2 concentrations.

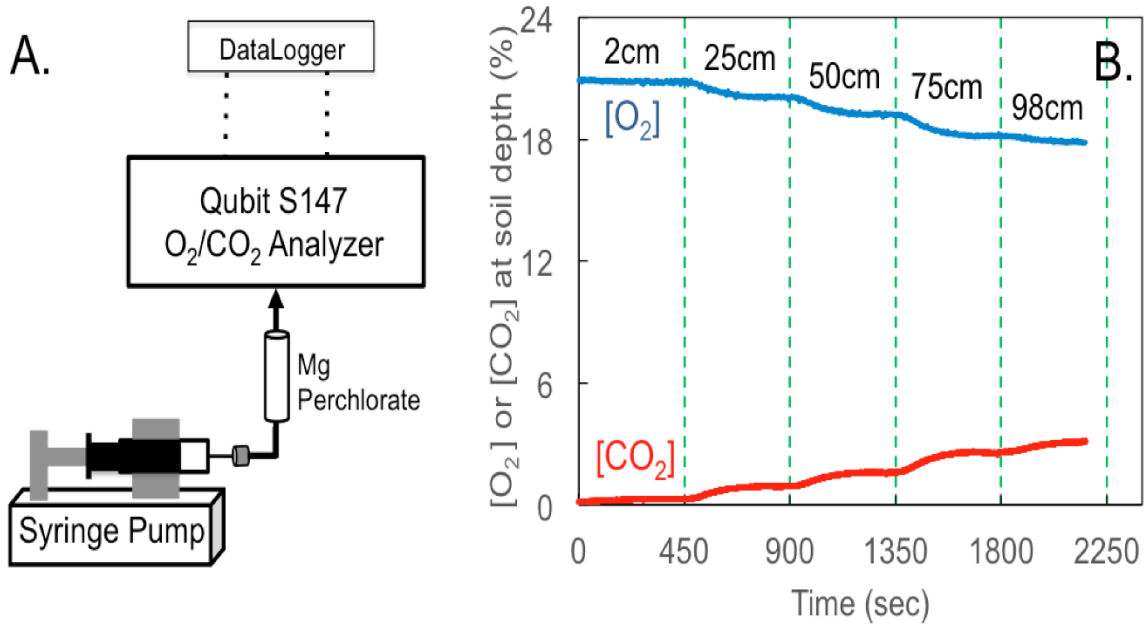

Figure 4-4: (Left) Shows the schematic of the soil air analyzing in GAS-1 for O_2 and CO_2 concentration measurements. Sample air was extracted from 2cm, 50, 75 and 98cm depths in the soil column. (Right) shows the example of the $[O_2]$ and $[CO_2]$ % at the soil depths measured in the S147.

To test the model prediction for the concentration gradients, CO_2 and O_2 in soil air were measured in GAS-1 by extracting 60 mL of soil air from each of the soil sampling ports over a 3-minute period (~20 mL/min). All these soil air samples were passed into GAS-1 for analysis through a magnesium perchlorate drying column (20 mL volume) at a flow rate of 10 mL/min by the syringe pump as shown in Figure 1-4A. The outputs from the GAS-1 were logged into a datalogger (Model no. LABQUEST2, Vernier Technology) before they were filtered and processed in an excel spreadsheet. Figure 1-4B shows an

example of the processed raw data for the simultaneous measurements of the O_2 and CO_2 concentrations in soil air extracted from different depths of the soil column.

4.2.1 Gas Analysis Systems (GAS-2 and GAS-3)

Since the gas analysis system (GAS-1) described in Figure 1-4A did not have the sensitivity and precision to measure gas exchange rates and gas concentration differentials between bulk air and the soil surface, a second gas analysis system (GAS-2) was constructed to measure soil gases in the controlled lab setup as shown in Figure 1-5. This was later upgraded to the final GAS-3 for field measurements (Figure 4-6). Central to these GAS-2 and GAS-3 systems were a Differential Oxygen Analyzer (Model S104 DOX, Qubit Systems Inc, Kingston, Canada) based on galvanic fuel cells and an infrared gas analyzer (model Li-7000, LiCOR, Lincoln, NB, USA). The IRGA of the GAS-2 can measure CO_2 mixing ratios in the sample stream over the range of 0 – 1000 ppm, while the DOX can measure a differential of ±1000 ppm against a reference gas stream.

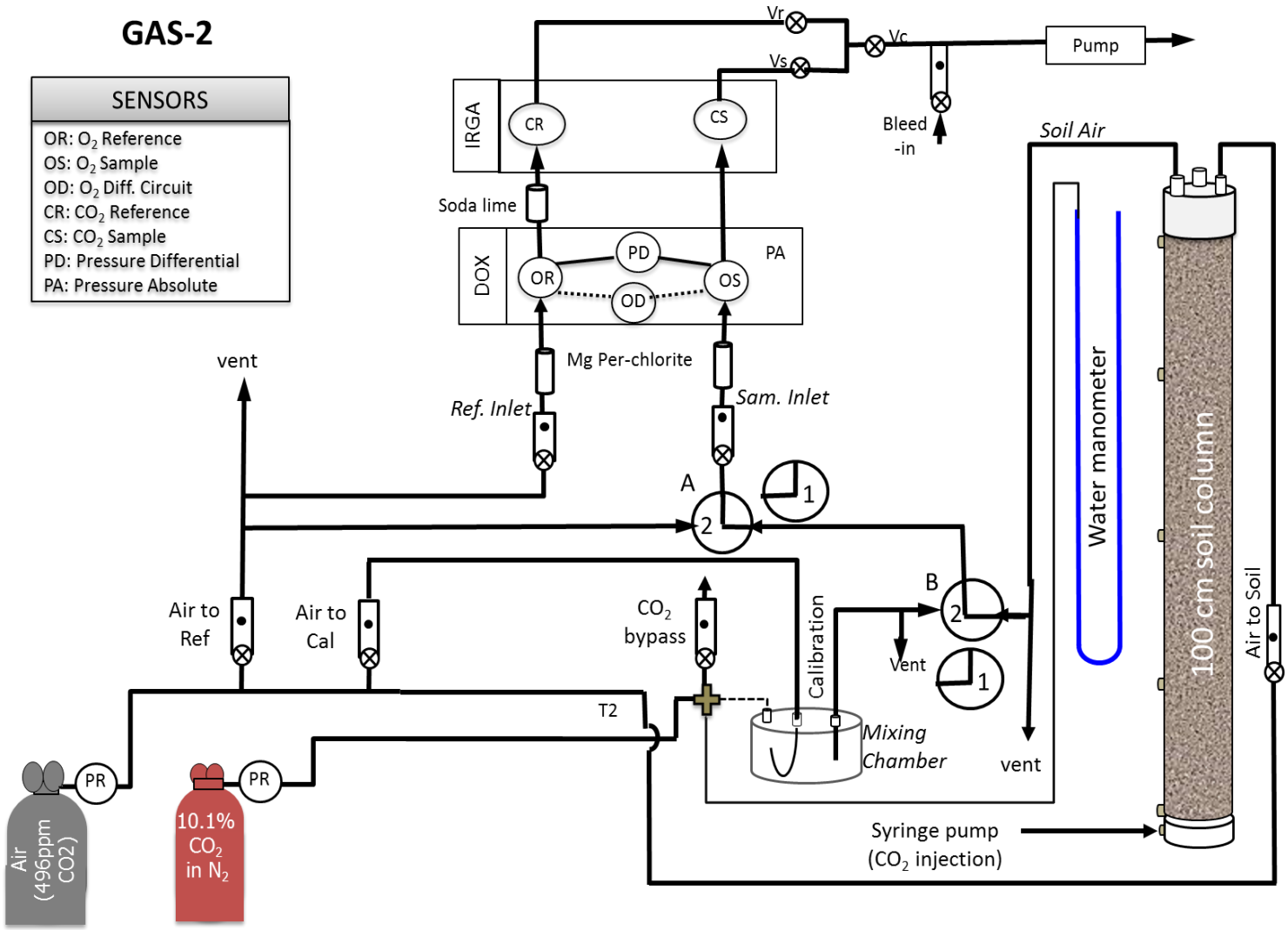

Figure 4-5: Schematic of the GAS-2A used for the measurement of gas exchange rates (GER/RQ) for CO_2 and O_2 and the concentration differentials (GCR) for CO_2 and O_2 between bulk air and the surface of the soil. The latter measurements were used to calculate the gas Concentration ratio as described in the text. A-B, 3-way valves showing positions 1 and 2; Cal, Calibration gas; DOX, Differential Oxygen Analyzer; IRGA, Infrared Gas Analyzer; PR, Pressure Regulator; R or RefGas, Reference gas = CO_2 scrubbed room air; Vr, Vs and Vc, Valves for reference, sample and common flows, respectively.

4.2.2 Standard use of the GAS-2

The GAS-2 system was used for measuring the gas exchange ratio (GER) at the headspace of the closed soil column by flowing reference air into and out of the capped column. It was operated by switching every 5 minutes, the gas streams supplying the sample side of the DOX (OS) and IRGA between the reference gas, and one of the other gas streams while monitoring the output of the O_2 differential (OD), Pressure Differential (PD) and IRGA CO_2 sample signal (CS). All measurements were made relative to the reference gas stream of breathing grade 496 ppm CO_2 air from a cylinder.

The following sequence of gases being supplied to the sample stream (the reference gas stream always receives the reference gas): 'Reference Gas (Ref)', 'Calibration (CalGas)', and 'Soil Flux'. The measurement for GAS-2 is given in Figure 1-5.

a) **Reference gas** [Valve position A1, Figure 1-5]. When the reference gas is provided to both sides of the DOX, the flows are adjusted (Typically by adjusting Vs and V_r) to ensure that no pressure differential exists between the sample and reference streams. The DOX output is also zeroed. The voltage reading of CO_2 concentration and the oxygen differential as CS^R and OD^{Cal} are logged for this valve position in the GAS-2.

b) **Calibration gas** [Valve position B1, A2, Figure 1-5]. The CalGas stream was created by mixing the reference gas with a low flow of a Calibrating gas containing 10.1% CO_2 in N_2. The resulting CalGas will have an elevated CO_2 concentration compared to the reference stream, and the O_2 concentration would be diluted. Since

CO_2 concentration in the calibrating gas (10.1%) was half of the O_2 concentration in air (20.9%), the difference in the O_2 and CO_2 concentration between the CalGas and the reference gas would be nearly 0.50. In this way, the CalGas treatment serves to lock the IRGA and DOX analyzers together and provide a regular check on whether they are maintaining their calibration with respect to each other over time. The reading of CO_2 concentration and O_2 differential in the CalGas stream w.r.t the reference gas (CA^{Cal} and OD^{Cal}) are logged from this step of the system.

c) **Gas exchange measurements** [Valve positions B2 and A2, Figure 1-5]. In this mode, a known flowrate of reference gas (typically 130 to 250 mL/min) is provided to the headspace of the soil column where it picks up CO_2 and contributes O_2 to the metabolic activity within the soil column. The flowrate of the gas is chosen to create a CO_2 concentration in the effluent gas stream that is similar to, or slightly greater than (up to 50% higher) the concentration measured in room air. The reading of oxygen and CO_2 as CS^{SF} and OD^{SF} in the effluent gas stream relative to the reference gas are collected from this position of the GAS-2 which are used to calculate the gas exchange rates (GER) for the two gases from the soil column.

4.2.3 Standard use of the GAS-3

The GAS-2 system was used by switching every 3 to 10 minutes, the gas streams supplying the sample side of the DOX (OS) and IRGA between the reference gas, and one of the other gas stream while monitoring the output of the O_2 differential (OD), Pressure

Differential (PD) and IRGA CO_2 sample signal (CS). All measurements were made relative to the reference gas stream of CO_2-scrubbed room air.

A typical run would involve the following sequence of gases being supplied to the sample stream (the reference gas stream always receives the reference gas (CO_2 scrubbed room air): 'Reference Gas (Ref)', 'Calibration Gas (CalGas)', 'Room Air', 'Soil Surface Air' and 'Soil Flux'. The measurement procedure of the GAS-3 is shown in Figure 1-6:

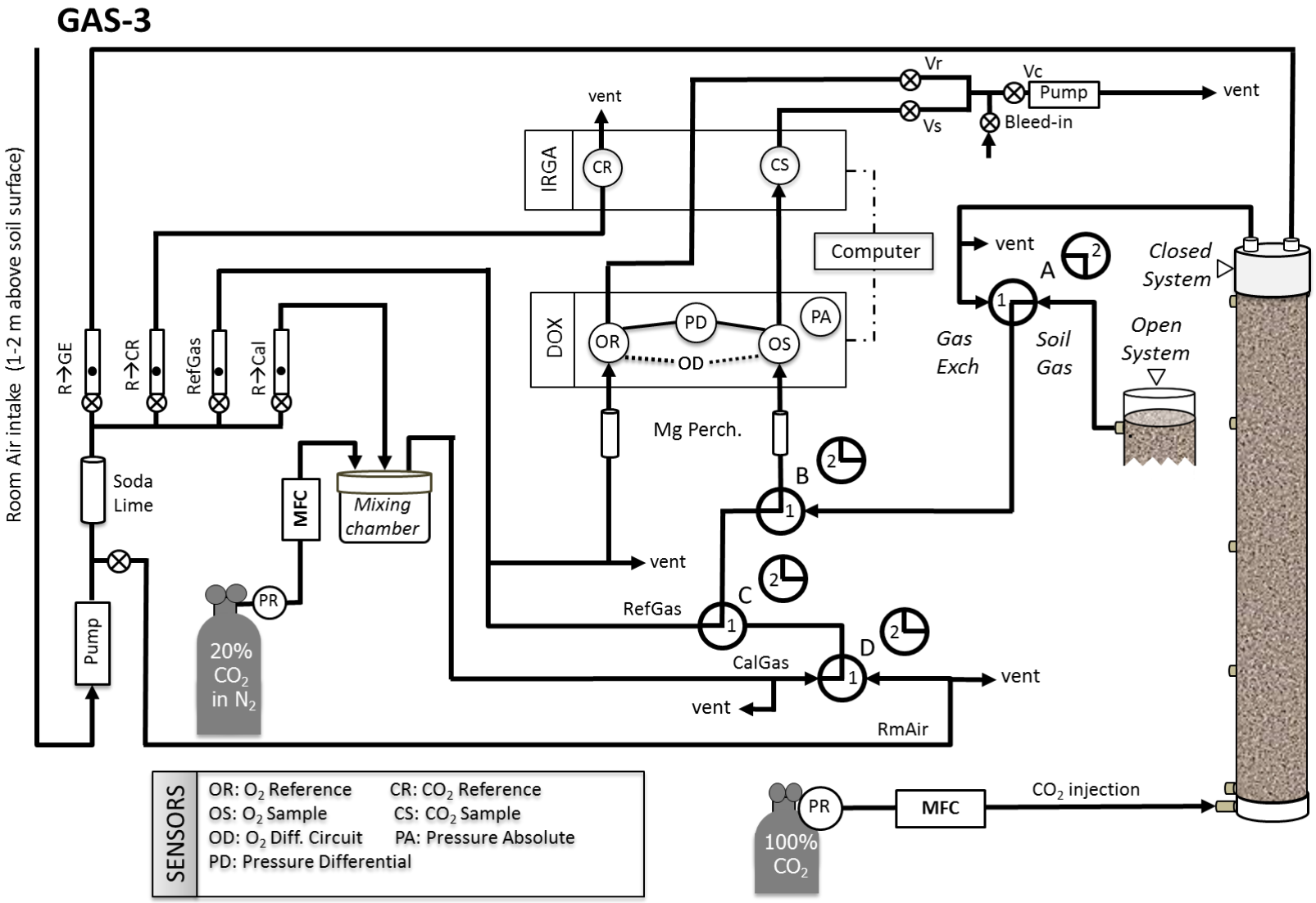

Figure 4-6: Schematic of the GAS-3 used for the measurement of gas exchange rates (GER/RQ) for CO_2 and O_2 and the concentration differentials (GCR) for CO_2 and O_2 between bulk air and the surface of the soil. The latter measurements were used to calculate the gas Concentration ratio as described in the text. A-D, Three way valves showing positions 1 and 2; Cal, Calibration gas; DOX, Differential Oxygen Analyzer; IRGA, Infrared Gas Analyzer; MFC, Mass Flow Controller; PR, Pressure Regulator; R or RefGas, Reference gas = CO_2 scrubbed room air; Vr, Vs and Vc, Valves for reference, sample and common flows, respectively.

i. **Reference gas** [Valve positions C1 and B1, Figure 1-6]. CO_2-free reference gas is provided to both sides of the DOX. Same flow rates are maintained (adjusting Vs and Vr, Figure 1-6) to ensure that no pressure differential exists between the sample and reference streams. The reading of CO_2 and oxygen differential as CA^R and OD^R as zero for this position.

ii. **Calibration gas** [Valve positions D1, C2 and B1, Figure 1-6]. For GAS-3, the CalGas stream was created by mixing the CO_2 scrubbed room air with a gas of 20.04% CO_2 in N_2. Since the CO_2 concentration in the calibrating gas (20.04%) was similar to the O_2 concentration in air (20.9%), the difference in the O_2 and CO_2 concentrations between the CalGas and the reference gas would expected to be 0.95. Deviation from this ratio would work as a regular check on the GAS-3 whether the DOX and IRGA maintained their calibration with respect to each other over time. The readings of CO_2 concentration in the CalGas as CA^{Cal} and oxygen differential w.r.t reference air OD^{Cal} are measured for this position of GAS-3.

iii. **Reference gas** [Valve positions C1 and B1, Figure 1-6].

iv. **Room air** [Valve positions D2, C2 and B1, Figure 1-6]. Since room air is scrubbed of CO_2 to create the reference gas, when it is compared with untreated room air, the IRGA will provide a measure of the CO_2

concentration in the room air. The DOX analyzer will also show a differential in O_2 concentration since the CO_2 removal from the room air would have increased the fractional O_2 concentration in the reference gas. The reading of CO_2 concentration in the untreated room air (CA^{Rm}) and oxygen differential w.r.t CO_2 free room air (OD^{Rm}) are collected from this position.

v. **Reference gas** [Valve positions C1 and B1, Figure 1-6].

vi. **Soil Surface Gas** [Valve positions A1 and B2, Figure 1-6]. In this mode, sample gas is drawn through a syringe placed either at the soil surface or up to 1 cm below the surface of the soil. As with other gas samples, the CO_2 concentration and oxygen differential (CA^{SS} and OD^{SS}) in soil air are measured relative to the reference gas.

vii. **Reference gas and the conversion to a closed system** [Valve positions C1 and B1, Figure 1-6]. Once the DOX and IRGA outputs have equilibrated to the reference gas, the soil column is prepared for measurements of net gas exchange by sealing a cap on the top of the soil column, thereby converting it from an ‘open system’ to a ‘closed system’ as shown in Figure 1-6.

viii. **Gas exchange measurements** [Valve positions A2 and B2, Figure 1-6]. In this mode, with the headspace closed, a known flow rate of reference gas (typically 130 to 250 mL/min) is provided to the headspace of the soil column where it picks up CO_2 and contributes O_2 to the metabolic activity within the soil column. The flowrate of the gas is chosen to create a CO_2 concentration in the effluent gas stream that is similar to, or slightly greater than (up to 50% higher) the concentration measured in room air. The DOX and IRGA provide the steady-state CO_2 concentration and O_2 differential (CA^{SF} and OD^{SF}) in the effluent gas stream relative to the reference gas and the information is used to calculate the gas exchange rates (GER) for the two gases from the soil column.

4.2.4 Calibration of GAS-2 and GAS-3

The complete calibration of the GAS-2 and 3 were done sequentially as the following steps.

1. Calibration of the Infra-Red Gas Analyzers (IRGA) model Licor-7000 for CO_2 measurements in CR and CS cells of the system
2. Calibration of the Oxygen Sensors (OR, OS) and Pressure sensors (PD) in the DOX
3. Calibration of the DOX using the IRGA Li-7000 analyzer

4.2.4.1 Calibration of IRGA analyzer Licor-7000:

The CO_2 analyzer was calibrated for two points (Figure 1-7). Initially, by flowing a reference gas (e.g. 496ppm CO_2 dry air) both in the 'CR' (reference) and 'CS' (sample) cells we matched the first point for CO_2 concentration at 'exact value' to '496'. After that,

flowing a 496 ppm CO_2 gas in 'CR' cell and another 1000 ppm CO_2 dry gas in 'CS' cell we matched the 2nd point for CO_2 concentration to the exact value of '1000'. After the calibration, the IRGA was tested by flowing certified CO_2 gas of 380ppm CO_2, 491ppm and 1000ppm into the CS cells respectively. The concentration readings of these gases were plotted with corresponding voltages. The slope and intercept of this relationship equation were used to measure the CO_2 concentration in the gas stream flowing through 'CS' cell with respect to the reference gas flowing in the 'CR' cell.

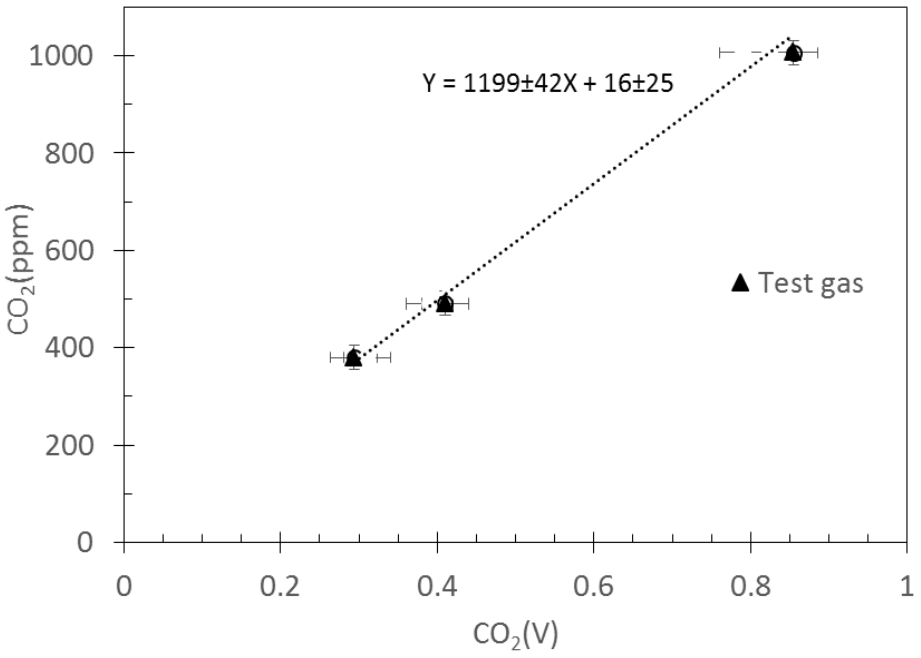

Figure 4-7: Calibration graph of IRGA (Li-7000) in GAS-2

4.2.4.2 Calibration of oxygen sensors and Pressure Differential sensors:

To measure differential O_2 concentration in the sample OS cell with respect to the reference OR cell, the OD sensor of the DOX was calibrated using a built-in Differential Pressure (PD) sensor between the cells. Complete calibration of the OD sensor required absolute O_2 sensors (OR and OS) calibration and the Differential Oxygen (OD) sensor calibration using the PD sensor.

(a) Reference O_2 ***(OR) and Sample*** O_2 ***(OS) sensors calibration:***

Before using the GAS-2 for the tests, we had to perform the 'Absolute Oxygen Sensors' calibration for OR and OS of the DOX. The calibration was run in the 'calibration command' mode of the DOX. It started with the calibration of 'Sample O_2' (OS) sensor. In this calibration, flowing '20.95% O_2 air' at same flow rate in both cells, 'First Point' of two-point linear calibration of the OS sensor was set as pO_2 (kPa) value. [i.e. pO_2 (kPa) = Atmospheric Pressure x 20.95%]. Then flowing an oxygen free gas (pure N_2 gas) in both cells, 'Second Point' was locked to pO_2 (kPa) = 0.00. The OR sensor was also calibrated in similar way. The built-in DOX software used these two-points to calculate the differential concentration of O_2, as OD(V), in any sample gas stream (w.r.t OR cell).

(b) ***Pressure Differential Sensor Calibration:***

The DOX comes with an absolute pressure (PA) sensor inside it. For our measurements, we used the factory calibration of this PA sensor. We only calibrate the sensitive differential sensor (PD) which, also built-in, is connected between the OR and OS cells of

the DOX which measure the pressure and the total Oxygen differential (OD) between them. It is, therefore, critical to calibrate the PD sensor prior to any gas analysis test.

PD calibration was carried out in three steps; it was first calibrated with a small water manometer (Figure 1-8 and Figure 1-9). Second, correction for the PD effect on the OD measurements as the partial pressure difference (PD(Pa)) between the cells (that may arise during the experiments due to switching among the channels to flow different gases through the sample channel) will create an artifact in oxygen differential between the cells (Figure 1-10 and Figure 1-11). Finally, OD (V) due to the PD(Pa) effect was converted to the OD(ppm).

Calibration of PD with the manometer gives the equivalent pressure (PA) for PD (V). It was done by disconnecting the inlets of the DOX and plugging the outlets. Then 'OR' inlet was left open to room air and 'OS' inlet was connected with the left arm of the manometer with a T-piece. With injection and pulling air from the 'T' by a syringe, PD (V) and OD(V) from the DOX and the corresponding water height (cmH_2O converted to Pa) from the manometer were recorded.

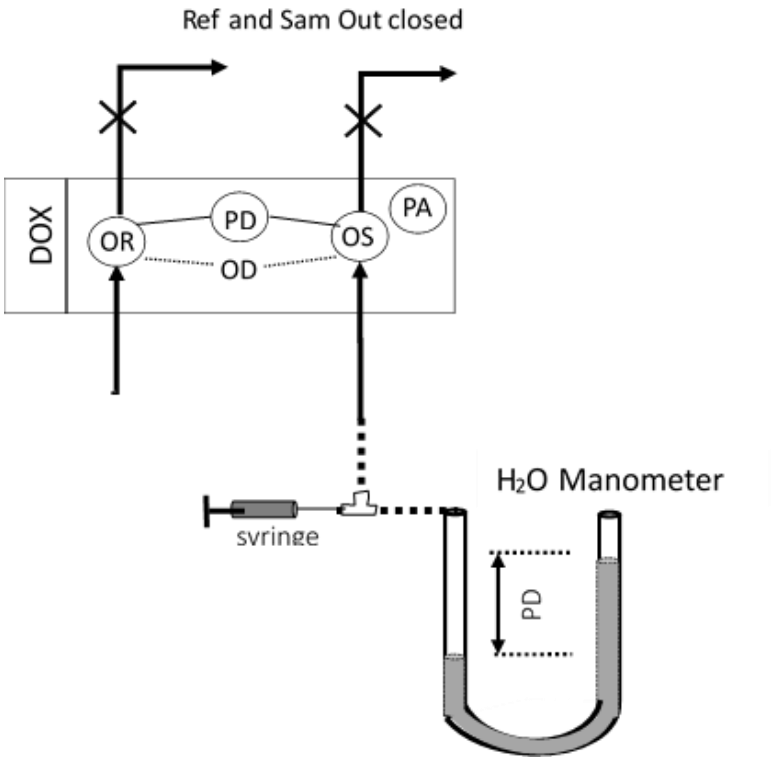

Figure 4-8: Schematic of the differential pressure (PD) sensor calibration using water manometer.

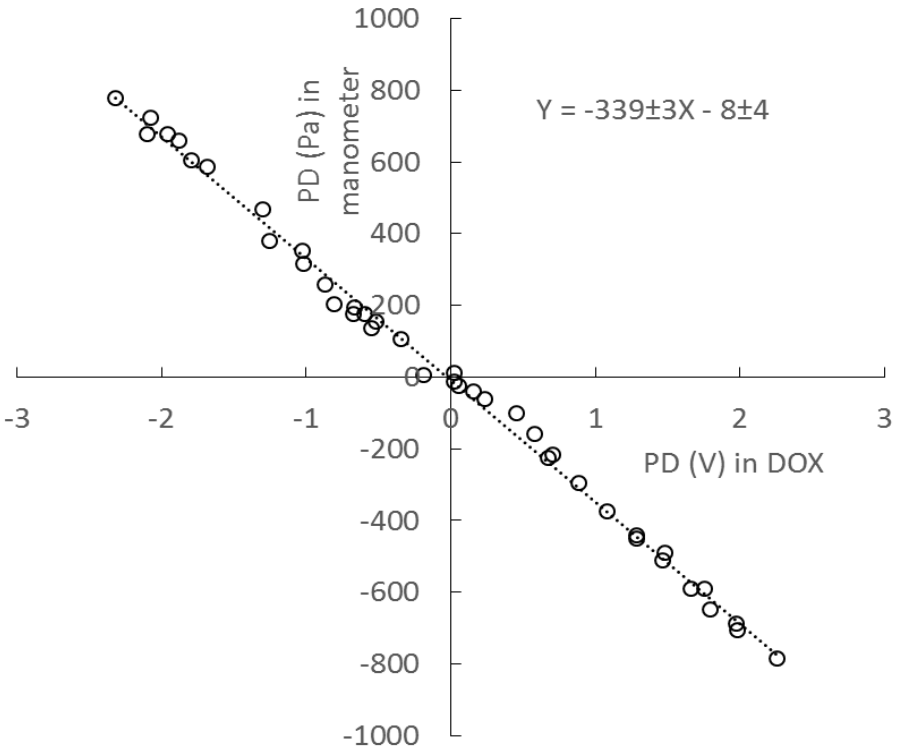

Figure 4-9: Equivalent Differential Pressure (Pa) (converting manometer water column height reading to pressure) with PD (V) reading for induced air pressure in O_2 sample cell (OS) w.r.to Ref cell.

(c) Calibration of Differential Pressure (PD) effect on the Oxygen Differential (OD) sensor

The sequential switching of four different gas streams (Ref, Calb Gas, Room Air, and Soil Air) in the sample cell (Figure 1-6) may alter the initial pressure balance (PD = 0.00V) between the cells that will lead to errors in our measurement of OD. A standard correction

method has been prepared for our gas analysis system to correct for this PD effect on OD measurements and the following protocol was prepared.

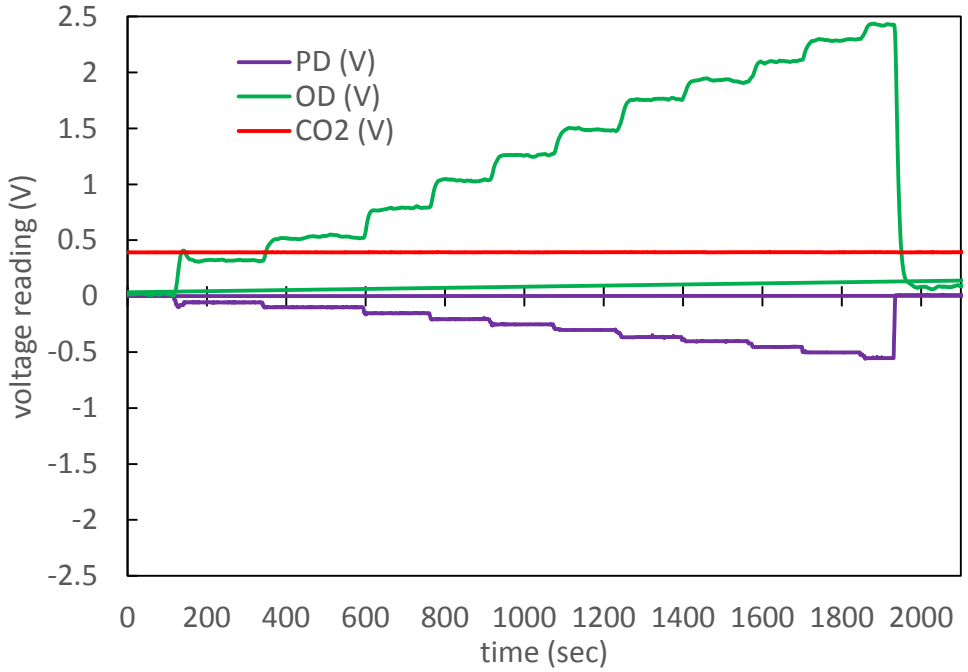

Figure 4-10: PD (V) effect on OD(V) (while CO_2 (V) remained unaffected)

First, by PD (V) =0.00 is set by flowing the same Ref gas (for example, 20.97%O_2 air) both in R and S cells at the same flowrates and both the OR(V) and OS(V) are adjusted to 1.35V. Next, the pressure difference (PD(V)) between the cells is changed by varying flow rates in the sample cells (with V_s valve) (Figure 1-10 shows an example of PD(V) effect on OD(V) while CO_2 concentration remain unchanged). The PD (V) affects the differential oxygen reading, OD(V), proportionally. Hence we use the slope and intercept of the *PD(V) vs OD(V)* relationship (not given here) to filter out the additional OD(V) effect. The PD(V)

is also converted to the equivalent PD(Pa) using the relationship of the PD (V) with Differential Pressure (Pa) from the Figure 1-9. The converted PD (Pa) and corresponding OD (V) from the DOX when RefGas was flowing into both the inlets of the GAS-2 is (Figure 1-11):

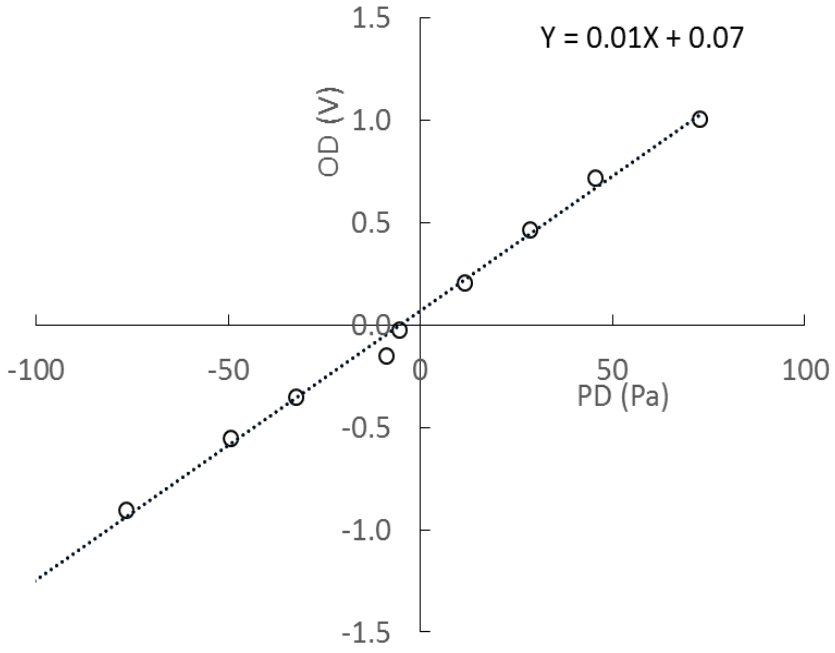

Figure 4-11: PD (Pa) effects OD (V) reading in the DOX analyzer

(d) Converting the measured OD (V) for the PD effect to OD(ppm)

In the gas analysis system, Oxygen Differential in a sample stream is collected as OD (V) which needs to be converted to our desired 'ppm' unit. PD (Pa) found in previous step was multiplied by the oxygen percentage (O_2 = 20.95%) to convert to equivalent pressure differential of oxygen OD (Pa), which was converted to OD (mol/m^3) using the ideal gas

law. The conversion equation, given below, was used to convert OD (mol/m^3) to OD (ppm):

$$OD(ppm) = OD(mol/m^3) \times 1000 \times MolarVol(L)$$

4.2.4.3 Calibration of DOX using IRGA Li-7000

In our gas exchange experiment, we use a gas as 'Internal Calibration' which is the stream of a gas from a mixture chamber. In this mixture chamber two streams of gases (with known but different O_2 and CO_2 %) are mixed to make a gas. This gas (Cal Gas) has a different concentration of CO_2 and O_2 gases depending on the sources gases that get mixed in the chamber.

For example, the CalGas from the mixtures of 20.95% O_2 and 496 ppm CO_2 air with 10.10% CO_2 (in N_2) gas will have (independent of their flow rates into the mixture chamber) Gas Exchange Ratio (GER, which is the ratio of concentration differentials of the source gases) as:

$$GER = \frac{\Delta CO_2}{\Delta O_2} = \frac{10.10 - 0.0496}{20.95 - 0.0} = 0.48 \qquad (4.3)$$

Similarly, for gas from the mixture of 20.97% O_2 and 496CO_2 air with 20.04%CO_2 (in N_2) will have the GER value:

$$GER = \frac{\Delta CO_2}{\Delta O_2} = \frac{20.04 - 0.0496}{20.97 - 0.0} = 0.95 \qquad (4.4)$$

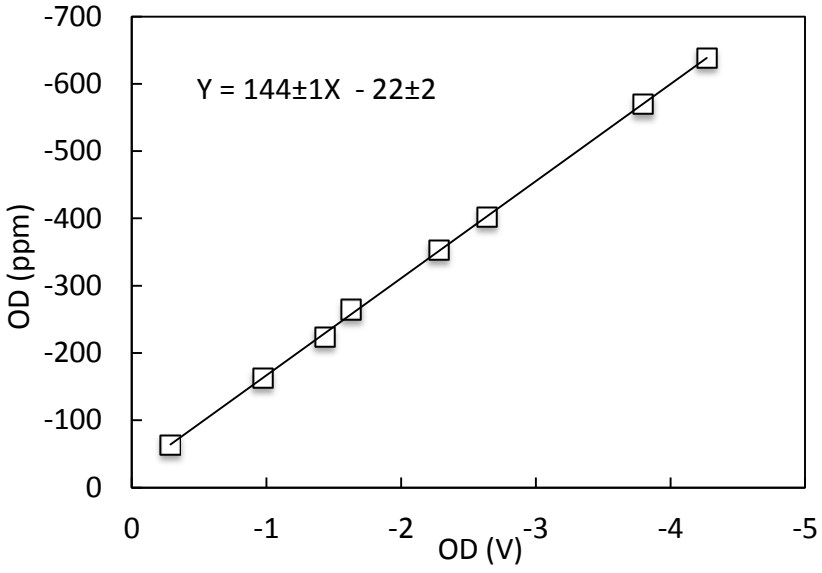

Figure 4-12: Expected OD (ppm) vs Measured OD (V)

For calibration of Differential Oxygen, OD (V), sensor in the DOX, the expected OD (ppm) in the mixture gas is calculated by dividing the CO_2 mixing ratio (measured in CO_2 analyzer) with the GER value (0.48 or 0.95). By changing the flow of one of the source gases into the mixture chamber, we change the CO_2 concentration (ppm) of the mixture gas and hence can calculate the corresponding OD (ppm).

This calibration equation of 'Expected OD (ppm) vs Measured OD (V)' is then used to convert OD (V) to OD (ppm) for calculation of GER. The value of GER for 'Cal Gas' worked as the standard to check our measurement regularly, as the deviation of GER from 0.48 or 0.95 was considered as the alarm if we required any re-calibration of the GAS or flushing the channels with reference gas.

4.2.5 Haldane correction for net gas volume

Willms et al (1997) showed that if a biological system does not have a CO_2 evolution and O_2 consumption ratio of $1:1$, it affects the net volume of the gas entering into and leaving a system and requires correction (Haldane correction) to find the net gas exchange within the system. After analyzing our preliminary results for measurements of soil RQ, a correction was followed in calculating the net gas volume and the relative concentration of the O_2 and CO_2 gases at near surface. Since studies shows that the ratio of CO_2 production and O_2 consumption rates in regular soils may vary within a range of 0.68 – 1.10, it may create an artifact in the fractional volume of the gases in our measurements of CO_2 (ppm) and OD (ppm) [Dilly, 2001; Andersen, 1997]. The Haldane correction, therefore, was applied to filter out the noise in our analysis prior to further measurements of soil RQ (GER) at surface both for the regular and leak added soil.

The correction for our OD (pa) and ΔCO_2 (pa) measurements in our gas exchange system is given below (Willms et al., 1997):

$$OD_{corrc}^{Pa} \approx OD^{Pa} + \left[\frac{\Delta CO_2^{Pa} + OD^{Pa}}{1 - \frac{OA^{kPa}}{PA^{kPa}}} \right] \times \frac{OA^{kPa}}{PA^{kPa}} \qquad (4.5)$$

Where, OD^{Pa} is the OD measured in Pascal

OD_{correc} is the corrected OD in Pascal

OA is the absolute Oxygen concentration in kPa

PA is the absolute atmospheric pressure in kPa

For the absolute atmospheric pressure (89kPa) for Calgary and the composition of O_2 and CO_2 gas used in GAS-2 as 20.95% and 0.0496% respectively, eq. 4.5 equation can be written as:

$$OD_{corrc}^{ppm} \approx OD^{ppm} + \left[\frac{\Delta CO_2^{ppm} + OD^{ppm}}{1 - 0.2095}\right] \times 0.2095 \tag{4.6}$$

$$\Delta CO_{2,corrc}^{ppm} \approx \Delta CO_2^{ppm} + \left[\frac{\Delta CO_2^{ppm} + OD^{ppm}}{1 - 0.0496}\right] \times 0.0496 \tag{4.7}$$

The ratio of differential CO_2 and O_2 at soil surface for the closed soil column headspace, w.r.t reference air, was calculated using eq. 4.8.

$$\frac{\Delta CO_2^{ppm}}{OD^{ppm}} = \frac{CS^R - CS^{SF}}{OD^R - OD^{SF}} \tag{4.8a}$$

After applying Haldane corrections of eq. 4.6 and 4.7, the GER at soil surface becomes:

$$GER = \frac{\Delta CO_{2,corrc}^{ppm}}{OD_{corrc}^{ppm}} \tag{4.8b}$$

CO_2 flux was measured using CO_2 concentration differential between inlets and outlets of the gas streams for the closed soil column headspace (eq. 4.9).

$$CO_2 Flux = F_r \times \frac{[CO_2]_{inlet}^{ppm} - [CO_2]_{outlet}^{ppm}}{A} = F_r \times \frac{\Delta CO_{2,corrc}^{ppm}}{A} \tag{4.9}$$

A unique acronym was used when CO_2 and O_2 at the soil surface were measured w.r.t room air for soil open to ambient air (i.e., GCR by GAS-3 in Figure 4-6). It was calculated as shown in equation (4.10).

$$GCR = \frac{CS^{Rm} - CS^{SS}}{OD^{Rm} - OD^{SS}} \quad (4.10)$$

Where,

CS – CO_2 mixing ratio (ppm)

OD – O_2 differential (ppm)

SS – Soil air from the near surface of the open column

R – Reference air

Rm – Room Air

SF – Soil flux at the headspace of the closed system

F_r – Flow rate into the chamber (m^3/sec)

A – Area of the soil surface (m^2)

Note that for CO_2 flux calculation $\Delta CO_{2,corrc}^{ppm}$ was converted from mixing ratio (ppm) to concentration (mol/m^3) using the ideal gas equation for standard temperature and pressure at 25^0C and 89 kPa, respectively.

4.3 Results and discussion

4.3.1 Characterization of soil properties:

Physical properties for SOIL-A and B, measured after they were placed in the soil columns, are shown in Table 4-2.

Table 4-2: Measured physical properties SOIL-A and B in the soil columns

Soil Column	Bulk Density (gm/cm^3)	Air Porosity (V/V)	Water Content (V/V)
SOIL-A	1.41±0.03	0.27±0.04	0.15±0.01
SOIL-B	1.26±0.06	0.30±0.02	0.18±0.03

The average bulk density of the SOIL-A was found to be comparatively higher than SOIL-B, while SOIL-A had lower porosity (total 42%, V/V) than SOIL-B (48%, V/V). The profiles for O_2 and CO_2 (%) across the depths of SOIL-A and SOIL-B were measured along with their water content and soil porosity over several months with GAS-1. The profiles of these two soils are given in the following Figure.

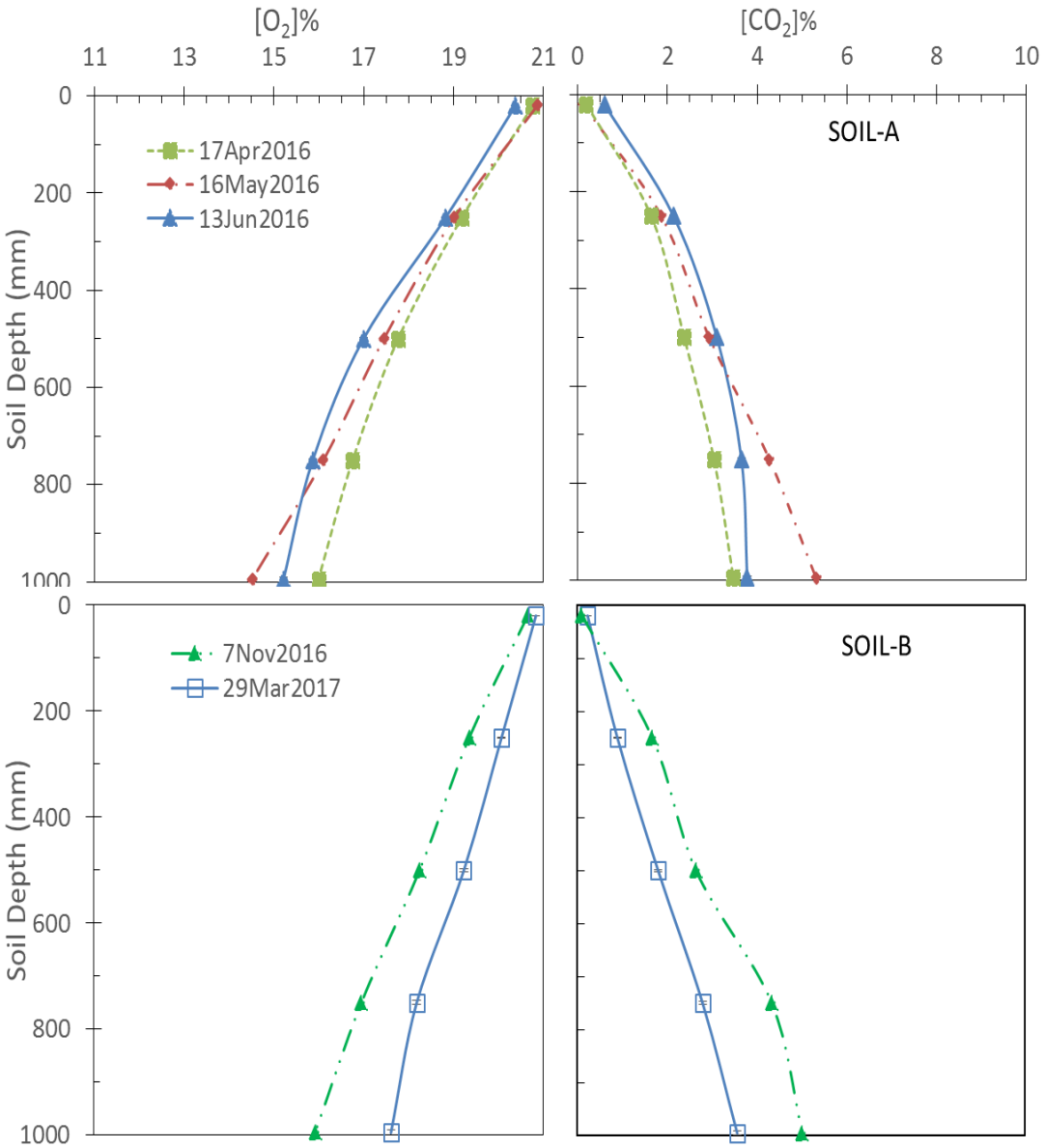

Figure 4-13: Measured gradients for O_2 and CO_2 in SOIL-A (upper panel) and SOIL-B (lower panel). Three trials were performed over 3-months for SOIL-A (with 18% of water) and two trials over 4-months period for SOIL-B column (with a decrease of water content from 18% to 14%). Errors are of ±0.14% for O_2 and ±0.33% CO_2 are not shown for simplicity. Note that CO_2 and O_2 profiles for 29Mar2017 for SOIL-B was measured after the soil was flushed of CO_2 for one day and left open to room air for several weeks.

Figure 1-13 demonstrates that the measured O_2 and CO_2 (%) within the soil columns follow expected stoichiometric relationships, a decrease of O_2 is observed while a gradual increase of CO_2 occurs with increasing depths in the soils. For SOIL-A, we see that both concentration gradients for all trials increases with time over the measurement period with a minor discrepancy at 100 cm below the surface. This increase in gradients might have occurred due to the settling of the soil particles after they were placed in the column that led to more dense soil layers gradually from the surface to 100 cm depth and reduced gas diffusivities as a consequence of the soil compaction changes (Czyz, 2004). Concentration of O_2 over the 1-m depth of SOIL-A column ranges from about 20.70% at near-surface to 15 – 16% (with max ΔO_2 of 6.4%), while CO_2 concentration ranges from about 0.10% to 5.3% (with max ΔCO_2 of 5.2%). The higher gradient of O_2 indicates that carbon substrates in the SOIL-A column had less oxygen content than carbon substrates in SOIL-B. It is likely because SOIL-A was collected near academic buildings and was in the lab for several months before the measurements.

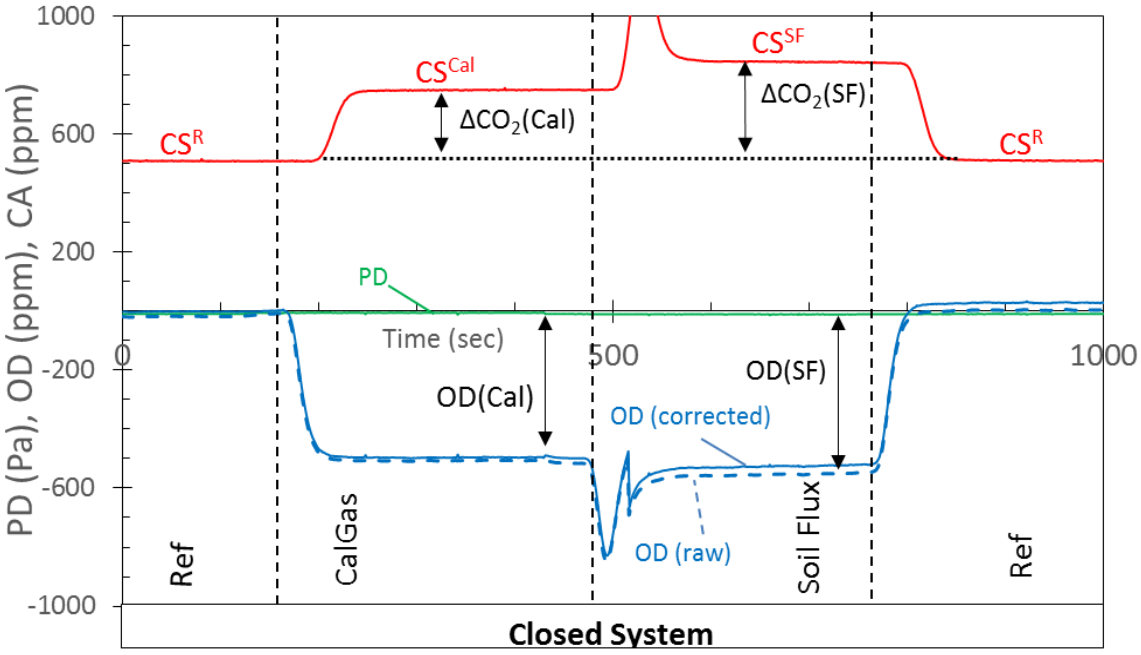

Figure 4-14: PD (Pa), OD (ppm), and CS (ppm) data for gas analysing for both soil column open and closed system. Before and after running CalGas, Room Air, Soil Surface, and Soil Fluxes in sample cell, GAS was flushed by flowing 'R' gas both in reference and sample cells. Green, blue and red lines represent PD (Pa), OD (ppm) and CS (ppm) respectively, while 'dashed' blue line is for raw OD and 'solid' blue line for pressure corrected OD line.

Before and after every measurement cycle of gases (Ref, CalGas, and Soil Flux air) in the GAS-2, the system was set for 'zero' voltage differences for PD(V) and OD(V) by running 'R' gas in both reference and sample channels to avoid voltage drift for OD(V) in the DOX. Figure 1-14 shows that both the CO_2 (ppm) and OD (ppm) readings in the GAS-2 system reached stability immediately after switching the valves of different gas streams during the measurements which reflects the precision of the analysis system.

The data from the system was collected as raw voltages in the data logger, which was then filtered for noise and corrected for the PD (V) effect on OD (V) (as discussed in the calibration section (c)).

Table 4-3 : SOIL-A characteristics for three replicate measurements using GAS-2 on 13 Jun 2016. The CalGas was created by mixing a 10.1% CO_2 in N_2 gas and Breathing air of 0.0496% CO_2 with 20.95% O_2.

Replicate	CalGas			Soil Flux			
	ΔCO_2 (ppm)	**ΔO_2 (ppm)**	**GER**	**ΔCO_2 (ppm)**	**ΔO_2 (ppm)**	**SR (µmol/m²/s)**	**GER (RQ)**
1	220	466	0.47	366	542	3.76	0.67
2	224	468	0.48	330	482	3.38	0.68
3	218	469	0.46	337	521	3.47	0.65

From Table 4-3 we see that the CO_2 flux (SR) for SOIL-A was 3.54±0.19 µmol/m^2/s. Also, for 'CalGas' of expected GER 0.48, the average of three repetitions in GAS-2 measured a GER of 0.46±0.02; which is an excellent agreement. Using GAS-2, the closed system GER of SOIL-A ('Soil Flux' section in Figure 4-14) was found to be 0.66±0.02. Similarly, for three consecutive measurements the average CO_2 flux for SOIL-B was 4.04±0.18 µmol/m^2/s and GER was found as 0.99±0.02 [Table 4-4].

It is important to note that in this thesis one essential parameter for model simulation was the RQ of both soils used for the tests. RQ for these soils were measured as the gas exchange ratio (GER) for closed system soil columns. Possible reasons for

different GER values found for SOIL-A and SOIL-B (representing their RQ as well) include soil physical properties, biological activities, and the environmental conditions (water content and temperature) in soils. For instance, RQ ranges from 0.6 to 1.0 for regular aerobic soils (Andersen & Scagel, 1997) and often higher than 1.0 under anaerobic conditions when there is an abundance of alternative electron acceptors like NO_3^-. Soils rich in glucose like carbon substrates and which are completely mineralized can have RQ of 1.0; and soils of organic-managed conventional farmland can have RQ >1 with a wide range from 0.50 to 1.10 (O. Dilly, 2001).

Between the two soils used in these tests, the RQ of SOIL-A was found to be comparatively lower than SOIL-B. Reasons for this difference, as discussed above, were related to the properties of SOIL-A and B and composition of organic matter at the sampling sites where these soil were collected (O. Dilly, 2001; Fischer & Blažka, 2015). SOIL-A was collected from a non-farmland soil which was not managed for many years. It is, thus, possible for this soil to have substrates with less oxygen and giving lower RQ values. Furthermore, the SOIL-A sampling site was near a construction site that may have contaminated the soils with oils/diesel and affected soil microbial activity that led to lower values of RQ (Moller et al., 1996). This lower RQ for SOIL-A could also be the result of the additional consumption of oxygen in the biotic (e.g. nitrification) process or by the conversion of CO_2 into calcium carbonate (Kettlewell, 2004; Moller et al., 1996).

SOIL-B, on the other hand, was collected from a community garden where soil was tilled annually and had visible leaves and litter mixed within the soil. The higher RQ values of SOIL-B are also in agreement with other studies that show that organic-managed soils

can have a RQ of 1.10 due to root exudates growing in the soil before collection [Dilly, 2001].

The respiration rates measured for SOIL-A and SOIL-B columns (3.54±0.19 μmol/m^2/s and 4.04±0.18 μmol/m^2/s, respectively) are in the range of soils CO_2 flux measured by other researchers across the world. For example, work done by (Turcu et al., 2005) in soil columns shows a range of soil CO_2 flux about 0.1 – 2.2 μmol/m^2/s in the soil columns, and the measurements done by (Brydie et al., 2013) show a respiration range of 0.5 – 6 μmol/m^2/s for a set of field and lab soil tests.

These measured GER values for closed soil columns (hence soil RQ) with corresponding CO_2 respiration rates were used as an input for the model in simulating O_2 and CO_2 concentration profiles for both the soils and predicting the GCR (ΔCO_2: ΔO_2) at the soil surface.

4.3.1 Model vs Measurements: O_2 and CO_2 profiles for estimating soil tortuosity, τ

Appropriate input values required for the simulation of the proposed soil model described in the model chapter (Chapter 3), such as physical characteristics (air porosity and water content), respiratory values (soil RQ, respiration rates), were established in the previous sections. Here measured O_2 and CO_2 profiles for SOIL-A and B were compared to the model for a range for tortuosity typical to these types of soils (Figure 1-15; top and lower panels).

The range of tortuosity factor (τ =2, 3, 4,5) chosen for our model simulation was based on the research of Moldrup et al (2001) which showed that soils with sandy and loamy type texture and having about 20% of their volume as water have a tortuosity between 2 to 5 (Moldrup et al., 2001).

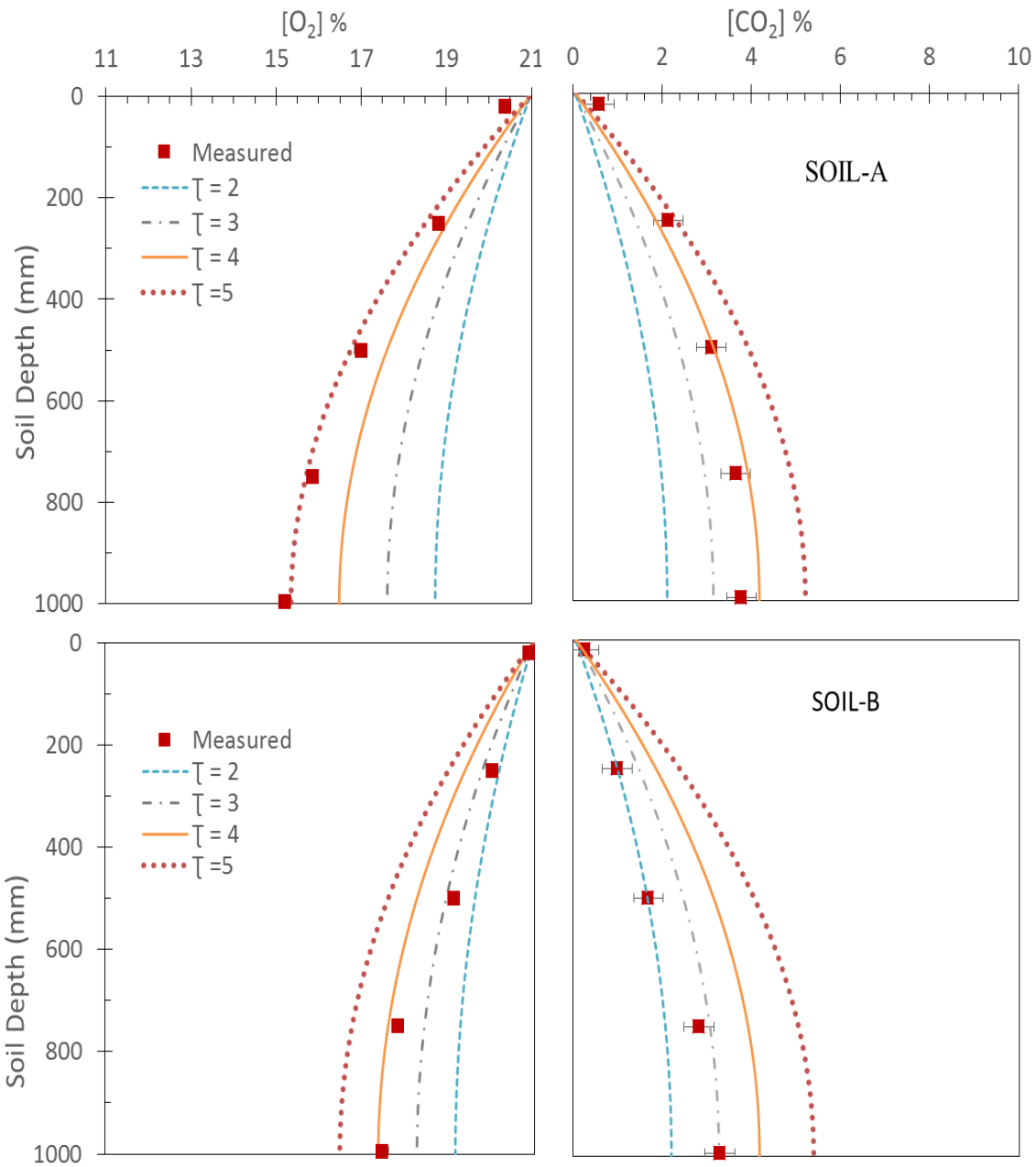

Figure 4-15: Measured $[O_2]$ and $[CO_2]$ %at depths with model predictions for tortuosity factor, τ = 2, 3, 4 and 5. For SOIL-A (top panel) model simulation used a respiration rate of 3.54 µmol/m^2/s, and an RQ of 0.66 (measured on 13 Jun 2016). For SOIL-B (lower panel), the model used a respiration rate of 4.04 µmol/m^2/s, and an RQ of 0.99 (measured on 29 Mar 2017).

From Figure 1-15 (top panel), we find a model predicted O_2 profile across the soil column for SOIL-A that matched measured concentrations for the assumption of $\tau = 4 – 5$, while the CO_2 profile matched for $\tau = 4$.

From the comparison of the measured and the model gradients for SOIL-B (Figure 1-15, lower panel) we see that for the CO_2 profile, $\tau = 2$ matches the CO_2% from the surface to 50 cm depth of soil, while CO_2% measured below 50 cm to 1m is in good agreement for $\tau = 3$. In the same Figure, for the O_2 profile, model predictions follow the same trend as measured up to 50 cm from the surface when $\tau = 3$; and below 50 cm for $\tau = 4$.

For both SOIL-A and B, we see that the average tortuosity of these soils are lower for CO_2 compared to O_2 gas. It is likely that a portion of total CO_2 gases in soils diffused faster through soil water content which was facilitated due to the nearly 30 times higher solubility of CO_2 in water than O_2.

In both cases the model provides a reasonable approximation for the measured results. For both of CO_2 and O_2 profile predictions a tortuosity of 4 to 5 was for SOIL-A and a tortuosity of 3 to 4 was used for SOIL-B. Since the model predictions represent the soil gas profiles best, model simulations for the regular and leak added soil gases profiles during the tests used values of tortuosity within this range. However, further studies are required for better measurement of for soil tortuosity (both in gas and liquid phase) and its variations with soil depths. Soil studies are beyond the scope of the work presented here but could form the basis for future research.

From the comparison of model and the measured concentration gradients for the measured fluxes and GER, we see our model predictions were reasonably good and justified that the model of GCR should work.

4.3.1 Gas concentration ratio (GCR) measurements using GAS-3

The gas exchange system, GAS-2, was tested for soil characteristics against a cylinder gas which is not ideal for field measurements. A better comparison of the near surface O_2 and CO_2 could be made with actual ambient air (similar to the field measurements). Therefore, a modified gas analysis system, GAS-3, was made to use ambient air as a reference as shown in Figure 1-6. The modified GAS-3 system introduced additional tubing for drawing room air from 1-2 m above the soil column which was then used (after CO_2 was scrubbed) as gas for 'Ref' and 'Room Air' channels in GAS-3. In this version, we had the sequence of *'Ref', 'CalGas', 'Soil Surface', 'Soil Flux'* air in the sample cell (Figure 1-16).

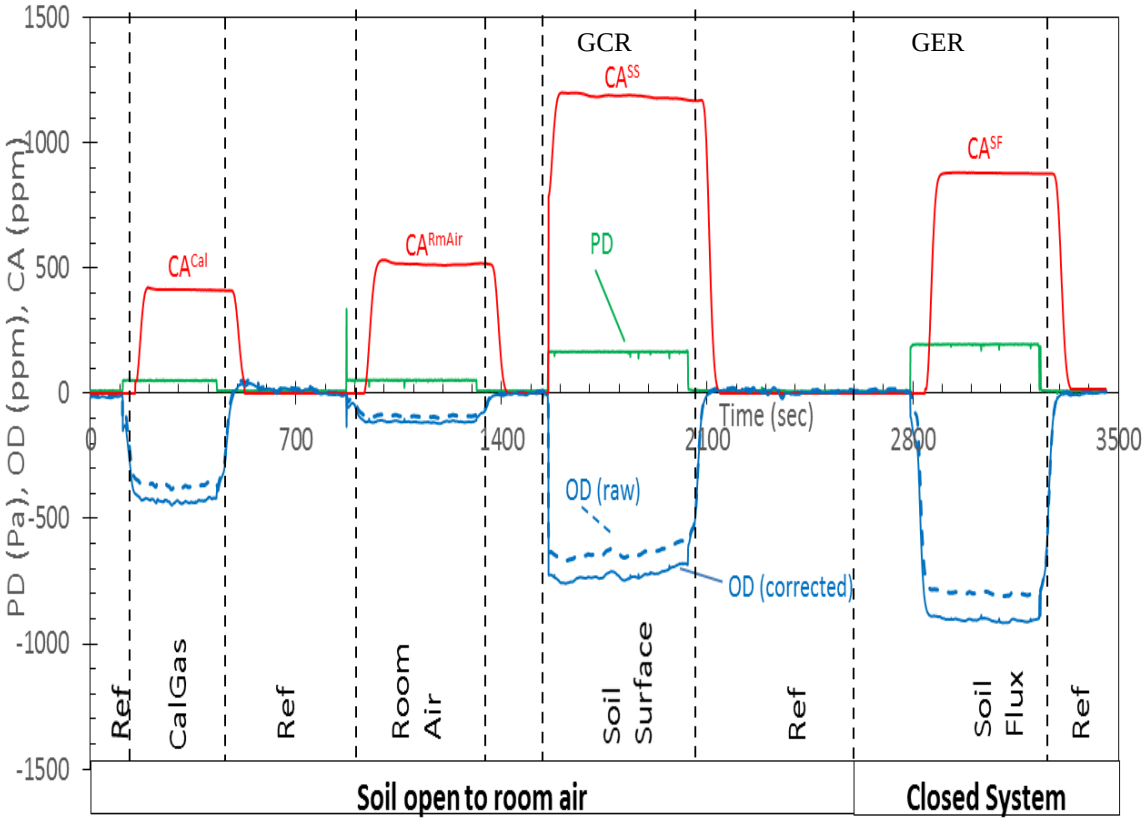

Figure 4-16: PD (Pa), OD (ppm), and CA (ppm) data for gas analysis for both soil column open and closed systems. Before and after running CalGas, Room Air, Soil Surface, and Soil Fluxes in sample cell, GAS-3 was flushed by flowing Ref gas both in reference and sample cells. Green, blue and red lines represent PD (Pa), OD (ppm) and CA (ppm) respectively, while the 'dashed' blue line is for raw OD and 'solid' blue line for pressure corrected OD.

The figure above demonstrates that before switching to a different gas in the sample channel the OD(ppm), CO_2(ppm), and PD(Pa) between 'Ref' and 'Sample' cells of the GAS-3 were set to reference zero position. This was set by running the 'RefGas' in both channels.

For GAS-3, adjusting the valve positions, different streams of gases were drawn into the sample channel which led to a pressure differential (PD) between the 'Ref' and 'Sample' cells of the DOX analyzer. The artifact associated in the OD measurements due to this sudden PD was corrected by the calibration method discussed in section 4.2.6.2(c). The GAS-3 used the mixture of the CO_2 scrubbed room air with 20.04% CO_2 in N_2 as the internal 'CalGas'. The readings for CO_2 and OD were stable for every gas into in the sample cell against the reference room air except the gas from near surface soils where OD^{ss} slightly fluctuated during the run time. This discrepancy occurs as the soil column was open to room air and variation of the ambient pressure affects the differential pressure sensor of the DOX (and hence the OD reading).

Table 4-4: SOIL-B characteristics in GAS-3 for three consecutive sequences for soil tested on 7th Nov 2016.

CalGas			Room Air			Soil Surface			Soil Flux			
ΔCO_2	**ΔO_2**	**GER**	**ΔCO_2**	**ΔO_2**	**GER**	**ΔCO_2**	**ΔO_2**	**GCR**	**ΔCO_2**	**ΔO_2**	**SR**	**GER (RQ)**
ppm	**ppm**	**-**	**ppm**	**ppm**	**-**	**ppm**	**ppm**	-	**ppm**	**ppm**	**µmol/m²/s**	-
415	431	0.95	521	120	NA	673	449	1.50	695	712	4.24	0.98
404	417	0.97	513	117	NA	658	444	1.48	689	710	4.00	0.97
395	408	0.97	521	113	NA	675	445	1.52	686	671	3.88	1.02

From the measured data given in Table 4-4, we see that for 'CalGas' the GAS-3 can repeatedly measure the GER of 0.96±0.02 against the expected value of 0.95; which is a very good precision for the gas measurement. This validates the accuracy of the measurements of GER for the 'Room Air' as 2.43±0.02; and the measurement of GCR for 'Soil Flux' at near surface as 1.5±0.3. Measuring the GCR at the soil surface, in GAS-3, improves the technique of checking our hypothesis of monitoring an anomaly in the differential gas concentration ratio at near-soil surface. The inclusion of the GCR in the measurements advances our method for CO_2 monitoring in two ways:

i) Differential concentrations measured with respect to background ambient air to reflect field monitoring conditions.

ii) Open soil column surface avoids the chance of pressure build up at the soil surface and possible artifacts in OD readings.

4.3.2 Leak detection by GCR measurements using GAS-3 for SOIL-B

Two CO_2 leak detection tests, five months apart from each other, were carried out on the SOIL-B column using GAS-3. In these tests, pure CO_2 gas was injected into the bottom chamber of the soil column as a representation of leaked CO_2 reaching 1-m depth. An automatic flowmeter (range of 0 – 1 ml/min) was used for the injection of CO_2 into SOIL-B.

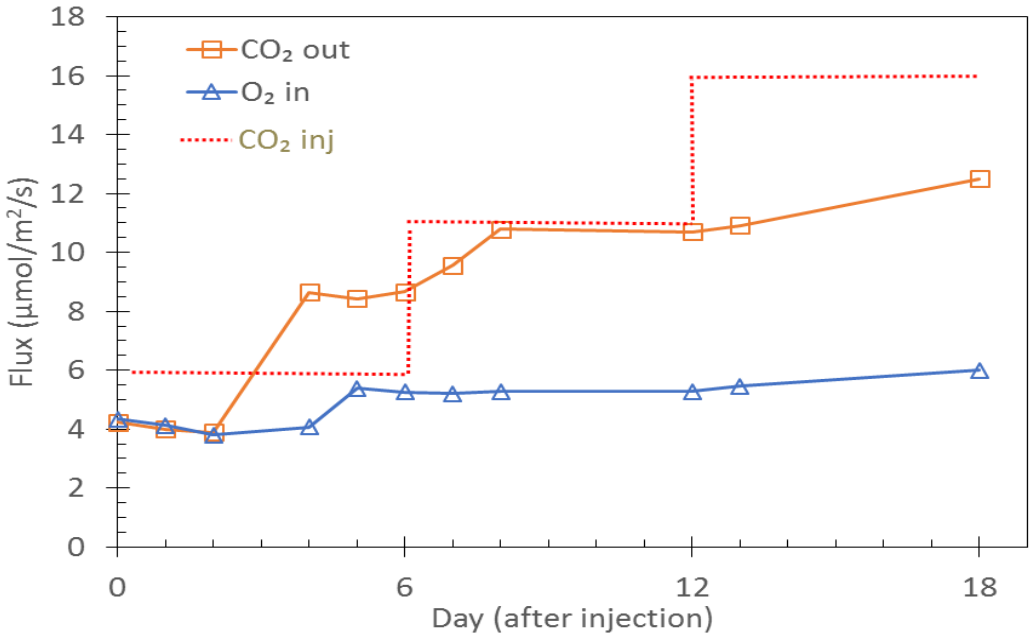

Figure 4-17: CO_2 and O_2 fluxes from and into the soils during Test-1 for injection of CO_2 at 1m depth. Flux measurements at the surface was started at time t = 0, prior to injection, and continued during the injection.

Before introducing any leaked CO_2, soil properties such as respiration rates, RQ, total porosity, and water content were measured. After each leak simulation test, the columns were flushed with room air using a vacuum pump at a speed of approximately 1 L/min and

left for several weeks to let the soil microbial activity reach a natural equilibrium state. For the first injection of pure CO_2 we chose the lower rates within the range of typical soil respiration rates to avoid possible build-up of pressure in soil layers which could affect gas diffusion. Initially, we injected at a rate of 0.08 – 0.21 mlCO_2/s (equivalent to soil respiration rates of 6 – 16 μmolCO_2/m^2/s). The first injection of CO_2 (6 μmol/m^2/s) was continued for five days, then increased by 5 μmol/m^2/s on the 6^{th} and 12^{th} days. The total CO_2 injection period in the soil column continued for 18 days (Figure 1-17).

During the injection period, O_2 and CO_2 flux at the surface were measured continuously to check their stability. The measured values of O_2 and CO_2 fluxes, Figure 4-17, at the soil surface shows that CO_2 fluxes from the soil started to increase gradually two days after injection and continued rising, while the O_2 fluxes into the soils remained almost constant during entire injection period. The lack of change in O_2 flux confirms that our injection of extra CO_2 did not create any noticeable air pressure inside the soils that could affect gas diffusion.

4.3.2.1 Comparison of Model and measured GCR for SOIL-B

The GCR (ΔCO_2: ΔO_2) measurements for two individual CO_2 leak simulations into SOIL-A and SOIL-B columns (referred as Test-1 and Test-2 respectively) were carried out. However the results for SOIL-A were not appropriate for realistic field conditions and provided the impetus to develop the GAS-3 system that could be applied under real-world filed conditions. SOIL-A results are given in Appendix-1 and this chapter gives the details of CO_2 leak tests performed on SOIL-B. Measured GCR was compared with the

corresponding model predictions for each injection rate. Measured GCR values for SOIL-B in Test-1 are in agreement with the model predictions for all leak tests (Figure 1-18)

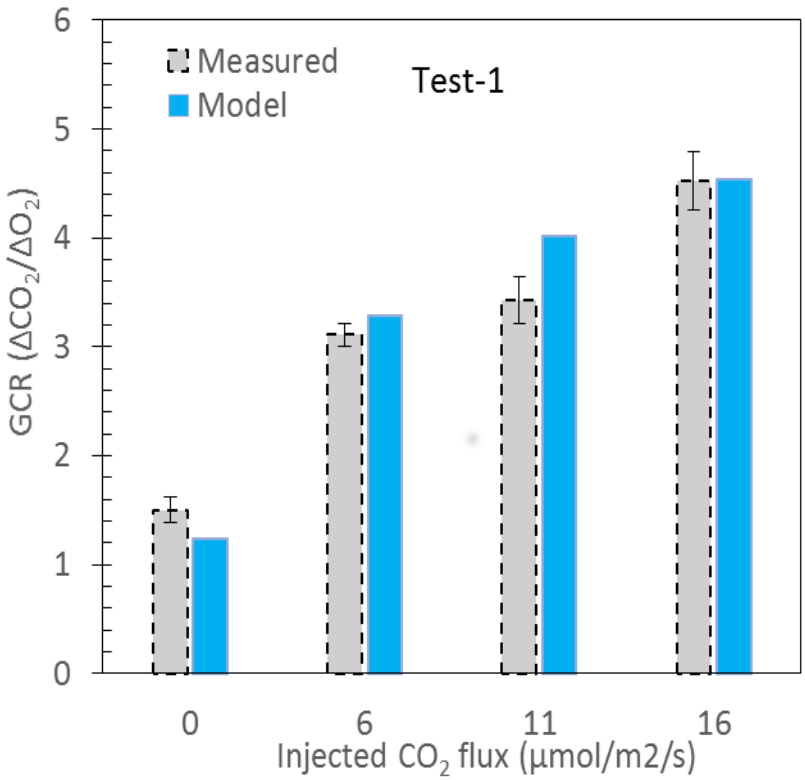

Figure 4-18: Comparison of measured and model predicted GCR for different rates of CO_2 injection. Model simulation used the respiration rate of 4 µmol/m2/s, RQ of 0.99, and 18% water that were found in soil before the test.

As shown in Figure 1-18, when no CO_2 was injected into the soil column the GCR was 1.52±0.02 which is 1.17 times higher than the model predicted. The GCR values increased

2 times from the base levels with the addition of a CO_2 leak of 6 μmol/m^2/s. This increasing trend of GCR continued with the incremental injection rates and became 2.3-times and 4.3-times higher than the background for leaks of 9 μmol/m^2/s and 15 μmol/m^2/s respectively. This comparison of measured and model data confirms that GCR values can be used reasonably in detecting any CO_2 leaks ≥ 6 μmol/m^2/s.

4.3.1 Detection limit of the GCR method

The results of the GCR test for different leak simulations for SOIL-B in the previous section, verify our proposed method of detecting steady small scale leaks from belowground by analyzing the relationship of the GCR in near-surface soil layers (w.r.t ambient air) along with soil respiration and RQ values. These tests (along the tests done for SOIL-A as well, given in Appendix-1) on the soils with different biological activities confirm that our model can be used to detect leaks as small as 6 μmol/m^2/s given that the soil properties are known.

As a proposed tool for the detection of leaked CO_2, the following figure gives the limit of the GCR measurements at near-surface soils for a wide range of soil RQ. The range of RQ was mainly chosen from previous studies discussed and our measurement on two soils described here. Figure 4-19 shows the model predicted GCR values (w.r.t ambient air) for soil RQ ranging from 0.40 to 1.60. This demonstrates that GCR and soil RQ have a linear relationship; that is, higher soil RQ will lead to higher GCR values at the surface. According to the model, the maximum expected GCR value of a regular biotic soil should lie under 2.0; exceeding this number can be taken as an indication that a CO_2 leak invaded the soil column (Figure 4-19).

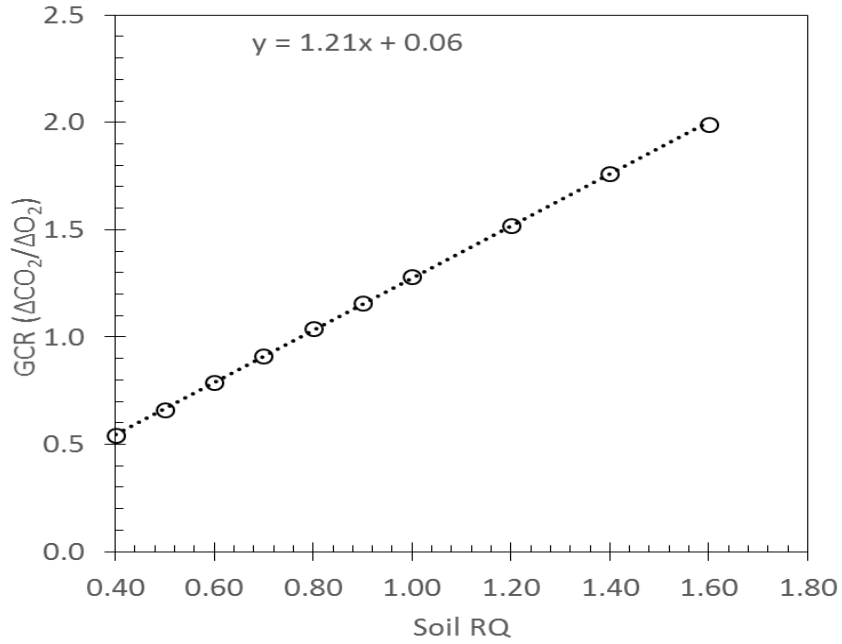

Figure 4-19: The expected biological range of the GCR at the near-surface soil for a possible range of soil RQ (based on the model).

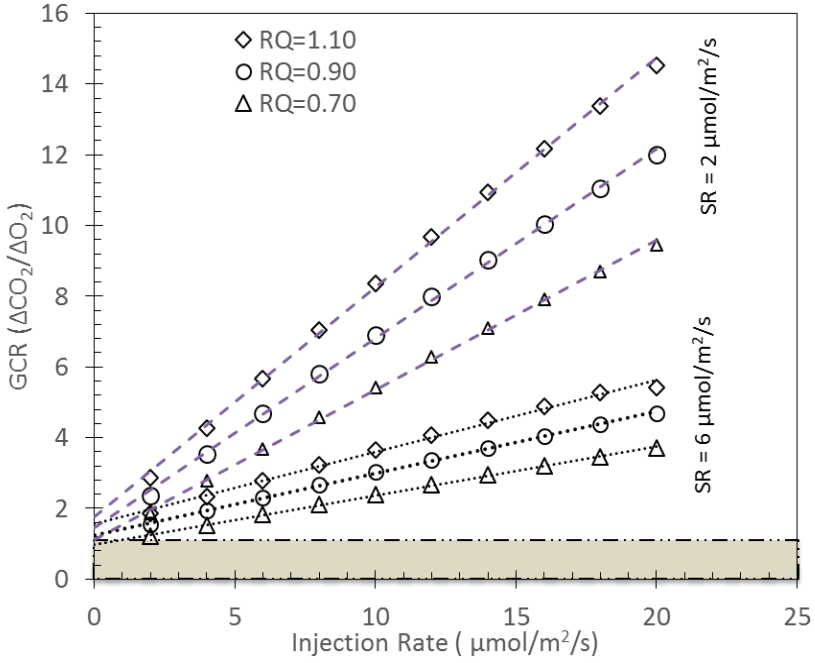

Figure 4-20: Model detection limit of the GCR for various RQ and soil respiration rates.

Our model also shows that the respiration flux of soils is also important for the detection limit by using GCR measurements. In Figure 1-20, we see that the detection limit of the method is lower if the soil has lower respiration rates. For example, detection of any leak ≥ 4 $\mu mol/m^2/s$ will be comparatively easier for SR of 2 $\mu mol/m^2/s$ than for respiration of 6 $\mu mol/m^2/s$. Similarly, the detection limit shifts towards higher values for RQ of 0.70 to 1.10 at any respiration rate. However, the level of difficulty will increase for the detection of small scale leaks discussed here if the background soil respiration flux is comparatively higher (shaded region in the Figure 1-20).

Chapter 5. **Carbon sequestration in soil**

5.1 Introduction

Monitoring CO_2 leaks from the results of leak added tests for GCR measurements in the previous chapter support the feasibility of using this technique in CO_2 leak characterization. However, the observed O_2 and CO_2 concentrations during the entire period of artificial CO_2 leaks in the soil showed some extent of discrepancy with the expected concentration gradients. Since the soil was prepared to have homogenous properties and no air pockets across the column where CO_2 can accumulate, it was thought that injected CO_2 would eventually reach the soil surface once equilibrium conditions were established in the soil column. The measured flux (Figure 1-17) shows that a 2 day of delay was evident in allowing CO_2 to pass through the soil along a presumably tortuous path. The injected CO_2 was eventually released to the atmosphere, but the magnitude of the flux was smaller than anticipated. For example, with an existing background of about 4 $\mu mol/m^2/s$, the addition of 6, 5, and 5 $\mu mol/m^2/s$ over 3 steps during 18 days of injection was expected to elevate the maximum surface flux to near 20 $\mu mol/m^2/s$, while the highest measured flux was about 13$\mu mol/m^2/s$.

5.2 Methods

To test this possible accumulation of CO_2 in soil, another test (Test-2) with continuous measurement of soil O_2 and CO_2 profiles was carried out during the injection in the SOIL-

B column. In this Test-2, the concentration of O_2 and CO_2 were recorded for different depths (using GAS-1) with time for the entire period of the CO_2 injection along with the GAS-3 measurements. Before this test, SOIL-B column was flushed with room air and left to dry for several weeks to reach natural equilibrium between O_2 consumption and CO_2 production rates within the column. Prior to the injection of CO_2, the measurements of GAS-3 for the SOIL-B column for three consecutive sequences are given in Table 5-1 below, where we find that RQ of the soil decreased significantly to 0.78 from the previously measured average of 0.99 (reported in Chapter 4 for SOIL-B Test-1).

During the injection of CO_2, 60 ml of soil air was extracted at 4hr, 8hr, 18hr, 24hr for the first day of injection and later for every 24hr. This was performed for each depth (2, 50, 25, 98 cm). Soil air samples were run using GAS-1 system for the measurement of the O_2 and CO_2 concentrations.

5.3 Results and Discussion

Soil respiration rates measured (Table 5-1) before the injection tests shows that biological activity was reduced compared to the previous Test-1 (possible reasons are discussed in later sections). The trend in the surface flux (Figure 1-1) during the injection period was similar to what was found in Test-1, showing the difference between measured and expected CO_2 levels at the soil surface. A detailed analysis of this discrepancy along with model simulations on the soil profiles for added leaks and the possibility of enhanced CO_2 sequestration is discussed in the subsequent sections.

Table 5-1: SOIL-B characteristics in GAS-3 for three consecutive sequences for soil tested on 29Mar 2017.

CalGas			Room Air			Soil Surface			Soil Flux			
ΔCO_2	**ΔO_2**	**GER**	**ΔCO_2**	**ΔO_2**	**GER**	**ΔCO_2**	**ΔO_2**	**GCR**	**ΔCO_2**	**ΔO_2**	**SR**	**GER (RQ)**
ppm	ppm	-	ppm	ppm	-	ppm	ppm	-	ppm	ppm	µmol/m²/s	-
335	350	0.96	512	98	NA	636	531	1.20	520	663	2.11	0.78
314	321	0.98	490	77	NA	668	559	1.20	525	674	2.13	0.78
303	317	0.96	505	86	NA	624	507	1.23	503	663	2.04	0.76

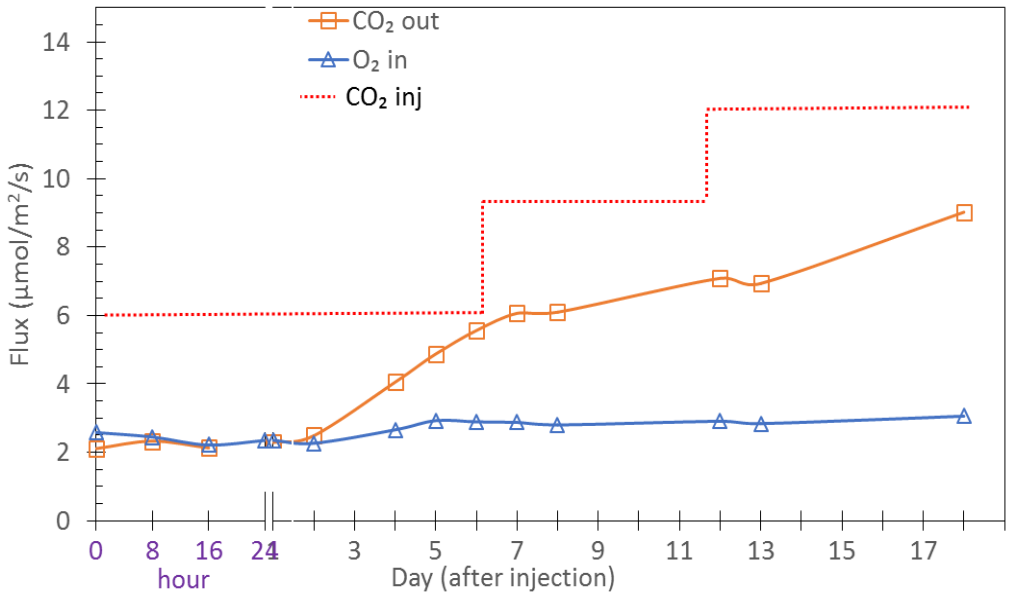

Figure 5-1: CO_2 and O_2 fluxes from and into the soils during injection of CO_2 at 1-m depth (Test-2 for SOIL-B).

Figure 1-2 shows the gradual change in the O_2 and CO_2 profiles in the SOIL-B column during injection at a rate of 6 µmol/m^2/s for the first 5-days (for simplicity, concentration profiles measured during the 6th to 18th were not plotted here).

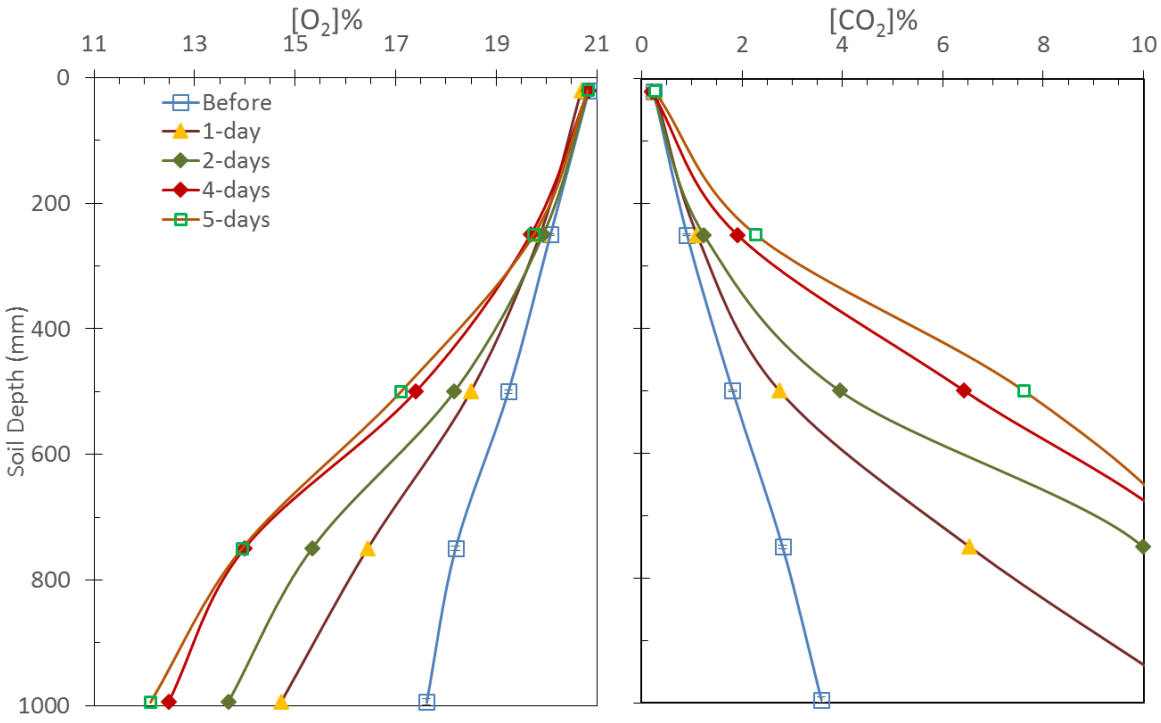

Figure 5-2: Changes in O_2 and CO_2 mixing ratios during the injection of 6 µmol/m^2/s for the first 5-days for SOIL-B.

The results for CO_2 and O_2 (%) were compared with the model predictions for similar leak rates (Figure 1-3). We find that our model can predict the concentration profiles for the CO_2 leak added soil column reasonably well. An overestimate of about 4.7% in O_2 and 5.5% underestimate in CO_2 is observed at 50 cm depth. However, model predictions

underestimated both the concentrations below 50 cm to 1m depth; for O_2 it gave almost 27% overestimation, while CO_2 could not be measured after the 5th day as its concentration at the lower levels (98cm and 75cm) reached the maximum limit of 10% that the Qubit S147 analyzer of GAS-1 can measure.

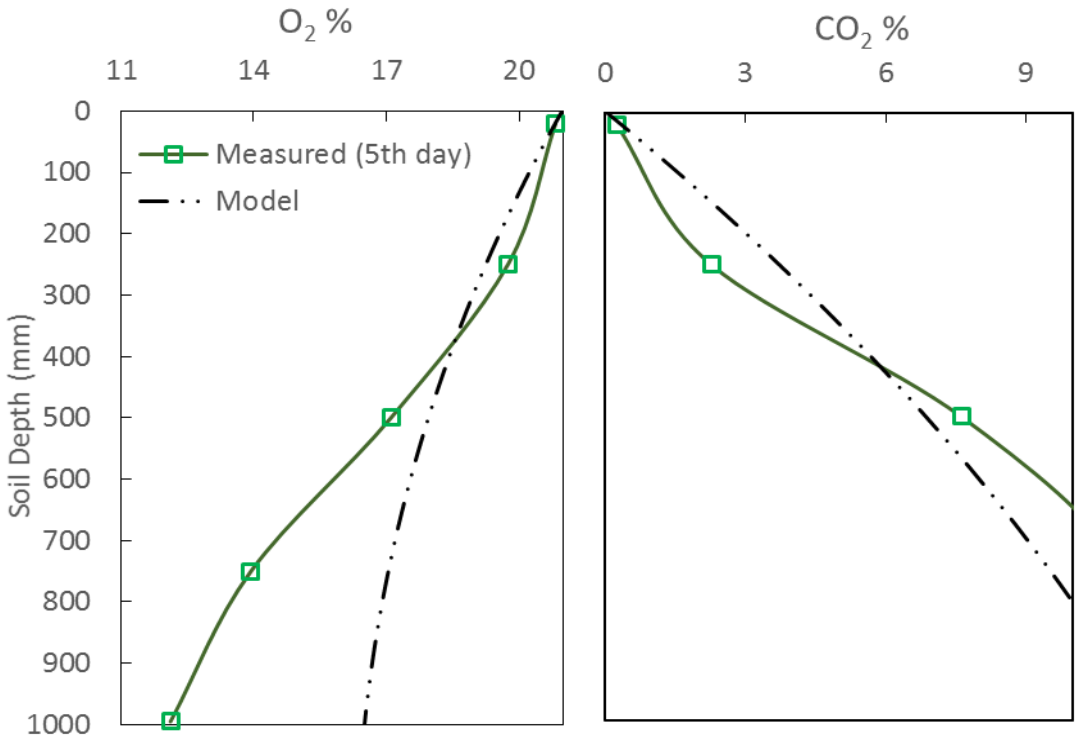

Figure 5-3: Comparison of measured (solid line) and model predicted (dot-dashed) O_2 and CO_2 profiles at the 5th days during the injection of CO_2 at a rate of 6µmol/m^2/s. Model simulations used the same environmental and physical properties (SR of 2.11 µmol/m^2/s, water content of 14%) measured and estimated ϒ of 3 for SOIL-B prior to CO_2 injection at Test-2 (Table 5-1).

5.3.1 Comparison of model and measured GCR for SOIL-B

The measured GCR values at the SOIL-B surface in Test-2 were compared with model predictions in Figure 1-4. Although, the model overestimated the GCR for all the three injection rates (6, 9, and 12 µmol/m^2/s respectively), the comparison once again confirms that a leak of ≥ 6 µmol/m^2/s can easily be distinguished from the background GCR of the soil.

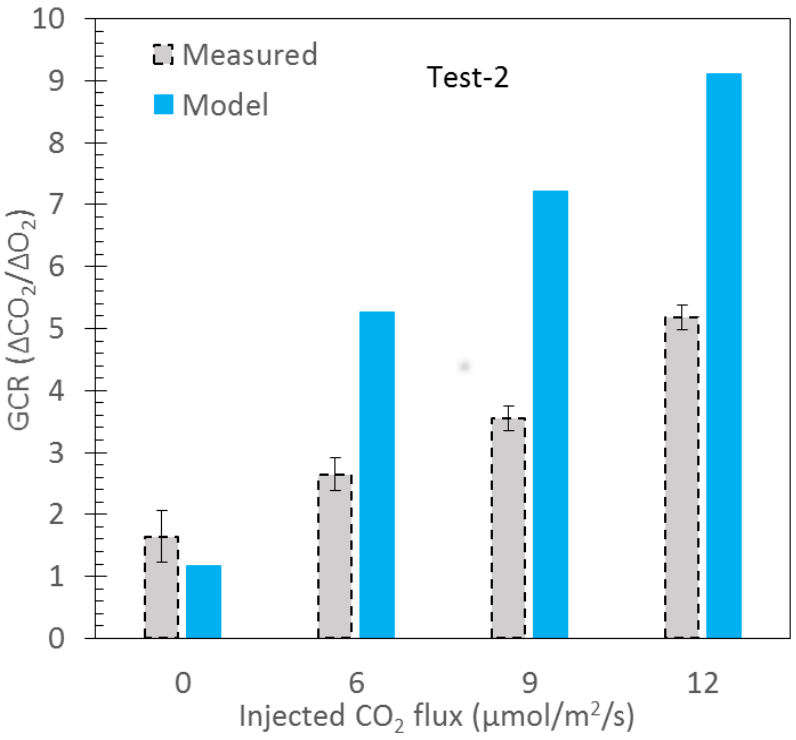

Figure 5-4: Comparison of measured and model predicted GCR for different rates of CO_2 injection during Test-2 for SOIL-B. Model simulation used respiration rate of 2.31 µmol/m^2/s, RQ of 0.78, and 14% water content found in soil before the test.

From Figure 1-4, we see that when no leak was injected into the soil column the GCR was 1.64±0.41 for Test-2. The GCR increased 1.62 times from the base level with the addition of a CO_2 leak of 6 μmol/m^2/s. This increasing trend of GCR continued and was about 2 and 3 times larger than the base case with no leak for the injection of leaks of 9 and 12 μmol/m^2 /s respectively.

Although the Test-1 model predictions for different leak scenarios are comparable with the measured GCR, it should be kept in mind that the soil in Test-1 was freshly packed in the column and the microbial activity was high. In contrast, for Test-2, when the soil was nearly two months older, the model highly overestimated the GCR (Figure 1-4). This overestimation of GCR values could arise since only addition of leaked CO_2 in soils and their contribution in gaseous phase diffusion was considered in the model, and conversion of gaseous CO_2 into the liquid phase (HCO_3^- and CO_3^{2-} species) and its possible accumulation in soil layers, was not counted. Liquid phase CO_2 and carbonate species might have played a higher role in CO_2 leak added soil than was found for normal soil conditions, which was not factored in during the model runs displayed here. Soils exposed to CO_2 and the possible carbon sequestration mechanisms are relevant topics for further research.

5.3.2 CO_2 accumulation in soil column

The accumulation of injected CO_2 in soil was calculated in two different ways: by i) measuring the flux from the soil column before and during the injection period, and ii) measuring the mixing ratio gradients before and after the injection.

The soil respiration rate (CO_2 flux) was measured before the injection and for simplicity it was considered that it would remain constant during the injection period. The total estimated amount of injection was about 1461 ml of CO_2 over the 12-days (out of 18 days injection period to avoid the artifacts of time delays CO_2 takes to reach surface).

The volume of accumulated CO_2 in the soil column was estimated from the difference in CO_2 concentration (both gas and liquid phase) before and after the injection. In this estimation, the volumes of gaseous and dissolved CO_2 in soil water were measured from the known soil air porosity (28%) and water content (15%) in the column and assuming that the gaseous and aqueous phase reach an equilibrium condition. The amount of CO_2 that can possibly have accumulated in the soil column was about 380 ml which is 26% of total injected CO_2; and more surprisingly, 34% of the accumulated CO_2 was found as dissolved CO_2(w) in soil water. The reasons for this relatively high volume of CO_2 sequestration in soil may include a range of factors: i) availability of pure CO_2 accelerated the dissolution of CO_2 into water due to its high solubility and this CO_2 was converted to be stored in aqueous phase carbon compounds; ii) injected CO_2 occupied in the air pockets in soil that might have created by the adverse effects of pure CO_2 on soil properties by creating O_2 deficiency (Zhou et al., 2013) in soil, or decreasing soil pH and nutrient concentrations that resulted in lower microbial activity (Zhao et al., 2017).

This accumulation of CO_2 in soil also indicates that there was a possibility of artifacts in the total injection amount which may occur due to any pressure in the injection chamber that could affect the injection flow rate. Some error also may arise in the mixing ratio measurement of CO_2 at 75 and 98 cm from the surface which was calculated by the extrapolation of the data as these concentrations were higher than the limits GAS-1 could measure. This suggests that further rigorous analysis is required to investigate the accumulation of the leaked CO_2 in the soils and its impact on the biotic and non-biotic activities in near-surface soils as little to no literature is available.

Chapter 6. **Conclusions**

6.1 Summary

In CCS, CO_2 is injected into the sub-surface and is expected to remain there permanently. While this may be the case for the majority of the CO_2 injected, fractures, faults or abandoned wells may allow a portion (estimated at ≤0.01% of the carbon stored per year, (Keeling et al., 2011; Leuning et al., 2008; Miles et al., 2005)) to leak back to the atmosphere. While small, such leaks undermine the effectiveness of geological storage and create a potential for a health hazard to animals or humans at the soil surface. For example, if only 10% of the CO_2 from a 0.01% leak made it to the surface in a storage site containing 20 Mt CO_2, more than 200 L/min would be venting to the atmosphere. If this gas entered the atmosphere over a 1000 m^2 land area, the average flux would be more than 144 μmoles/m^2/sec, a rate about 20 times that observed in a typical soil (Leuning et al., 2008; Risk et al., 2002). Since CO_2 is heavier than air, the CO_2 may accumulate on the surface and asphyxiate air-breathing species.

As discussed in Chapter 1 (Introduction) and Chapter 2 (Literature review) of this dissertation, the early detection of CO_2 leaks will be important for the economics and public acceptability of CCS. The objective of the work reported in this dissertation, was to develop the theory and practical data to describe a relatively low-cost approach to identifying a CO_2 leak at the rate of 10's of μmoles CO_2/m^2/sec and to be able to distinguish it from normal biological fluxes of CO_2 in soils.

The theoretical work described in Chapter 3 was needed to understand how a wide range of soil conditions (such as temperature, water content, biological activity or soil respiratory quotient (RQ= CO_2 production/ oxygen uptake)) would impact measureable characteristics of soil gas flux in the presence or absence of a CO_2 leak.

Questions included how well we understand the near-surface soil gas exchange dynamics. What are the relative roles of key variables such as soil properties and environment in this exchange? And what contribution does the aqueous phase in soils make in the transport of gases?

To address these questions, a one-dimensional steady-state model of gas reaction and diffusion was built and used (Chapter 3). This model considered both the gaseous and aqueous phase reaction and diffusion of O_2 and CO_2 in the top metre of a soil typical of Alberta, Canada. It showed that under typical conditions for soil pH and water content in Alberta, there would be no significant facilitated diffusion of CO_2 by HCO_3^- and CO_3^{2-} in the aqueous phase of soils.

This insight justified the creation of a subsequent model in which gases were only considered to move within the gas phase. However in this model, both diffusion and bulk pressure flow were considered in addition to the biochemical processes consuming O_2 and releasing CO_2. The pressure flow of gases could occur when the RQ deviated from 1.0, when there was an atmospheric pressure change or when there was a CO_2 leak entering near-surface layers of soil.

This model predicted that it should be possible to quantify and differentiate from ‘natural processes’, a CCS leak below the acceptable leaks as mentioned by Keeling et al (2011) and Miles et al (2005) using one of two metrics:

i) The mass flow of gas from the soil to the atmosphere,

ii) The ratio of the CO_2 and O_2 concentration gradients (Gas Concentration Ratio, $GCR=\Delta CO_2 : \Delta O_2$) between the soil surface and bulk air.

A laboratory-based experimental system was set up to test the feasibility of the GCR method (Chapter 4). The system incorporated a 1 m long soil column connected to a gas exchange system with instruments that included an infrared CO_2 analyzer and a differential O_2 analyzer.

Results of the controlled lab tests (Chapter 4 and Chapter 5) showed good agreement with the modeling studies for the use of GCR as a metric to identify CO_2 leaks from CCS storage sites of as low as 6 $\mu molCO_2/m^2/s$. While a promising technology, additional work is required to convert these findings into a practical method for the early detection of CO_2 leaks from CCS sites.

6.1 Recommendation of Future Studies

To improve our understanding of soil gas exchange and enhance the sensitivity of GCR measurements, future research should focus on the following areas:

a) In our model the ratio of CO_2 release against O_2 uptake (RQ) in soils was considered to be constant in every soil layer for the simplicity of the model; while it may vary depending on the pre-existing substrate quality and O_2 availability (Godley, 2004; Oliver Dilly, 2003). The substrate quality and their level of degradation need to be taken into consideration in our model as research shows that due to the synthesis of

lipids from carbohydrates the RQ fluctuates from 0.50 to 1.30 (Araújo et al., 2013)

.

b) Research is also needed to investigate the effect of soil drying during the long incubation periods, as the recent work of Fischer et al (2015) showed that both CO_2 production and O_2 consumption rates decreased and RQ dropped to 0.40 within the first 20 days of incubation for the reduction of soil water content. In contrast, from the same studies, it was also found that drying of soil for longer incubation periods (>20 days) can elevate the soil RQ by releasing more CO_2 from soil water. Therefore more work is needed here as our lab tests on soil in the column were incubated for more than a month and that might have contributed to our RQ measurements to some extent.

c) A recent study (Zhao et al., 2017) showed that elevated CO_2 from naturally leaking sites reduced the total organic carbon content, nutrient availability and pH in soils. It also found that an atmospheric concentration of 11.2% CO_2 had an adverse effect on the biogeochemical reactions of plants. Further work is needed on the effect of elevated CO_2 from belowground on soil respiration.

d) In this project, model predictions were tested only in a controlled lab setup with sieved and disturbed soils. Conducting these tests in-situ with a leak of CO_2 from belowground could give more realistic outcomes. Because atmospheric pressure change, wind flow at soil surface, the boundary between soil and atmosphere (due to grasses or shrubs) could all affect gaseous diffusion in soil, introducing these factors and their impact on the GCR measurements would improve the reliability of the proposed method.

e) Given the results obtained in this thesis, there is justification to design and build a portable gas analysis system that could be taken into the field to carry out the measurement of GCR in real time.

Overall, it can be concluded that the GCR in near-surface soils will carry the signature of the underlying biogeochemical reactions of soil. It is expected that, after more improvements on the areas that were ignored initially, measurements of the GCR at the soil surface may lead to identifying the invading CO_2 from the below ground carbon storage and can be used for characterizing the early leak detection at CCS sites.

References:

ACIS. (2012). Current and Historical Alberta Weather Station Data. Retrieved November 6, 2017, from https://agriculture.alberta.ca/acis/alberta-weather-data-viewer.jsp

Andersen, C. P., & Scagel, C. F. (1997). Nutrient availability alters belowground respiration of ozone- exposed ponderosa pine. *Tree Physiology*, *17*(6), 377–387.

Araújo, A. S. F., Cesarz, S., Leite, L. F. C., Borges, C. D., Tsai, S. M., & Eisenhauer, N. (2013). Soil microbial properties and temporal stability in degraded and restored lands of Northeast Brazil. *Soil Biology and Biochemistry*, *66*, 175–181. https://doi.org/10.1016/j.soilbio.2013.07.013

Armstrong, K., & Styring, P. (2015). Assessing the Potential of Utilization and Storage Strategies for Post-Combustion CO_2 Emissions Reduction. *Frontiers in Energy Research*, *3*(March), 1–9. https://doi.org/10.3389/fenrg.2015.00008

Ball, B. C. (1981). Modelling of Soil Pores As Tubes Using Gas Permeabilities, Gas Diffusivities and Water Release. *Journal of Soil Science*, *32*(4), 465–481. https://doi.org/10.1111/j.1365-2389.1981.tb01723.x

Bandyopadhyay, A. (Ed.). (2014). *Carbon Capture and Storage: CO_2 Management Technologies*. Apple Academic Press. 106 pp

Bazzaz, F. a. (1990). The Response of Natural Ecosystems to the Rising Global CO_2 Levels. *Annual Review of Ecology and Systematics*, *21*(1990), 167–196. https://doi.org/10.1146/annurev.es.21.110190.001123

Beaubien, S. E., Ciotoli, G., Coombs, P., Dictor, M. C., Krüger, M., Lombardi, S., Pearce, J. M., West, J. M. (2008). The impact of a naturally occurring CO2 gas vent on the shallow ecosystem and soil chemistry of a Mediterranean pasture (Latera, Italy). *International Journal of Greenhouse Gas Control*, *2*(3), 373–387. https://doi.org/10.1016/j.ijggc.2008.03.005

Bellante, G. J., Powell, S. L., Lawrence, R. L., Repasky, K. S., & Dougher, T. A. O. (2013). Aerial detection of a simulated CO2 leak from a geologic sequestration site using hyperspectral imagery. *International Journal of Greenhouse Gas Control*, *13*, 124–137. https://doi.org/10.1016/j.ijggc.2012.11.034

Brydie, J., Faught, B., Olson, M., Underwood, A., & Drozdowski, B. (2013). The laboratory simulation and field verification of seasonal soil-respired CO_2 flux at a proposed CCS project site. *Energy Procedia*, *37*, 4041–4048. https://doi.org/10.1016/j.egypro.2013.06.304

Cahill, A. G., Marker, P., & Jakobsen, R. (2014). Hydrogeochemical and mineralogical effects of sustained CO 2 contamination in a shallow sandy aquifer: A field-scale controlled release experiment. *Water Resources Research*, *50*(2), 1735–1755. https://doi.org/10.1002/2013WR014294

Campbell, G. S. (1985). *Soil Physics with BASIC: Transport Models for Soil-Plant Systems*. Elsevier B.V. 14-15 pp.

Canada NIR. (2017). *Canada's greenhouse gas emissions projections 2016*. Retrieved from https://www.canada.ca/en/environment-climate-change/services/climate-change/publications/2016-greenhouse-gas-emissions-case.html

Celia, M., Bachu, S., Nordbotten, J., Kavetski, D., & Gasda, S. (2005). Modeling Critical Leakage Pathways in a Risk Assessment Framework : Representation of Abandoned Wells. *4th Annual Conference on Carbon Capture and Sequestration DOE/NETL*, (MAY), 1–9 pp.

Chadwick, R. A., Arts, R. J., Bentham, M., Eiken, O., Holloway, S., Kirby, G., Pearce, J. M., Williamson, J. P., Zweigel, P. (2010). Review of monitoring issues and technologies associated with the long-term underground storage of carbon dioxide. *Geological Society Special Publication*, *313*(1), 257–275. https://doi.org/10.1144/SP313.15

Crovetto, R. (1991). Evaluation of Solubility Data of CO2 in H2O from 273 K to the critical point of water. *Journal of Physical and Chemical Reference Data*, *20*(3).

Curiel Yuste, J., Baldocchi, D. D., Gershenson, A., Goldstein, A., Misson, L., & Wong, S. (2007). Microbial soil respiration and its dependency on carbon inputs, soil temperature and moisture. *Global Change Biology*, *13*(9), 2018–2035. https://doi.org/10.1111/j.1365-2486.2007.01415.x

Czyz, E. A. (2004). Effects of traffic on soil aeration, bulk density and growth of spring barley. *Soil and Tillage Research*, *79*(2 SPEC.ISS.), 153–166. https://doi.org/10.1016/j.still.2004.07.004

Dawson, B., & Spannagle, M. (2009). *The Complete Guide to Climate Change*. Routledge. 9-13 pp.

Dessler, A., & Parson, A. E. (2010). *The Science and Politics of Global Climate Change* (Second). Cambridge University Press. 12-15 pp.

Dilly, O. (2001). Microbial respiratory quotient during basal metabolism and after glucose amendment in soils and litter. *Soil Biology and Biochemistry*, *33*(1), 117–127. https://doi.org/10.1016/S0038-0717(00)00123-1

Dilly, O. (2003). Regulation of the respiratory quotient of soil microbiota by availability of nutrients. *FEMS Microbiology Ecology*, *43*(3), 375–381. https://doi.org/10.1016/S0168-6496(02)00437-3

Downie, D. L., Brash, K., & Vaughn, C. (2009). *Climate Change: A Reference Handbook*. ABC-CLIO, Inc.

Environment of Canada. (2014). National Inventory Report 1990-2012: Greenhouse Gas Sources and Sinks in Canada - Executive Summary, 14. Retrieved from http://ec.gc.ca/ges-ghg/3808457C-9E9E-4AE3-8463-05EE9515D8FE/NIR2014-Exec Sum-Web-Final.pdf

Fischer, Z., & Blažka, P. (2015). Soil Respiration in Drying of an Organic Soil, (September), 181–192.

Friedmann, J., & Herzog, H. (2006). Geological Carbon Sequestration. In *MIT Report: Future of coal in a carbon constrained world* (pp. 43–76).

Gasda, S. E., Bachu, S., & Celia, M. A. (2004). Spatial characterization of the location of potentially leaky wells penetrating a deep saline aquifer in a mature sedimentary basin. *Environmental Geology*, *46*(6–7), 707–720. https://doi.org/10.1007/s00254-004-1073-5

Gaumont-Guay, D., Black, T. A., Griffis, T. J., Barr, A. G., Jassal, R. S., & Nesic, Z. (2006). Interpreting the dependence of soil respiration on soil temperature and water content in a boreal aspen stand. *Agricultural and Forest Meteorology*, *140*(1–4), 220–235. https://doi.org/10.1016/j.agrformet.2006.08.003

Gendrin, A., Fiah, N. M., Poupeau, F., Pekot, L. J., & Garnett, A. (2013). Rewards and challenges of seismic monitoring for CO_2 storage: A fluid substitution study in the gippsland basin, Victoria, Australia. *Energy Procedia*, *37*, 4145–4154. https://doi.org/10.1016/j.egypro.2013.06.316

Gibbins, J., & Chalmers, H. (2008). Carbon capture and storage. *Energy Policy*, *36*(12), 4317–4322. https://doi.org/10.1016/j.enpol.2008.09.058

Gluyas, J., & Mathias, S. (Eds.). (2013). *Geological Storage of Carbon Dioxide (CO_2): Geoscience, technologies, environmental aspects, and legal frameworks*. Woodhead Publishing Ltd. 68-82 pp.

Godley, A. R. (2004). Factors Affecting the Soil Microbial Quality Measurements of Biomass Quotient and Respiration Quotient. *Water and Environment Journal*, *18*(May), 73–79. https://doi.org/10.1111/j.1747-6593.2004.tb00500.x

Greene, C. H., Huntley, M. E., Archibald, I., Gerber, L. N., Sills, D. L., Granados, J., Bill, C. M., Walsh, M. J. (2017). Geoengineering, marine microalgae, and climate stabilization in the 21st century. *Earth's Future*, *5*(3), 278–284. https://doi.org/10.1002/2016EF000486

Györe, D., Gilfillan, S. M. V., & Stuart, F. M. (2017). Tracking the interaction between injected CO_2 and reservoir fluids using noble gas isotopes in an analogue of large-scale carbon capture and storage. *Applied Geochemistry*, *78*, 116–128. https://doi.org/10.1016/j.apgeochem.2016.12.012

Haefeli, S., & Bosi, M. (2004). *Carbon Dioxide Capture and Storage Issues – Accounting and Baselines Under the United Nations Framework Convention on Climate Change (UNFCCC)*. Paris: IEA information paper. Retrieved from http://www.iea.org/papers/2004/css.pdf

Harned, H., & Jr, R. D. (1943). The ionization constant of carbonic acid in water and the solubility of carbon dioxide in water and aqueous salt solutions from 0 to 50°. *Journal of the American Chemical Society*, *65*(4), 2030–2037. Retrieved from http://pubs.acs.org/doi/abs/10.1021/ja01250a059

Harris, J. M., Quan, Y., Xu, C., & Urban, J. (2006). Seismic Monitoring of CO_2 Sequestration. *Geophysics*, 1–8.

Hashimoto, S., & Komatsu, H. (2006). Relationships between soil CO_2 concentration and CO_2 production, temperature, water content, and gas diffusivity: Implications for field studies through sensitivity analyses. *Journal of Forest Research*, *11*(1), 41–50. https://doi.org/10.1007/s10310-005-0185-4

Herzog, H. J. (2001). New technologies could reduce carbon dioxide emissions to the atmosphere while still allowing the use of fossil fuels. *Environmental Science & Technology*, *35*(7), 148A–153A.

Ide, S. T., Friedmann, S. J., & Herzog, H. J. (2006). CO_2 leakage through existing wells: current technology and regulations. *8th International Conference on Greenhouse Gas Control Technologies*, 1–6.

IEAGHG. Qunatification Techniques for CO_2 Leakage, 2012/02, Janurary, 2012.

IPCC. (2005). *Special Reports on Carbon Dioxide Capture and Storage*. (L. Metz, Bert; Davidson, Ogunlade; de Coninck; Loose, Manuela; Meyer, Ed.). Cambridge University Press. https://doi.org/10.1002/anie.201000431

IPCC. (2007). IPCC Fourth Assessment Report (AR4). *Ipcc*, *1*, 976. https://doi.org/ISSN: 02767783

IPCC. Summary for Policymakers, Climate Change 2013: The Physical Science Basis. Contribution of Working Group I to the Fifth Assessment Report of the Intergovernmental Panel on Climate Change (2013). https://doi.org/10.1017/CBO9781107415324

IPCC. (2014). *Climate Change 2014: Mitigation of Climate Change. Contribution of Working Group III to the Fifth Assessment Report of the Intergovernmental Panel on Climate Change*. (O. Edenhofer, K. R. Pichs-Madruga, Y. Sokona, E. Farahani, S. Kadner, T. Z. and J. C. Seyboth, A. Adler, I. Baum, S. Brunner, P. Eickemeier, B. Kriemann, J. Savolainen, S. Schlömer, C. von Stechow, & Minx, Eds.). Cambridge University Press.

Jassal, R., Black, A., Novak, M., Morgenstern, K., Nesic, Z., & Gaumont-Guay, D. (2005). Relationship between soil CO_2 concentrations and forest-floor CO_2 effluxes. *Agricultural and Forest Meteorology*, *130*(3–4), 176–192. https://doi.org/10.1016/j.agrformet.2005.03.005

Jiang, X., Akber Hassan, W. A., & Gluyas, J. (2013). Modelling and monitoring of geological carbon storage: A perspective on cross-validation. Applied Energy, 112, 784–792. https://doi.org/10.1016/j.apenergy.2013.01.068

Ji, Y. (2016). *Developing Radioactive Carbon Isotope Tagging for Monitoring , Verification and Accounting in Geological Carbon Storage*. Phd thesis submitted to Columbia University. Retrieved from https://academiccommons.columbia.edu/download/fedora_content/download/ac:193901/CONTENT/Ji_columbia_0054D_13114.pdf

Karberg, N. J., Pregitzer, K. S., King, J. S., Friend, A. L., & Wood, J. R. (2005). Soil carbon dioxide partial pressure and dissolved inorganic carbonate chemistry under elevated carbon dioxide and ozone. *Oecologia*, *142*(2), 296–306. https://doi.org/10.1007/s00442-004-1665-5

Kayler, Z. E., Sulzman, E. W., Rugh, W. D., Mix, A. C., & Bond, B. J. (2009). Characterizing the impact of diffusive and advective soil gas transport on the measurement and interpretation of the isotopic signal of soil respiration. *Soil Biology and Biochemistry*, *42*(3), 435–444. https://doi.org/10.1016/j.soilbio.2009.11.022

Keeling, R. F. (1988). Measuring Correlations Between Atmospheric Oxygen and Carbon-Dioxide Mole Fractions - a Preliminary-Study in Urban Air. *Journal of Atmospheric Chemistry*, *7*(2), 153–176. https://doi.org/10.1007/BF00048044

Keeling, R. F., Manning, A. C., & Dubey, M. K. (2011). The atmospheric signature of carbon capture and storage. *Philosophical transactions.Series A, Mathematical, Physical, and Engineering Sciences*, *369*(1943), 2113–2132. https://doi.org/10.1098/rsta.2011.0016

Kettlewell, B. (2004). *The relationship between carbon dioxide and oxygen exchange during nitrification*.PhD thesis submitted to Dept. of Biology, Queen's University.18-22.

Kharaka, Y., Thordsen, J., Abedini, A., Beers, S., & Thomas, B. (2017). Changes in the Chemistry of Groundwater Reacted with CO_2: Comparison of Laboratory Results with the {ZERT} Field Pilot. *Procedia Earth and Planetary Science*, *17*, 241–244. https://doi.org/https://doi.org/10.1016/j.proeps.2016.12.043

Layzell, D. B., Gaito, S. T., & Hunt, S. (1988). Model of gas exchange and diffusion in legume nodules - I. Calculation of gas exchange rates and the energy cost of N2 fixation. *Planta*, *173*(1), 117–127. https://doi.org/10.1007/BF00394496

Leeuwen, C. Van, & Meijer, H. A. J. (2015). Detection of CO_2 leaks from carbon capture and storage sites with combined atmospheric CO_2 and O_2 measurements. *International Journal of Greenhouse Gas Control*, *41*, 194–209. https://doi.org/10.1016/j.ijggc.2015.07.019

Leung, D. Y. C., Caramanna, G., Maroto-Valer, M. M., Gendrin, A., Fiah, N. M., Poupeau, F., Pekot, L. J., Garnett, A., Benso, S., Cole, D. R, Harris, J., Quan, Y., Xu, C., Urban, J. (2006). Seismic Monitoring of CO_2 Sequestration. *Geophysics*, *37*(5), 1–8. https://doi.org/10.1016/j.rser.2014.07.093

Lee, K. K., Lee, S. H., Yun, S. T., & Jeen, S. W. (2016). Shallow groundwater system monitoring on controlled CO2 release sites: a review on field experimental methods and efforts for CO2 leakage detection. Geosciences Journal, 20(4), 1–15. https://doi.org/10.1007/s12303-015-0060-z

Leuning, R., Etheridge, D., Luhar, A., & Dunse, B. (2008). Atmospheric monitoring and verification technologies for CO2 geosequestration. *International Journal of Greenhouse Gas Control*, *2*(3), 401–414. https://doi.org/10.1016/j.ijggc.2008.01.002

Lewicki, J. L., Oldenburg, C. M., Dobeck, L., & Spangler, L. (2007). Surface CO_2 leakage during two shallow subsurface CO2 releases. *Geophysical Research Letters*, *34*(24), 2–7. https://doi.org/10.1029/2007GL032047

Lindroth, R. L. (2010). Impacts of Elevated Atmospheric CO_2 and O_3 on Forests: Phytochemistry, Trophic Interactions, and Ecosystem Dynamics. *Journal of Chemical Ecology*, *36*(1), 2–21. https://doi.org/10.1007/s10886-009-9731-4

Liu, G. (2012). Carbon Dioxide Geological Storage : Monitoring Technologies Review. In G. Liu (Ed.), *Greenhouse Gases - Capturing, Utilization and Reduction* (pp. 299–338). In Tech. https://doi.org/10.5772/2521

Lloyd, J., & Taylor, J. A. (1994). On the Temperature Dependence of Soil Respiration. *Functional Ecology*, *8*, 315–323.

Loh, Z., Leuning, R., Zegelin, S., Etheridge, D., Bai, M., Naylor, T., & Griffith, D. (2009). Testing Lagrangian atmospheric dispersion modelling to monitor CO_2 and CH4 leakage from geosequestration. *Atmospheric Environment*, *43*(16), 2602–2611. https://doi.org/10.1016/j.atmosenv.2009.01.053

Mann, M. E., & Jones, P. D. (2003). Global surface temperatures over the past two millennia. *Geophysical Research Letters*, *30*(15), 15–18. https://doi.org/10.1029/2003GL017814

Meinshausen, M., Meinshausen, N., Hare, W., Raper, S. C. B., Frieler, K., Knutti, R., Frame, D., Allen, M. R. (2009). Greenhouse-gas emission targets for limiting global warming to 2 degrees C. *Nature*, *458*(7242), 1158–1162. https://doi.org/10.1038/nature08017

Miles, N. L., Davis, K. J., & Wyngaard, J. C. (2005). Detecting leaks from bellowground CO2 reservoirs using Eddy Covariance. In D. C. Thomas & S. M. Benson (Eds.), *Geologic Formations-Results from the CO_2 Capture Project: Vol 2-Geologic Storage of Carbon Dioxide with Monitoring and Verification* (Vol. 2, pp. 1031–1044). Elsevier Ltd.

Moldrup, P., Olesen, T., Komatsu, T., Schjonning, P., & Rolston, D. E. (2001). Tortuosity, Diffusivity, and Permeability in the Soil Liquid and Gaseous Phases. *Soil Science Society of America Journal*, *65*, 613–623. https://doi.org/10.2136/sssaj2001.653613x

Moller, J., Winther, P., Lund, B., Kirkebjerg, K., & Westermann, P. (1996). Bioventing of diesel oil-contaminated soil: Comparison of degradation rates in soil based on actual oil concentration and on respirometric data. *Journal of Industrial Microbiology*, *16*(2), 110–116. https://doi.org/10.1007/BF01570070

NOAA. (2017a). Climate at a Glance. Retrieved November 9, 2017, from https://www.ncdc.noaa.gov/cag/

NOAA. (2017b). Trends in Atmospheric Carbon Dioxide. Retrieved November 2, 2017, from https://www.esrl.noaa.gov/gmd/ccgg/trends/global.html#global

Oertel, C., Matschullat, J., Zurba, K., Zimmermann, F., & Erasmi, S. (2016). Greenhouse gas emissions from soils — A review, *76*, 327–352. https://doi.org/10.1016/j.chemer.2016.04.002

Pacala, S. (2004). Stabilization Wedges: Solving the Climate Problem for the Next 50 Years with Current Technologies. *Science*, *305*(5686), 968–972. https://doi.org/10.1126/science.1100103

Pak, N. M., Rempillo, O., Norman, A.-L., & Layzell, D. B. (2016). Early atmospheric detection of carbon dioxide from carbon capture and storage sites. *Journal of the Air & Waste Management Association*, *66*(8), 739–747. https://doi.org/10.1080/10962247.2016.1176084

Park, Y. C., Huh, D. G., & Park, C. H. (2012). A pressure-monitoring method to warn CO 2 leakage in geological storage sites. *Environmental Earth Sciences*, *67*(2), 425–433. https://doi.org/10.1007/s12665-012-1667-2

Qi, Y., Xu, M., & Wu, J. (2002). Temperature sensitivity of soil respiration and its effects on ecosystem carbon budget: Nonlinearity begets surprises. *Ecological Modelling*, *153*(1–2), 131–142. https://doi.org/10.1016/S0304-3800(01)00506-3

Rackley, S. A. (2007). *Carbon Capture & Storage* (2nd ed.). Butterworth-Heinemann, Oxford, UK. 595-598 pp.

Richardson, K., Steffen, W., & Liverman, D. (2011). *Climate change, Global Risks, Challenges and Decisions*. Cambridge: Cambridge University Press. 218-428 pp.

Risk, D., Kellman, L., & Beltrami, H. (2002). Carbon dioxide in soil profiles: Production and temperature dependence. *Geophysical Research Letters*, *29*(6), 1087. https://doi.org/10.1029/2001GL014002

Roberts, J. J., Gilfillan, S. M. V., Stalker, L., & Naylor, M. (2017). Geochemical tracers for monitoring offshore CO2stores. International Journal of Greenhouse Gas Control, 65(June), 218–234. https://doi.org/10.1016/j.ijggc.2017.07.021

Romanak, K. D., Bennett, P. C., Yang, C., & Hovorka, S. D. (2012). Process-based approach to CO2 leakage detection by vadose zone gas monitoring at geologic CO2 storage sites. *Geophysical Research Letters*, *39*(15), 2–7. https://doi.org/10.1029/2012GL052426

Romanak, K., Sherk, G. W., Hovorka, S., & Yang, C. (2013). Assessment of alleged CO2 leakage at the Kerr farm using a simple process-based soil gas technique: Implications for carbon capture, utilization, and storage (CCUS) monitoring. *Energy Procedia*, *37*, 4242–4248. https://doi.org/10.1016/j.egypro.2013.06.326

Romanak, K., Yang, C., & Darvari, R. (2017). Towards a Method for Leakage Quantification and Remediation Monitoring in the Near-surface at Terrestrial CO2 Geologic Storage Sites. *Energy Procedia*, *114*(November 2016), 3855–3862. https://doi.org/10.1016/j.egypro.2017.03.1517

Sawyer, D., Harding, R., Pozlott, C., & Dickey, P. (2008, November). Carbon Capture and Storage — The Environmental and Economic Case and Challenges. *A Pembin Institute - ISEEE Thought Leader Forum*. Retrieved from www.pembina.org

Schaeffer, M., & van Vuuren, D. (2012). *Evaluation of IEA ETP 2012 emission scenarios*. Retrieved from papers2://publication/uuid/CB0F1E91-808C-4DD1-8777-7B7776CA454F

Schieman, C., Graham, A., Gelfand, G., McFadden, S. P., Tiruta, C., Hill, M. D., & Grondin, S. C. (2009). Weather and chinook winds in relation to spontaneous pneumothoraces. *Canadian Journal of Surgery*, *52*(5), 151–155.

Schütze, C., Lau, S., Reiche, N., Sauer, U., Borsdorf, H., & Dietrich, P. (2013). Ground-based remote sensing with open-path fourier- Transform infrared (OP-FTIR) spectroscopy for large-scale monitoring of greenhouse gases. Energy Procedia, 37, 4276–4282. https://doi.org/10.1016/j.egypro.2013.06.330

Schloemer, S., Furche, M., Dumke, I., Poggenburg, J., Bahr, A., Seeger, C., Vidal, A., Faber, E. (2013). A review of continuous soil gas monitoring related to CCS - Technical advances and lessons learned. *Applied Geochemistry*, *30*, 148–160. https://doi.org/10.1016/j.apgeochem.2012.08.002

Shackley, S., & Gough, C. (Eds.). (2006). *Carbon Capture and Its Storage : An Integrated Assessment*. Ashagte Publishing Ltd., UK. Chapter 2.

Šimůnek, J., & Suarez, D. L. (1993). Modeling of carbon dioxide transport and production in soil: Model development. *Water Resources Research*, *29*(2), 487–497. https://doi.org/10.1029/92WR02225

Smith, S. D., Huxman, T. E., Zitzer, S. F., Charlet, T. N., Housman, D. C., Coleman, J. S., Fenstermaker, L. K., Seemann, J. R., Nowak, R. S. (2000). Elevated CO_2 increases productivity and invasive species success in an arid ecosystem. *Nature*, *408*(6808), 79–82. https://doi.org/10.1038/35040544

Stangeland, A. (2007). A model for the CO_2 capture potential. *International Journal of Greenhouse Gas Control*, *1*(4), 418–429.

Stauffer, P. H., Keating, G. N., Middleton, R. S., Viswanathan, H. S., Berchtold, K. A., Singh, R. P., Pawar, R. J., Mancino, A. (2011). Greening coal: Breakthroughs and challenges in carbon capture and storage. *Environmental Science and Technology*, *45*(20), 8597–8604. https://doi.org/10.1021/es200510f

Turcu, V. E., Jones, S. B., & Or, D. (2005). Continuous soil carbon dioxide and oxygen measurements and estimation of gradient-based gaseous flux. *Vadose Zone Journal*, *4*(4), 1161–1169. https://doi.org/10.2136/vzj2004.0164

USDA. (1993). Examination and Description of Soils-Particle size distribution. In *Soil Survey Manual* (pp. 3–5). Soil Survey Division Staff - USDA Handbook. Retrieved from http://enviro-soil.com/soil-judging/reference_documents/Chpt.3ClayPercentageCoarseFragments_and_Texture_SoilSurveyManual1993.pdf

USDOE. (2012). *Best Practices for Monitoring , Verification , and Accounting of CO_2 Stored in Deep Geologic Formations – 2012 Update* (Second). U.S. Department of Energy. https://doi.org/DOE/NETL-2012/1568

USDOE. (2017). National Energy Technology Laboratory. Retrieved November 2, 2017, from www.netl.doe.gov/research/coal/carbon-storage-faqs/how-can-CO_2-be-stored-underground

Verkerke, J. L., Williams, D. J., & Thoma, E. (2014). Remote sensing of CO_2 leakage from geologic sequestration projects. *International Journal of Applied Earth Observation and Geoinformation*, *31*, 67–77. https://doi.org/10.1016/j.jag.2014.03.008

Waarum, I.-K., Blomberg, A. E. A., Eek, E., Brown, J., Ulfsnes, A., Carpenter, M.,

Grimsrud, T. S., Park, J., Cornelissen, G., Sparrevik, P. (2017). CCS Leakage Detection Technology - Industry Needs, Government Regulations, and Sensor Performance. Energy Procedia, 114(November 2016), 3613–3627. https://doi.org/10.1016/j.egypro.2017.03.1493

Werner, C., Chiodini, G., Voigt, D., Caliro, S., Avino, R., Russo, M., Brombach, T., Wyngaard, J., Brantley, S. (2003). Monitoring volcanic hazard using eddy covariance at Solfatara volcano, Naples, Italy. *Earth and Planetary Science Letters*, *210*(3–4), 561–577. https://doi.org/10.1016/S0012-821X(03)00127-4

White, F. M. (1991). *Viscous Fluid Flow* (2nd ed.). McGraw-Hill, Inc. 28 pp.

Wilcox, J. (2012). *Carbon Capture.* Springer. 18-23 pp. https://doi.org/10.1007/978-1-4614-2215-0

Willms, J. R., Dowling, a N., Dong, Z. M., Hunt, S., Shelp, B. J., & Layzell, D. B. (1997). The simultaneous measurement of low rates of CO2 and O2 exchange in biological systems. *Analytical Biochemistry*, *254*(2), 272–282. https://doi.org/10.1006/abio.1997.2416

Wilson, E., & Jerrad, D. (2007). *Carbon capture and sequestration: integrating technology, monitoring, regulation*. Blackwell Publishing, Ames, IA. 107-122 pp.

WMO. (2017a). Frequently ask question. Retrieved November 7, 2017, from camhttp://www.wmo.int/pages/prog/wcp/ccl/faq/faq_doc_en.html#top

WMO. (2017b). Wmo Greenhouse Gas. Retrieved from public.wmo.int/en/media/press-release/greenhouse-gas-concentrations-surge-new-record

Yiqi, L., & Zhou, X. (2006). *Soil Respiration and the Environment*. Academic Press. 17-157.

Yu, X., Zha, T., Pang, Z., Wu, B., Wang, X., Chen, G., Li, C., Cao, Ji., Jia, G., Li, X., Wu, H. (2011). Response of soil respiration to soil temperature and moisture in a 50-year-old oriental arborvitae plantation in China. *PLoS ONE*, *6*(12), 1–7. https://doi.org/10.1371/journal.pone.0028397

Zeebe, R. E. (2011). On the molecular diffusion coefficients of dissolved CO_2, HCO^{3-}, and CO_3^{2-} and their dependence on isotopic mass. *Geochimica et Cosmochimica Acta*, *75*(9), 2483–2498. https://doi.org/10.1016/j.gca.2011.02.010

Zhao, X., Deng, H., Wang, W., Han, F., Li, C., Zhang, H., & Dai, Z. (2017). Impact of naturally leaking carbon dioxide on soil properties and ecosystems in the Qinghai-Tibet plateau. *Scientific Reports*, *7*(1), 3001. https://doi.org/10.1038/s41598-017-02500-x

Zhou, X., Apple, M. E., Dobeck, L. M., Cunningham, A. B., & Spangler, L. H. (2013). Observed response of soil O_2 concentration to leaked CO_2 from an engineered CO_2 leakage experiment. *International Journal of Greenhouse Gas Control*, *16*, 116–128. https://doi.org/10.1016/j.ijggc.2013.03.005

Appendix A. **Leak Test for GER Measurements for SOIL-A**

Initially for SOIL-A, leak detection test was conducted for closed system GER measurement, where a NE-300 pump syringe was used to inject smaller rates of CO_2 from a 60ml syringe (within the range of soil respiration rates) into the bottom chamber of the soil column. As it required us to refill the syringe every time it was finished to maintain the continuous leaked CO_2 injection, we eventually had to switch to an automatic flowmeter (range of 0 – 1 ml/min) later for the injection at SOIL-B. Initially, we injected at rate equivalent to soil respiration rates of 2 – 6 umolCO_2/m^2 /s for Soil-A.

The GER values, as ratio of ΔCO_2 and ΔO_2 w.r.t reference air, at the headspace of enclosed the SOIL-A was recorded continuously for the entire injection period. The measured values of the GER are compared with the corresponding model predications for each injection leaks. The comparison bar graphs for all the three CO_2 leak added tests for the SOIL-A are given sequentially at the below figures:

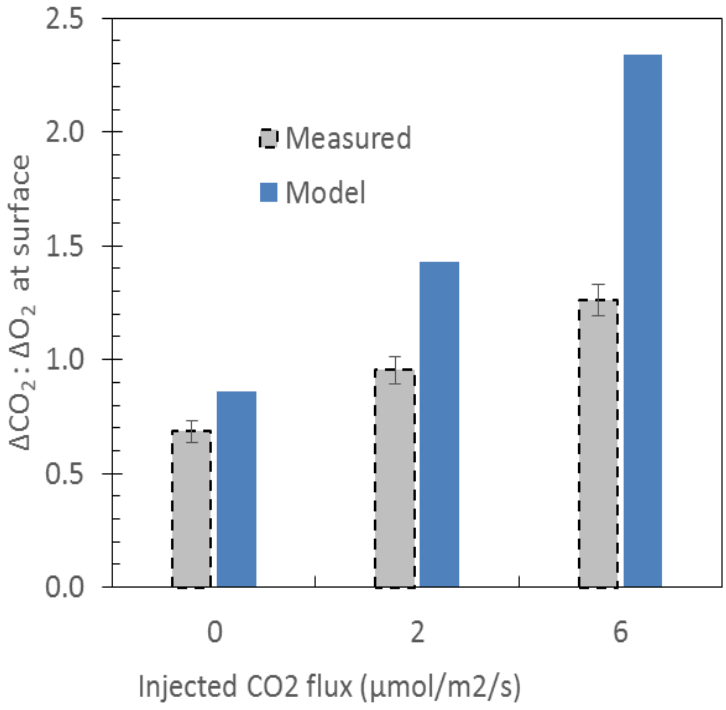

Figure A-1: Test-1 for leak detection at SOIL-A by GER measurement at soil surface. The measured GER and model predictions with CO_2 injections are compared for the respiration of 3.54 µmol/m2/s, RQ of 0.69, and 15% water in the soil column.

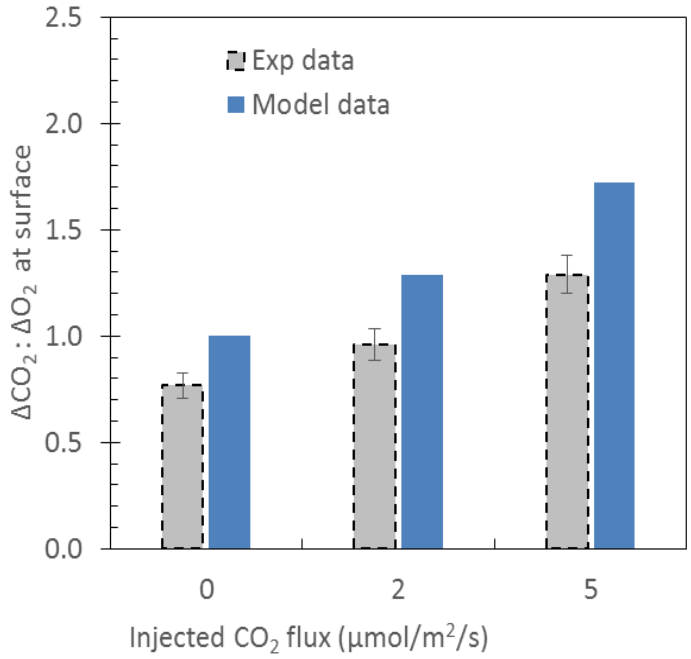

Figure A-2: Test-2 for SOIL-A; measured GER and the model predictions are compared for the respiration of 6 µmol/m2/s, RQ of 0.70, and water of 15%.

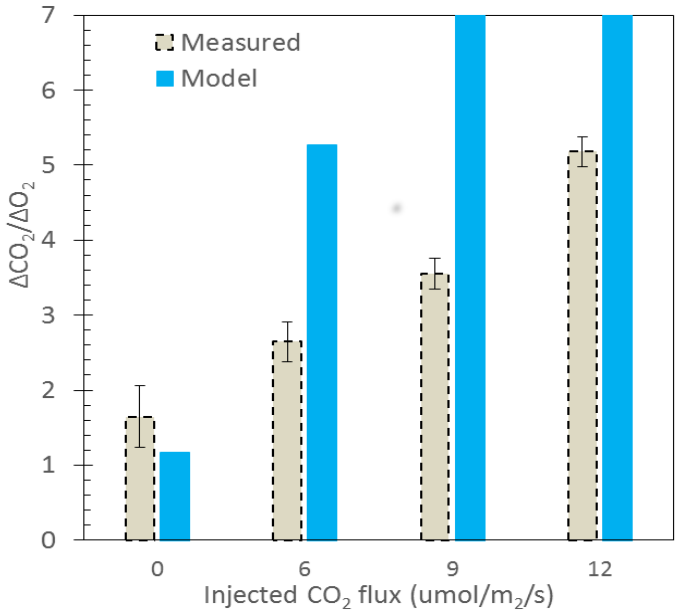

Figure A-3: Test-3 for SOIL-A; the measured GER and model predictions are compared for the respiration of 6.57 µmol/m2/s, RQ of 0.88, water content of 15%.

For SOIL-A, the natural GER $(\Delta CO_2 : \Delta O_2)$ were found as 0.69±0.05, 0.77±0.05, and 0.88±0.06 with different respiration rates of 3.54, 6.0, 6.57µml/m2/s respectively in the three tests. These graphs, Figure A-23 to Figure A-25, also the introduction of the injection of 2 mol/m2/s injection rates GCR values increased to 0.95±0.06, 0.96±0.06, and 1.17±0.08, which sees an average of approx. 32% increase from the corresponding natural GER levels. This increase went higher with the addition of CO_2 leak ≥ 5µmol/m2/s; for all three tests, the GER values were 1.26±0.07, 1.29±0.08, and 1.52±0.10 with average increase of 75% from the base level. It shows that GER measurement can easily distinguish any leaks higher than ≥5µmol/m2/s. Despite the model predictions of the GER show the similar increasing trend as the measured with the increasing injection rates, the model overestimated the GER for each leak added scenario.

However, model overestimate the GER for leak added scenario. This overestimation of the model is higher when the soil respiration rate is comparatively lower (seen for the test-1 where respiration was about 3µmol/m2/s). The reasons the model over predicts is that one/more processes important to soils subjected to CO_2 leaks is not incorporated into the model. This missing process will be discussed in the chapter five.

Appendix B. **Comparison of model and measurements for enhanced boundary between soil and ambient air**

After the initial measurements for the model variables (water content, RQ, and respiration rate), we tested our model predictions by comparing the measured concentrations of O_2 and CO_2 across the soil column having a boundary layer (due to dried leaves or grasses on surface) between the soil surface and ambient air.

A layer of 1- 2 cm thick glass wool was used, to make the boundary between the soil surface of the column and room air. The concentration of the O_2 and CO_2% in the air within this boundary were measured after a day and were found to be 19.11% and 1.63% respectively which are significantly different than room air composition (about 20.90 and 0.04%, respectively). These concentrations along with SR and RQ were used to simulate the O_2 and CO_2 profiles across the soil column. The comparison of model predictions and measured data for this special condition is given in Figure B-1.

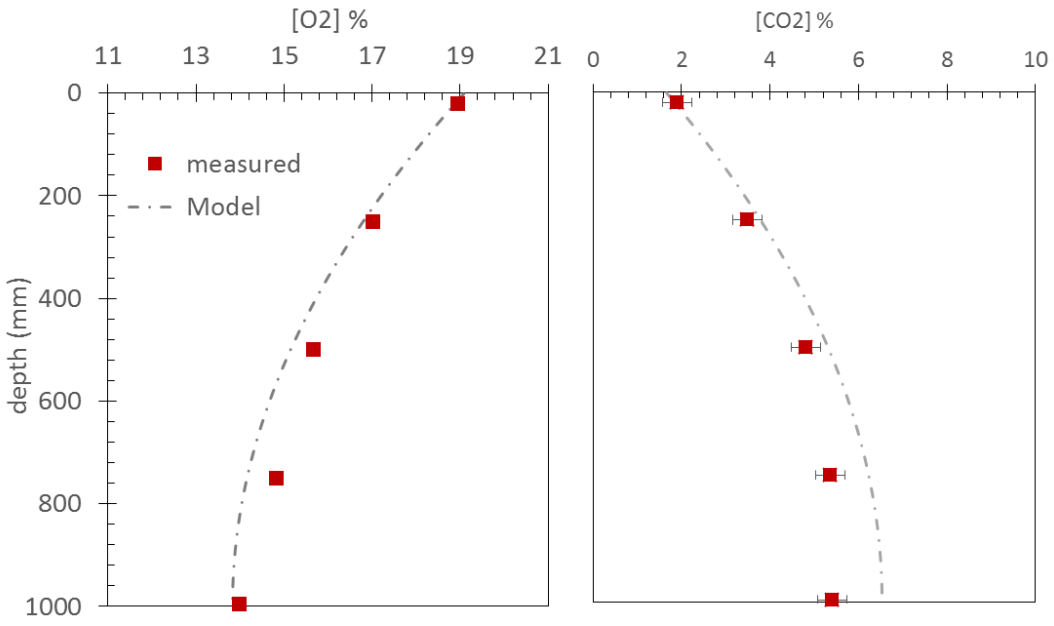

Figure B-1: Comparison of the model with measured O_2 and CO_2 profiles in soil column when the soil surface was covered by 1 – 2 cm of glass wool.

From the comparison, between model and measurement, we see that when the surface has a lower level of O_2 and higher CO_2, as expected for soil covered by litter, our model overestimates the CO_2 concentrations in soil and this overestimation increases with depth. For O_2 profiles, the model underestimates relative to measurements with depth. These discrepancies in model predictions and observed concentrations can be explained by the lower concentration of O_2 and higher concentration of CO_2 at the soil surface which, in turn, may affect the diffusion of both gases into or out of the soil layers, hence impacting biological respiration in the subsequent soil layers which was considered constant in all the layers in our model.

Appendix C. **Calculation of CO_2 accumulation in the soil column**

For the calculation, the measured soil properties used as given below,

Soil Porosity= 28%

Water content, W% = 18%

Total soil vol. = 8107 ml

CO_2 solubility at 25^0C = 0.83 (dimensionless)

Table C-1: Total CO_2 injection over 12 days

Injection Rate	**Total Period**		**Injected CO_2**	**Total vol.**
ml/min	Days	min	ml	ml
0.08	4	5760	460.8	1497.6
0.12	6	8640	1036.8	

The total actual amount of CO_2 for the soil column only is,

$$= 1497.6 \text{ ml of } CO_2 \quad (1)$$

The method of CO_2 accumulation is based on the measured (and extrapolated) CO_2 concentrations across the soil column before (Table 3) and after (Table 4) the injection period for 12 days.

Table C-2: From the concentration profile measured before injection

Depth	measured [CO2]	vol. of [CO_2]= air vol. x [CO2]%	Total [CO_2] in soil	Eqvt [CO_2](w)	Total [CO_2] (w)	Total [CO_2](g+w)
no.	*fraction*	*ml*	*ml*	*ml*	ml	*ml*
SA-1	0.24%	1.35		0.72		
SA-2	0.90%	5.12		2.73		
SA-3	1.58%	8.95	51.66	4.77	27.57	*79.23*
SA-4	2.81%	15.93		8.50		
SA-5	3.58%	20.31		10.84		

Table C-3: From the concentration profile measured 12 days after injection

Depth	measured [CO2]	vol. of [CO_2] = air vol. x [CO2]%	Total [CO_2] in soil	Eqvt [CO_2](w)	Total [CO_2] (w)	Total [CO_2](g+w)
no.	*fraction*	*ml*	*ml*	*ml*	ml	*ml*
SA-1	0.19%	1.06		0.56		
SA-2	3.59%	20.35		10.86		
SA-3	11.05%	62.71	299.76	33.46	159.94	459.71
SA-4	16.00%	90.80		48.45		
SA-5	22.00%	124.85		66.62		

From Table 3 and 4, we can estimate the total CO_2 accumulation during the injection as,

Total CO_2 accumulation = Total [CO_2](g+w) (after – before injection)

$$= 459.71 - 79.23 = 380.48 \text{ ml of } CO_2 \quad (2)$$

The calculation of CO_2 accumulation from the concentration difference method (Table 3 and 4) shows that total accumulation of gas CO_2 increased by about 6 times from background soil column. This accumulation of gas phase CO_2 enhanced the proportional liquid phase CO_2(w) (and the HCO_3 and CO_3^{2-}) as it shares approximately 35% of the total CO_2 in the soil column.